National Library of Canada
Acquisitions and Bibliographic Services Branch
395 Wellington Street
Ottawa, Ontario
K1A 0N4

Bibliothèque nationale du Canada
Direction des acquisitions et des services bibliographiques
395, rue Wellington
Ottawa (Ontario)
K1A 0N4

Your file Votre référence

Our file Notre référence

NOTICE

The quality of this microform is heavily dependent upon the quality of the original thesis submitted for microfilming. Every effort has been made to ensure the highest quality of reproduction possible.

If pages are missing, contact the university which granted the degree.

Some pages may have indistinct print especially if the original pages were typed with a poor typewriter ribbon or if the university sent us an inferior photocopy.

Reproduction in full or in part of this microform is governed by the Canadian Copyright Act, R.S.C. 1970, c. C-30, and subsequent amendments.

AVIS

La qualité de cette microforme dépend grandement de la qualité de la thèse soumise au microfilmage. Nous avons tout fait pour assurer une qualité supérieure de reproduction.

S'il manque des pages, veuillez communiquer avec l'université qui a conféré le grade.

La qualité d'impression de certaines pages peut laisser à désirer, surtout si les pages originales ont été dactylographiées à l'aide d'un ruban usé ou si l'université nous a fait parvenir une photocopie de qualité inférieure.

La reproduction, même partielle, de cette microforme est soumise à la Loi canadienne sur le droit d'auteur, SRC 1970, c. C-30, et ses amendements subséquents.

Canada

THE UNIVERSITY OF ALBERTA

DISSOLUTION KINETICS OF CARBONATES IN HYDROTHERMAL SOLUTIONS

©

BY

STEPHEN JAMES TALMAN

A thesis submitted to the faculty of graduate studies and research in partial fulfilment of the requirements for the degree of Doctor of Philosophy

DEPARTMENT OF GEOLOGY

Edmonton, Alberta

FALL 1992

National Library of Canada
Bibliothèque nationale du Canada

Canadian Theses Service
Service des thèses canadiennes

Ottawa, Canada
K1A 0N4

The author has granted an irrevocable non-exclusive licence allowing the National Library of Canada to reproduce, loan, distribute or sell copies of his/her thesis by any means and in any form or format, making this thesis available to interested persons.

L'auteur a accordé une licence irrévocable et non exclusive permettant à la Bibliothèque nationale du Canada de reproduire, prêter, distribuer ou vendre des copies de sa thèse de quelque manière et sous quelque forme que ce soit pour mettre des exemplaires de cette thèse à la disposition des personnes intéressées.

The author retains ownership of the copyright in his/her thesis. Neither the thesis nor substantial extracts from it may be printed or otherwise reproduced without his/her permission.

L'auteur conserve la propriété du droit d'auteur qui protège sa thèse. Ni la thèse ni des extraits substantiels de celle-ci ne doivent être imprimés ou autrement reproduits sans son autorisation.

ISBN 0-315-77222-0

Canada

THE UNIVERSITY OF ALBERTA

RELEASE FORM

NAME OF AUTHOR: Stephen James Talman

TITLE OF THESIS: Dissolution Kinetics of Carbonates in Hydrothermal Solutions

DEGREE: Doctor of Philosophy

YEAR THIS DEGREE GRANTED: 1992

Permission is hereby granted to THE UNIVERSITY OF ALBERTA LIBRARY to reproduce single copies of this thesis and to lend or sell such copies for private, scholarly or scientific purposes only.

The author reserves other publication rights, and neither the thesis nor extensive extracts from it may be printed or otherwise reproduced without the author's written permission.

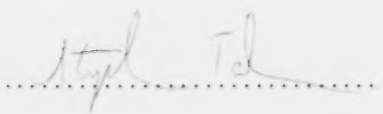

29 Lonsdale Dr., London

Ontario

N6G 1T4

Date: October 1, 1992

THE UNIVERSITY OF ALBERTA

FACULTY OF GRADUATE STUDIES AND RESEARCH

The undersigned certify that they have read, and recommend to the Faculty of Graduate Studies and Research for acceptance, a thesis entitled *Dissolution Kinetics of Carbonates in Hydrothermal Solutions* submitted by Stephen James Talman in partial fulfilment of the requirements for the degree of Doctor of Philosophy.

.....
Karlis Muehlenbachs - Supervisor

.....
Bill Gunter - Supervisor

.....
Bruce Nesbitt (Geology)

.....
Robert Luth (Geology)

.....
Hans Machel (Geology)

.....
Loren G. Hepler (Chemistry)

.....
Abraham Lerman - External Examiner
Northwestern University

Date: October 1, 1992

This thesis is dedicated to the memory of Chris Scarfe who was responsible for initiating this work. Although he supervised this work for less than a year before he was fatally struck, while jogging at 8 a.m., by an automobile operated by an impaired driver, he managed to excite my curiosity as few others have. I will always regret that I was never able to talk to Chris simply as a friend, rather than as a friend and a supervisor. Please - Don't drink and drive - or better yet - Don't drive.

ABSTRACT

Rates of dissolution of calcite and dolomite in CO_2 and HCl bearing aqueous solutions were experimentally evaluated in the temperature range between 100 and 200°C. The dissolution rate of both carbonates is strongly dependent on stirring rate. This stirring dependence indicates the presence of gradients in the composition of the solution surrounding the dissolving grains which demonstrates that the rate of reaction is partially transport limited. Rate expressions based on the composition of the bulk solution may be unsuitable for describing the rate data. The dependence of dissolution rate of calcite on solution composition can be described with a rate expression similar to the low temperature rate expression proposed by Plummer *et al.* (1978). The 100 and 150°C dolomite dissolution data was satisfactorily fitted with a low temperature rate expression, based on bulk solution composition, similar to that proposed by Busenberg and Plummer (1982); however, the 200°C data cannot be described with a similar rate expression.

A model for the dissolution based on a reaction rate that is dependent on the solution composition adjacent to the dissolving grains, but considers the diffusion of reactants towards the dissolving surface, is presented. The model includes electrostatically coupled diffusion coefficients, a consideration lacking in most other similar models. Although several parameters used in the model are estimated, the model predictions provide insights, otherwise inaccessible, into the reaction kinetics. The results demonstrate the need for well defined hydrodynamic conditions in order to interpret experimental results uniquely.

The model was adapted to consider situations, other than those studied experimentally, in which concentration gradients may form around dissolving or precipitating grains. Results from calculations modelling the incorporation of trace elements in precipitating calcite grains rate arising from diffusional processes, and the probable effect of introducing agents which form stable Ca–complexes on the rate of calcite dissolution.

ACKNOWLEDGEMENTS

I would like to thank Bill Gunter who, as a co–supervisor of my thesis, was always available to deal with my problems, scientific or otherwise. Karlis Muehlenbachs was placed in the unenviable position of inheriting three of Chris's PhD. students; however, he rose to the task and was rid of us all in as short an order as could be expected (considering that I was one of them). I am also grateful to the management of the Alberta Research Council for providing me with access to ARC's labs, computing facilities, lab technologists, and a very good library. Lab techs who were of particular help, and I can still remember, were Bernice Young, Nanik Khamil, and Larry Holloway. Also talks with the professional staff, particularly Ernie Perkins, Peter Tremaine, Gordon Bird, Ralph Jonasson, Zhihong Zhou and Linda Gray were welcomed. Finally, more thanks are due to Brain Wiwchar than I can possibly express.

I thank Jamey Hovey for his groundbreaking work in LaTeX, for his hospitality in Berkeley, and generally providing me with more rich food for thought than is good for one. Hugo Bianchi replaced Jamey in the ARC calorimetry lab, and as a source of confusing talk about chemistry. Haibo Huang also provided, near endless, hours of constantly witty and incredibly perceptive conversation, welcome relief from my work. Finally, Tom Dearman's hospitality, whether here or there, was always appreciated.

I would like to thank all the members of my examining committee for their support and for reading this. In particular, short talks with H.G. Machel focussed my attention on aspects of carbonate chemistry that I would likely have managed to overlook. Also, Loren Hepler provided many kind words and thoughts, usually when they were well needed.

The good folks at the Edmonton Bicycle Commuters gave as good as they took, and they took plenty. EBC provided me with a surrogate family in Edmonton, a little bit of insanity in an otherwise overly-sane city.

Karen Jensen drafted, with very little help from my sketches, many figures in this thesis. Thanks Karen. Also, Doug Barrett helped out in this department. Peter

Moller provided me with a pre-commercial release of his plotting program, Viking, which helped my work considerably. During the hectic last days Carl Mendoza provided much needed logistical support, and Wendy Allsopp gave me a timely, and much needed, hand.

A musical cast of thousands was involved in the preparation of this thesis. David Wisdom kept me awake, and sometimes even at work, many late nights. Sloth and CJSR managed most other nights.

Finally, I am grateful to the Alberta Oil Sands Technology and Research Authority for a postgraduate scholarship and their support for this project.

Contents

1 Introduction to Thesis **1**

1.1 Introduction and Outline 1

1.2 Review of literature 6

1.2.1 General review of rate processes 7

1.2.2 Temperature dependence of processes 10

1.2.3 Dependence of reaction rate on solution composition 11

1.2.4 Review of Carbonate Dissolution Kinetics 13

1.2.5 Reactor designs 15

2 Experimental Designs **21**

2.1 Introduction 21

2.2 Calcite Experiments 22

2.2.1 Reactants 22

2.2.2 Experimental details 25

2.3 Dolomite Experiments 28

2.3.1 Experimental details 28

3 Experimental Study of Calcite Dissolution Kinetics under Hydrothermal Conditions **33**

3.1 Introduction 33

3.2 Experimental Results 34

3.2.1 Solution Composition 34

3.2.2 Solubility Product of Calcite . . . 35
3.3 Data Reduction . . . 37
3.3.1 Rate Laws . . . 37
3.3.2 Evaluation of Rate Constants . . . 40
3.3.3 Temperature Dependance . . . 46
3.4 Conclusions . . . 49

4 Mixed Kinetic Control of Calcite Dissolution **50**
4.1 Introduction . . . 50
4.2 Theory . . . 52
4.2.1 Calcite Dissolution . . . 52
4.2.2 Diffusion in electrolyte solutions . . . 54
4.3 Mixed reaction control . . . 55
4.3.1 Numerical Scheme . . . 58
4.4 Results . . . 60
4.5 Implications for High Temperature Results . . . 72

5 Dissolution Rate of Dolomite in Hydrothermal Solutions **76**
5.1 Introduction and previous studies . . . 76
5.1.1 Stirring Dependence . . . 79
5.2 Results . . . 80
5.2.1 Stoichiometry of dissolution . . . 86
5.2.2 Determination of Rate Constants . . . 87
5.3 Conclusions . . . 97

6 Mixed Kinetics of Dolomite Dissolution **103**
6.1 Introduction . . . 103
6.2 Theory . . . 107
6.3 Numerical Results . . . 108
6.4 Applications to higher temperatures . . . 120

7 Implications and Applications to other Systems **124**

7.1 Application to Industrial Problems 124

7.2 Trace Element Partitioning 128

7.2.1 Zonations within Grain 128

7.2.2 Trace Element Partitioning and Precipitation Rates 130

8 Summary and Conclusions **136**

References **140**

Appendix A **151**

A.1 Raw data from the calcite experiments 151

A.2 Dolomite Experimental Details 156

A.2.1 Detailed notes on Experiments 156

List of Figures

1.1 Simulated data from a batch reactor. 17

1.2 Simulated data from an open reactor 19

2.1 Schematic drawing of autoclaves 23

2.2 Line profile scans of calcite surface 24

2.3 Schematic diagram of the stirred batch reactor 27

2.4 Schematic diagram of the flow through reactor system 31

3.1 Calcium concentration versus elapsed time for various experimental conditions 36

3.2 Dissolution rate plotted against Ω 38

3.3 Compositional fields displaying prominent reaction contributing to rate 45

3.4 Arrhenius plots of calcite rate constants 47

4.1 Calculated (H^+) *vs.* distance from the calcite surface 61

4.2 Calculated (Ca^{2+}) *vs.* distance from the calcite surface 62

4.3 Calculated (H_2CO_3) *vs.* distance from the calcite surface 63

4.4 Calculated (HCO_3^-) *vs.* distance from the calcite surface 64

4.5 Calculated (Cl^-) *vs.* distance from the calcite surface 65

4.6 Comparison of bulk and surface (H^+) 66

4.7 Plot of Ω *vs.* δ. 68

4.8 Comparison of back reaction rate with various aqueous complex concentrations 69

4.9 Calculated (H_s^+) as a function δ^{-1} 71

5.1 Traces of the rotating disk used by Herman and White 79
5.2 Measured rate of dolomite dissolution from three runs. 82
5.3 Rate of dolomite dissolution at 100°C less k_2 [H_2CO_3]$^{1/2}$ *vs.* [H^+]. . 91
5.4 Rate of dolomite dissolution at 100°C less $k_1(SR)$ [H^+] *vs.* [H_2CO_3]$^{1/2}$. 92
5.5 Rate of dolomite dissolution at 150°C less k_1 [H^+] *vs.* [H_2CO_3]$^{1/2}$ . . 96
5.6 The variation of $\log(k_2^D)$ as a function of $1000/T$. 98
5.7 The variation of $\log(k_3^D)$ as a function of $1000/T$. 99

6.1 Dissolution rates reported by Busenberg and Plummer (1982) 105
6.2 Stirring rate dependence on dolomite dissolution rate at 45°C (after Busenberg and Plummer, 1982) 106
6.3 Calculated solution composition *vs.* distance from the dolomite surface at $\delta = 7.0\mu$m and 25°C 109
6.4 Calculated solution composition *vs.* distance from the dolomite surface at $\delta = 25.0\mu$m and 25°C 110
6.5 Calculated solution composition *vs.* distance from the dolomite surface at $\delta = 7.0\mu$m and 45°C 111
6.6 Calculated solution composition *vs.* distance from the dolomite surface at $\delta = 25.0\mu$m and 45°C 112
6.7 Calculated solution composition *vs.* distance from the dolomite surface at $\delta = 7.0\mu$m and 65°C 113
6.8 Calculated solution composition *vs.* distance from the dolomite surface at $\delta = 25.0\mu$m and 65°C 114
6.9 Calculated solution composition *vs.* distance from the dolomite surface at $\delta = 7.0\mu$m and 100°C 115
6.10 Calculated solution composition *vs.* distance from the dolomite surface at $\delta = 25.0\mu$m and 100°C 116
6.11 (H^+(s) as a function of H^+(b) at 25, 45, 65 and 100°C 118

7.1 Calculated distribution coefficient as a function of precipitation rate . 134

List of Tables

2.1 Chemical analysis of Iceland spar 26
2.2 Summary of conditions for calcite experiments 26
2.3 Chemical analysis of dolomites 29
2.4 Summary of conditions for dolomite experiments 29

3.1 Values of thermodynamic constants used in the calculations 44
3.2 Comparison of experimental and extrapolated rate constants 44

4.1 Values of physical parameters 59
4.2 Bulk and surface concentration and dissolution rate calculated at 150°C 73
4.3 Comparison of calculated rates with those from empirical rate expression 74
4.4 Coefficients used to calculate the empirical rate listed in Table 4.3 . . 74

5.1 Table of internally consistent solution compositions from 100°C runs. 83
5.2 Table of internally consistent solution compositions from 150°C runs. 85
5.3 Table of internally consistent solution compositions from 200°C runs. 86
5.4 Inferred 100°C solution composition. 89
5.4 Inferred 150°C solution composition. 94
5.5 Inferred 200°C solution composition. 102

6.1 Values of physical parameters 123

A.1 Raw data from the calcite experiments 155
A.2 Comparison of carbonate analysis obtained using different sampling procedures 158
A.3 Analysis of cation standards. 159
A.4 Raw data from 100°C runs 160
A.5 Raw data from 150°C runs 162
A.6 Raw data from 200°C runs 163

Chapter 1

Introduction to Thesis

1.1 Introduction and Outline

Although there is a large body of literature dealing with the dissolution and precipitation kinetics of carbonate minerals, to date these studies have dealt exclusively with temperatures at or below 100°C. This thesis presents new experimental and theoretical results dealing with the dissolution of calcite and dolomite. Specifically, results of dissolution experiments at temperatures between 100 and 200°C and theoretical results describing the diffusive flux of material away from dissolving calcite and dolomite grains are given.

The thesis consists of 7 relatively self-contained chapters. Portions of the second and third chapters have been previously published in Talman *et al.* (1990), and a shorter version of the fifth chapter was published by Talman and Gunter (1992). The bulk of this introductory chapter introduces many of the concepts utilized in the subsequent chapters. The second chapter and a portion of the appendix describe the techniques used experimentally to determine the rate of calcite and dolomite dissolution; the experimental results and their interpretation are presented in two chapters (calcite in Chap. 3 and dolomite in Chap. 5). The treatment of the diffusive flux arising from the dissolution is presented in Chaps. 4 (calcite) and 6 (dolomite). Chapter 7 demonstrates possible applications of the results and concepts developed, particu-

larly those from Chap. 4, to various systems of industrial and geological relevance. Within the appendix to the thesis are tables of the original experimental data, as well as a description of how and why various experimental techniques were changed over the course of the work.

Different experimental techniques were used to study the rates of calcite and dolomite dissolution. Experimental variables included the pH and concentration of carbonic acid in the solution, temperature and stirring rate. Calcite dissolution was studied using a batch reactor (see Sec. 1.2.5 for a description of various reactor types). Batch reactors do not directly yield rate data, but rather give integrated rates of dissolution. Limitations associated with using batch reactor data in rate studies where the number of samples obtained during a run is small (as was the case in this study due to restrictions arising from the high experimental temperatures and pressures) are also discussed in Sec. 1.2.5. For the reasons discussed therein, the dissolution rates of calcite were not directly calculated from the batch reactor data, but rather, a proposed rate expression was integrated and this expression was compared to the batch reactor data. It was felt that this approach is more accurate than calculating the rate by numerical integration of the limited batch reactor data. This approach has generally not been used previously in rate studies of carbonates. The dolomite dissolution rate data were obtained using a flow through reactor.

The experimental results demonstrate that, as at lower temperatures, the rate of both calcite and dolomite dissolution are influenced by the activity of H^+ and H_2CO_3. A further important experimental variable is the stirring rate; this indicates that concentration gradients exist in the solution surrounding the dissolving solid. Stirring rate dependence has been previously documented for calcite (*e.g.* Rickard and Sjöberg, 1983), although the evidence for stirring rate dependence at low temperatures for dolomite is equivocal (compare Herman and White, 1985 with Busenberg and Plummer, 1982; Sec. 5.1). The rate expressions proposed by Plummer *et al.* (1978, see Sec. 1.2.4) for calcite dissolution were found to describe the high temperature data obtained here. The rate constants used to fit these equations to the data

(Table 3.2) were in reasonable agreement with values extrapolated in temperature using equations presented in Plummer *et al.* (1978); although, the value of one rate constant (k_2^C in Eqn. 3.1) decreases with temperature above about 120°C. Recently reported rates of calcite precipitation at 100°C (Shiraki and Brantley, 1992) are consistent with the rate expression and rate constants reported here. Interpretation of the dolomite rate data was more complex. The rate data at 100 and 150°C could be described with a rate expression of the form proposed by Busenberg and Plummer (1982); however, no expression of this form could fit the 200°C data. The rate constants in this expression (Table 5.7) were, for the most part, relatively consistent with the low temperature results of Busenberg and Plummer. Since one rate constant (k_1^D in Eqn. 5.2) was found to depend on the stirring rate, extrapolation of the low temperature results was not possible. The rate constant, k_1^D, becomes progressively more sensitive to changes in the stirring rate as the temperature increases.

Unlike most silicate minerals, some carbonate and sulphate minerals and many simple salts dissolve so rapidly that appreciable concentration gradients (reflected in the dependence of reaction rate on stirring rate) develop in the solution surrounding the grains. A model of the diffusive flux of reactants to, and reaction products from, the carbonate surface was developed. The model treats both electrostatic coupling between ions and speciation changes within a stagnant boundary layer of between about 5 and 50 μm thickness. The model describing the calcite system (Chap. 4) includes equations describing the behaviour of Ca^{2+}, CO_3^{2-}, HCO_3^-, H_2CO_3, $CaCO_3^\circ$, $CaHCO_3^+$, H^+, OH^-, and Cl^-. The dolomite model was simplified by considering fewer species (Chap. 6), equations describing the behaviour of Mg^{2+}, Ca^{2+}, H_2CO_3, HCO_3^-, H^+, and Cl^- were considered. This simplification is justified as long as the calculated concentration gradients remain small. The resulting system of coupled, non-linear, first order differential equations was solved numerically. Results of calculations describing the calcite and dolomite systems at 150°C are presented in Secs. 4.5 and 6.4 respectively and are used to interpret experimental results. However, the model was mainly used to predict the concentration profiles away from the grains at

lower temperatures because the input parameters for the model (transport and thermodynamic properties of the various solutes) are more accurately known at lower temperatures. Furthermore, good low temperature models are required before the less well constrained, high temperature, results can be interpreted unequivocally.

The calculations described above demonstrate that appreciable concentration gradients will form around calcite, but not dolomite, dissolving in dilute, acidic solutions at 25°C for values of the stagnant film thickness of 10–30 μm (compare Fig. 4.1 with Fig. 6.3). Appreciable concentration gradients will form around dissolving dolomite grains at temperatures above 65°C (Figs. 6.7 and 6.8). An assumption commonly used in the analysis of low temperature calcite dissolution rate data is that the reaction is diffusion limited (*i.e.* the surface of the crystal is in equilibrium with the adjacent solution see Lancia *et al.*, 1991; Plummer *et al.*, 1978; Chap. 4); however, the calculations clearly demonstrate that this is not the case (Fig. 4.7). A further result of importance is that the calculated concentration of hydronium at the surface of a calcite crystal is proportional to its concentration in the bulk solution at 25°C (Fig. 4.6). This allows the use of the bulk solution composition in rate expressions. The calculations also demonstrate that diffusional limitations on the dissolution rate are much greater at higher temperatures (Secs. 4.5 and 6.4).

The experimental results demonstrate that the rate of dissolution of both calcite and dolomite are controlled by the concentration of H^+ and H_2CO_3 in the solution. The rate expressions proposed by Plummer *et al.* (1976) for calcite, and Busenberg and Plummer (1982) for dolomite both have explicit dependence on both of these concentrations. The rate of dissolution is retarded by the presence of dissolved salts in solution; this is explicitly noted by the presence of a back reaction term in the rate expressions used (*e.g.* Eqn. 1.12). The dissolution of calcite readily proceeds to saturation at low temperatures (Plummer *et al.*, 1978), so relatively simple expressions based simply on the departure from equilibrium (reaction affinity) can be used for the back reaction term. In contrast, dolomite dissolution is strongly inhibited by commonly occurring ions (notably HCO_3^-) at lower temperatures. This requires that

the expression for the back reaction contain terms which inhibit the reaction, and are not necessarily related to the, readily evaluated, reaction affinity. This complicates the analysis of the rate data, particularly since the composition of solution adjacent to the grain cannot be measured. In order to develop an improved expression for the back reaction the solution composition adjacent to the grain must be calculated. This calculation can only be made if the stagnant layer thickness is known; future work on carbonate dissolution kinetics should use experimental systems designed with this in mind.

The calculated concentration gradients demonstrate several interesting features about carbonate dissolution kinetics. Predicted pH shifts between the bulk and surface solutions are on the order of only a half a pH unit (Sec. 4.3, Fig. 4.1). Previously published models based on diffusion limited calcite dissolution (*e.g.* Sjöberg and Rickard, 1984a) predict shifts of several pH units over the same stagnant film thickness. At higher temperatures the calculated pH shift is greater (about 1.5 of a pH unit at 150°C, see Table 4.2). The higher temperature calculations on calcite predicted that the behaviour of rate constant, k_2^C, which was observed experimentally to decrease with temperature, will become erratic at elevated temperatures (Sec. 4.5 and Table 4.4).

The model also demonstrates that concentration gradients developed around dissolving dolomite grains are, at least partially, responsible for the change in the reaction order with temperature which was observed by Busenberg and Plummer (1982) and here (Chap. 5; Sec. 6.3, Fig. 6.11). As well, the great natural variations between the dissolution rates of different dolomite samples at low temperatures will diminish at higher temperatures since the dissolution of dolomite becomes increasingly diffusion controlled.

Both the experimental and computational results demonstrate that diffusional processes become increasingly important in limiting the rate of dissolution of calcite and dolomite as temperature is increased. This is likely to be the case for many minerals with retrograde solubility, since the concentration gradient driving the diffusive

flux from the crystal will decrease as the solubility of the mineral decreases.

Throughout this work activities will be denoted with square brackets and concentrations (moles kg^{-1} water) with parentheses (see Faure, 1991, p. 186).

1.2 Review of literature

Equilibrium solubilities and phase relations of carbonate minerals have been studied extensively at both ambient temperatures (Frear and Johnston, 1929; Mackenzie *et al.*, 1983) and higher temperatures (Sharp and Kennedy, 1965; Holland and Malinin, 1979; Fein and Walther, 1987). The behaviour of carbonate minerals in hydrothermal systems is particularly relevant to secondary oil recovery. Carbonates can affect porosity during diagenesis (Wood, 1986) and steam assisted oil recovery, and carbonate equilibria calculations be used to estimate the partial pressure of CO_2 in fluids produced during secondary oil recovery (Gunter and Perkins, 1991).

The incentive for studying the kinetics of dissolution and precipitation of carbonates at temperatures greater than 100°C has been lacking, because most traditional applications are based on the assumption of carbonate equilibrium. However, kinetic considerations may become important when the relative reaction rates of two minerals are similar, as in the case of carbonate diagenesis, or when a solution is subjected to conditions that change more rapidly than mineral equilibria can be established. Kinetic data at higher temperatures are needed if computer simulations of mid–ocean ridge processes (e.g. Bowers and Taylor, 1985) are to be improved.

Industrial processes generally are much more rapid than geological processes, and consequently, rate data are required to model industrial processes at most temperatures. Steam-assisted oil recovery is an example of an industrial process which will bring reactive aqueous solutions at temperatures similar to those used in this study into contact with carbonate minerals. Until recently, there were very few kinetic data on any minerals under hydrothermal conditions; however, rates are now available for several minerals (quartz - Rimstidt and Barnes, 1980; Bird *et al.*, 1986; feldspars -

Lagache, 1976; fluorite - Posey-Dowty *et al.*, 1986; also Helgeson *et al.*, 1984; Wood and Walther, 1983). Rate data are virtually non-existent for the carbonate system in solutions above 80°C. Early work on the rates of dissolution of common minerals under near-surface conditions was done by King and Liu (1933, calcite) and Correns and von Engelhardt (1938, potassium feldspar). Subsequent studies have been numerous, most in the past 20 years. Much of this work followed from seminal works by Wollast (1967) and Paces (1973), which were studies of dissolution kinetics in the laboratory and the field. The following section will present aspects of the previous work that are relevant to this study.

The dissolution reaction

$$A(s) \rightarrow A^{\circ}, \qquad 1.1$$

in which A(s) is used to represent a solid phase and A° is in solution, is a simple reaction that will be used, for illustrative purposes, in this chapter.

1.2.1 General review of rate processes

Theoretical aspects of dissolution kinetics are well described in the geochemical literature (*e.g.* Berner, 1978; 1981; Lerman, 1979; Lasaga, 1981; Dibble and Tiller, 1981)

Dissolution kinetics may be limited by the rate of transport of reactants towards the reacting surface, the rate of reaction between the reacting surface and the solution, or a combination of transport and reaction rate. Reactions limited by the first and second processes are said to be transport and surface reaction controlled respectively, the third is said to be controlled by mixed kinetics. Consequences of these limits on reaction rate are discussed by Berner (1978) and Dibble and Tiller (1981). The dissolution kinetics of virtually all minerals at near-surface conditions are surface reaction controlled; however, the rate of dissolution of some salts is diffusion controlled (Berner, 1978; Lasaga, 1990).

Observations that can be made to distinguish surface and diffusion controlled reactions (Berner, 1978). The rate of increase of reaction rate with temperature tends

to be greater for surface controlled reactions than for diffusion controlled reactions. The rate of surface controlled reactions is independent of stirring rates whereas the rate of diffusion controlled reactions are stirring dependent. Finally, surface controlled reactions tend to produce roughened surfaces whereas diffusion controlled reactions tend to smooth the dissolving grains. However; stirring rate dependence does not ensure that a reaction is diffusion controlled, nor does the presence of etch pits ensure that a reaction is surface controlled.

In a diffusion controlled reaction the solution at the mineral/solution interface is saturated with respect to the solid, and the rate of reaction is dependent on a characteristic length over which the solution can support a concentration gradient. This length is determined by the hydrodynamic conditions near the solid. If reaction 1.1 is diffusion controlled, and if the diffusion coefficient of A° is D_{A°, the rate, r_{Diff}, at which A(s) dissolves is given by

$$r_{Diff} = \frac{D_{A^\circ}}{\delta}((A^\circ_{eq}) - (A^\circ_b)). \qquad 1.2$$

The stirring rate dependent term, δ, in the above expression, is the distance over which a concentration gradient is supported, and (A°_{eq}) and (A°_b) are the equilibrium and bulk concentrations of A°. δ is a hydrodynamic parameter, its value is dependent on the physical parameters associated with the fluid (*e.g.* viscosity, flow velocity) and the solid surface (*e.g.* surface geometry and roughness); values of δ cited in the literature tend to be between 10 and 100 μm (Nielsen, 1964); however, in low energy environments (*e.g.* low flow or stirring rate) larger values may be reasonable. High stirring rates are associated with low values of δ, and hence higher dissolution rates.

In surface controlled reactions no such concentration gradient develops; the reaction rate is simply related to the bulk solution composition. The rate expression 1.2 is similar to one commonly assumed for surface controlled reactions, with the modification that the term D_{A°/δ is replaced by a single, experimental rate constant, k_s, divided by (A°_{eq}), and that concentrations are replaced by activities, to give

$$r_s = k_s\left(1 - \frac{[A^\circ_b]}{[A^\circ_{eq}]}\right). \qquad 1.3$$

Alternative, transition state based, rate expressions have been utilized recently (Lasaga, 1981; 1990; Aagaard and Helgeson, 1982; Murphy and Helgeson, 1989); however, for the brief and algebraically simple discussion following, only the rate expressions 1.2 and 1.3 will be considered. Furthermore, the solution will be assumed to be ideal (*i.e.* $[A^\circ] = (A^\circ)$).

Mixed reaction kinetics arise when a solid dissolves sufficiently rapidly to allow some appreciable concentration gradient to form in the solution adjacent to the surface, yet slowly enough that the solution near the grain remains undersaturated with respect to the dissolution. This is certainly the case for calcite dissolution in many solutions at room temperature. If the volume of solution in which there is a concentration gradient (stagnant layer) is much less than the volume of solution into which the mineral is dissolving (bulk solution) a significant quantity of mineral may pass through the stagnant layer without appreciably changing the bulk solution composition. After a transient response during which the concentration gradient around the grain changes, a steady state gradient will be reached within this stagnant layer. In this steady state the concentration of A° at the surface, (A°_s), will be such that the flux of A° away from the crystal will be equal to the rate of introduction of A° by dissolution. The diffusive flux of A° away from the surface, J_D, is

$$J_D = \frac{D_{A^\circ}}{\delta}((A^\circ_s) - (A^\circ_b)); \qquad 1.4$$

the flux due to the dissolution of A(s), J_s, is

$$J_s = k_s\left(1 - \frac{(A^\circ_s)}{(A^\circ_{eq})}\right). \qquad 1.5$$

As a simplification the parameter $k_D = D_{A^\circ}/\delta$ is introduced. Equating J_D to r_s and solving for (A°_s) gives

$$(A^\circ_s) = \frac{k_D(A^\circ_b) + k_s}{k_D(A^\circ_{eq}) + k_s}(A^\circ_{eq}), \qquad 1.6$$

and the rate of dissolution, r_m, is given by

$$r_m = \frac{k_s k_D}{k_D + k_s}\frac{(A^\circ_{eq}) - (A^\circ_b)}{(A^\circ_{eq})}. \qquad 1.7$$

1.2.2 Temperature dependence of processes

The manner in which rate constants for elementary reactions change with temperature is commonly described with the Arrhenius equation

$$k(T) = k_0 \exp(-E_a/RT), \qquad 1.8,$$

in which E_a is the activation energy, k_0 the pre-exponential factor, R the gas constant, and T the temperature. The Arrhenius equation is applicable to many rate processes, although there may be complications in that the two parameters k_0 and E_a may be temperature dependent. Changes in these parameters are indicative of a change in reaction mechanism.

The case of mixed kinetics discussed above does not represent rate control by a single elementary reaction, but rather two parallel reactions. Because mixed kinetics is important in carbonate dissolution, the temperature dependence of the rate of such reactions is developed below. Although the case treated below is considerably simpler than the treatment of mixed dissolution of carbonates presented in Chapters 4 and 6, it has the advantage of being algebraically tractable, and numerical solutions are not required.

The change in both k_D (assume constant δ) and k_s with temperature can be described by Eqn. 1.8, with the value of E_D (the diffusion activation energy) about 20 kJ/mole (Berner, 1978) and E_s (surface reaction activation energy) on the order of 100 kJ/mole (Murphy and Helgeson (1989) cite values for silicates between 40 and 140 kJ/mole).

The apparent activation energy can be evaluated from the derivative of $\log r_m$ with respect to $1/RT$ at constant (A_b°). Differentiating the log of Eqn. 1.7 with respect to $1/RT$ gives

$$\frac{d \log r_m}{d1/RT} = -\frac{\Delta A E_s k_D + E_D k_s + \Delta H^\circ k_s}{k_s + \Delta A k_D}, \qquad 1.9$$

in which ΔH° is the enthalpy of reaction 1.1, and ΔA is (A_{eq}°) - (A_b°). It can be seen that the expression for any rate constant will be complex, and will involve both

the activation energies of the two rate processes as well an enthalpy of reaction. If $\Delta A k_D \gg k_s$, Eqn. 1.9 becomes

$$\frac{d \log r}{d1/RT} = -E_s; \tag{1.10}$$

if $k_s \gg \Delta A k_D$, Eqn. 1.9 becomes

$$\frac{d \log r}{d1/RT} = \Delta H^\circ - E_D. \tag{1.11}$$

Eqns. 1.10 and 1.11 are the appropriate equations for what are known as surface controlled and diffusion controlled reactions. It is interesting to note that the rate of a diffusion controlled reaction will decrease with temperature if $\Delta H^\circ - E_D$ is greater than 0.

Since the activation energies associated with diffusion are generally less than those associated with surface reactions, the ratio k_D/k_s should decrease with temperature. This observation has led some authors to conclude that transport processes should be rate limiting at high temperatures (*e.g.* Lasaga, 1990, p. 20). However, transport processes will not limit reaction rates if the solubility of a mineral increases with temperature more rapidly than the ratio k_D/k_s decreases. If a mineral has retrograde solubility, transport control will, in most instances, limit reaction rates above some temperature.

1.2.3 Dependence of reaction rate on solution composition

The composition of the solution into which a mineral is dissolving can affect the reaction rate in many ways. Dissolution is driven by a departure from equilibrium, as a solution approaches saturation with respect to a mineral, the mineral will tend to dissolve less rapidly. This is the most fundamental, although not the only way that solution composition can affect dissolution rates.

Addition of electrolytes to a solution will alter reaction rates by changing the saturation state of the solution, by virtue of the electrolyte's effect on activity coefficients. As well, supporting electrolytes alter the diffusivities of ionic species, hence,

if a reaction rate is transport limited, there will be a further salinity dependence on reaction rate. Physical models of aqueous solutions can be used to predict the manner in which reaction rates are affected by these aspects of the solution composition with some certainty. Another obvious manner in which the solution composition can affect the reaction rate is if a new mineral precipitates on the dissolving surface. This will lead to a reduction of the rate of dissolution of the original substrate.

There are several other ways that solution composition can affect dissolution rates for which models are less well developed. The basis of many current models was the study of catalysis of gas phase reactions by solid surfaces and is described in standard texts of chemical kinetics (*e.g.* Glasstone *et al.*, 1941). Virtually all interfacial properties (*e.g.* surface charge, surface composition and edge free energy) can affect reaction rates; electrical, chemical and physical properties of the surface may appear in general rate expressions. Expressions for rates of crystal growth at kinks have explicit dependence on edge free energy (Zhang and Nancollas, 1990). Rate expressions based on surface complex concentrations are common (*e.g.* Chou and Wollast, 1985), and surface complex formation is dependent on surface electrical properties. Addition of any solute that affects the electrical, chemical or mechanical properties of the interface can affect reaction rates.

The surface charge of an interface determines the electric potential in its vicinity, and this potential enters directly into expressions for the equilibrium constant for the formation of surface complexes (Sposito, 1990). The distribution of surface complexes is of great importance in deriving a mechanistic model of the dissolution process. This is most easily shown by assuming that the dissolution reaction requires a specific surface geometry to proceed. The probability of that geometry of surface sites existing is reduced by adsorbed species, causing a reduction in reaction rate (see Wieland *et al.*, 1988).

Among the carbonate minerals, the surface properties of calcite are the most extensively studied. Calcite is much more reactive than most silicate minerals, and the calcite surface tends to be more dynamic than most other surfaces of geological

importance (Lahann and Siebert, 1982). Continuous restructuring of the calcite surface in aqueous solutions has been reported recently. For example, sorption of Cd on calcite surfaces appears to be a two step process, a rapid initial ion exchange with surface calcium ions, and a much slower uptake attributed to the incorporation of cadmium into calcite by recrystallization (Davis *et al.*, 1987). Thompson and Pownall (1989) report the formation of needle-like overgrowths, which they suggest may be aragonite, on calcite surfaces. The solution in which this putative aragonite was grown was was also dissolving calcite. They attribute this growth to a subsurface precipitation as described by Leaist (1987).

The ability of some solutes to affect the reaction kinetics of the carbonates has been well documented. For example the rate of calcite dissolution is greatly reduced by the addition of phosphates to the solution. Morse (1983) reports that a host of ions inhibits the rate of dissolution of calcite. Although rate expressions describing dissolution kinetics tend to be empirical at present (all the kinetic variables are not fully considered in present theories), investigation of relatively simple systems is required to provide insights into the factors affecting mineral dissolution rates.

1.2.4 Review of Carbonate Dissolution Kinetics

Dissolution kinetics of carbonate minerals is a subject that has been extensively studied in the past 20 years. The kinetics of calcite reactions are, by far, the best studied. Reviews on this subject are by Plummer *et al.* (1979) and Morse (1983) with more recent work being reported (Herman, 1982; Rickard and Sjöberg, 1983; Compton *et al.* 1984; 1990; Sjöberg and Rickard, 1984a; 1984b; Busenberg and Plummer, 1986; Chou *et al.*, 1989; Wallin and Bjerle, 1989; Dreybrodt and Buhmann, 1991). Studies on the kinetics of dissolution of other carbonates are relatively scarce; dolomite dissolution kinetics was studied by Lund *et al.* (1973); Busenberg and Plummer (1982), Herman (1982) and Chou *et al.* (1989). Other carbonates studied are aragonite (Chou *et al.*, 1989; Busenberg and Plummer, 1986) magnesite (Faux *et al.*, 1986; Chou *et al.* (1989), and witherite (Chou *et al.*, 1989).

These studies have been done on either simple aqueous systems or complex natural waters. The former studies were motivated by a desire to understand the mechanism by which the dissolution reaction proceeds, the latter by the belief that the mechanism is sufficiently dependent on solution composition to render meaningless any extrapolations from the simple systems under direct experimental observation to the more complex natural systems. Consequently, rate expressions proposed to fit the rate data in simple systems tend to be more complex than those used for more complex solutions. The complex solutions studied tend to be natural or synthetic sea water, whereas the simple solutions tend to be restricted to HCl and/or CO_2–bearing solutions. This thesis is restricted to study of these relatively simple solutions.

Plummer *et al.* (1978, referred to as PWP herein) as well as Busenberg and Plummer (1982; 1986) and Chou *et al.* (1989) found that carbonate dissolution rate data can be interpreted by assuming that the reaction proceeds by at least three parallel reactions, each of which dominates under different solution compositions. The general result of these studies is that the rate of dissolution, r, of these carbonates can be written as the difference between the rate of a forward reaction, r_f, and the rate of a backward reaction, r_b, or

$$r = r_f - r_b \tag{1.12}$$

where

$$r_f = k_1[H^+]^{n_1} + k_2[H_2CO_3^\circ]^{n_2} + k_3[H_2O]^{n_3} \tag{1.13}$$

and r_b a relatively more complex function of the solution composition (Busenberg and Plummer, 1982; 1986). The exponents n_i are all 1.0 except for dolomite in which case they are less than 1 and temperature dependent. It is also reported that the rate of calcite and dolomite dissolution is dependent on stirring rates at 25°C and 100°C respectively.

Several experimental techniques have been used to study the diffusion controlled aspect of calcite dissolution. These techniques include using a rotating calcite disk (Lund *et al.*, 1975; Herman, 1982; Rickard and Sjöberg, 1983; Sjöberg and Rickard, 1983; 1984a; 1984b; Compton and Daly, 1987; Compton *et al.*, 1989) and flow over

a flat calcite surface (Compton *et al.*, 1989). The advantage of these approaches is that the flow of the solution around the crystal is well defined; the characteristic diffusional length, δ, can be varied by changing either the rotation rate of the disk or the flow rate of the solution.

Although calcite dissolution kinetics have been extensively studied there are no rate data available for temperatures above 100°C. Data on the rate of calcite and dolomite dissolution at 100 to 200°C will be presented here. As well, it is commonly assumed (Sjöberg and Rickard, 1984a; Wallin and Bjerle, 1989) that calcite dissolution is a diffusion controlled reaction since there is some stirring rate dependence on the reaction rate. This assumption has been explored and justified by solutions to the diffusion equation describing the flux of solutes near the dissolving surface. This has been done by Plummer and Wigley (1976), Sjöberg and Rickard (1984b), Wallin and Bjerle (1989), although in an attempt to simplify the equations, various assumptions were made that are not necessary and may significantly affect the model results. A numerical solution to the complete set of equations describing the diffusion eliminates the need for these assumptions and is also presented here.

1.2.5 Reactor designs

Reactors, whether for high or low temperature systems, can be classified as either open or closed. Both systems are useful in certain circumstances (Levenspiel, 1972; Rimstidt and Dove, 1986; Posey-Dowty *et al.*, 1986). Several experimental designs have been used in the study of the dissolution kinetics of carbonates at low temperature. The relative merits and data reduction techniques required to analyse the data are discussed below.

Batch Reactors

The rate at which reaction 1.1 proceeds can be evaluated by simply immersing A(s) in solution, and either monitoring the mass loss of A(s), or the concentration of A°. Since no materials are being added to or removed from the system (save for some

aliquots of sample or some contamination from electrodes) this is called a closed or batch reactor. The introduction of one mole of A into a solution (total mass of solution, M kg) leads to an increase in A° of $1/M$ mol kg^{-1}, so an increase in A° of X mol kg^{-1} s^{-1} corresponds to a rate of dissolution of XM mol s^{-1}. Rates are generally normalized to surface area, A, so the rates are expressed as mol s^{-1} m^{-2}. The normalized rate of dissolution, r, is

$$r = \frac{XM}{A} = \frac{M}{A}\frac{d(A^\circ)}{dt}. \qquad 1.14$$

The rate of introduction of A° into solution is evaluated by numerically differentiating a concentration *vs.* time plot (e.g. Fig. 1.1).

A high temperature batch reactor may be as simple as a pressure vessel from which aliquots can be sampled periodically. Some form of agitation may be required, this is most easily achieved by rocking the pressure vessel, although magnetically coupled stirring devices may also be used. A practical difficulty arises with this approach in hydrothermal experiments since sampling the contents of the pressure vessel, without significantly disturbing the vessel, is complex. This puts limits on the amount of data that may be collected. Uncertainties in the numerical derivative are much greater than in low temperature studies, where a large numbers of concentration measurements can be obtained with relative ease.

Batch reactor data can be used to test any proposed rate expression; its validity can be checked with data from a single batch reactor run by integrating the proposed rate expression and comparing the integrated form to the data. Since there are a host of rate expressions describing calcite dissolution kinetics in solutions below 80°C, the hydrothermal dissolution experiments on calcite were done in a batch reactor, and the integrated rate expression was fit to the data.

Open Reactors

An open reactor are reactors into which there is a constant input of reactants. Some examples of open reactors are described in Levenspiel (1972) and Chou and Wollast (1984). One example is the stirred flow reactor. Such a reactor consists of a fixed

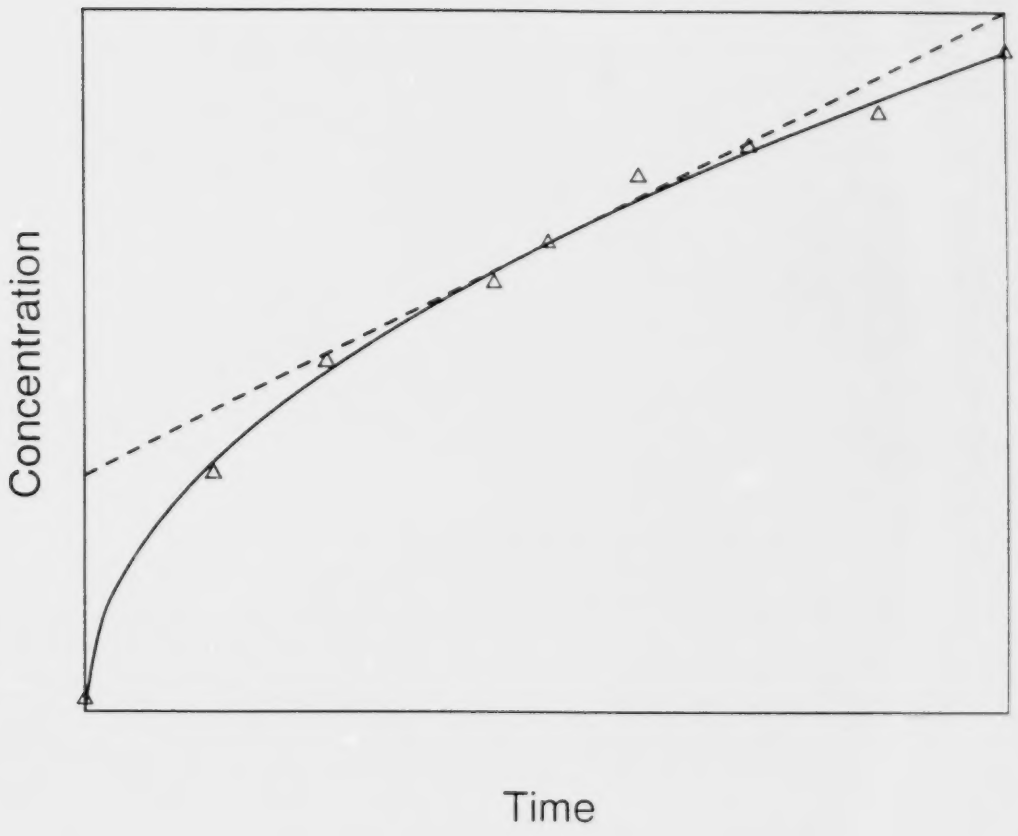

Figure 1.1: Simulated data from a batch reactor. The composition of the solution within the reactor is evaluated at various times (△). An empirical expression (solid line) is fit to the data and the rate of dissolution in a particular solution is given by the slope of the tangent to the fit curve (dashed line).

volume reactor vessel into which a reacting solution is constantly introduced. The solution in the reactor is homogenized by stirring so that the composition of the solution at the reactor outflow is the same as the composition within the reactor. The reaction rate is monitored by the composition of this outflow solution.

A plot of outflow solution composition, (A°_o), against time (Fig. 1.2) will show it changing with time, although it will tend towards a constant value. (A°) in the reactor changes according to the differential equation

$$\frac{d(A^\circ)}{dt} = \frac{d(A^\circ_o)}{dt} = \frac{1}{m}(J_i - J_o + Ar), \qquad 1.15$$

in which J_i and J_o represent the flux of A° into and from the reactor. These can be written, if the mass of solution in the reactor is not changing, as $J_i = f(A^\circ_i)$ and $J_o = f(A^\circ_o)$, in which f is the flow rate of solution through the reactor and (A°_i) is the inflow concentration. Substituting these expressions for the input and output fluxes in Eqn. 1.15 gives

$$\frac{d(A^\circ)}{dt} = \frac{f}{m}((A^\circ_i) - (A^\circ)) + \frac{Ar}{m}. \qquad 1.16$$

Eventually, (A°_o) will reach a steady state, A°_{ss}, (*i.e.* $d(A^\circ)/dt = 0$) after which time the rate of removal of reactants at the outflow will be balanced by the rate of addition of reactants by dissolution and from the input solution. Setting $d(A^\circ)/dt = 0$ and rearranging Eqn. 1.16 gives,

$$r = f\frac{(A^\circ_{ss}) - (A^\circ_i)}{A}. \qquad 1.17$$

This steady state is generally reached after about three reactor volumes of solution have passed through the reactor. This can be demonstrated by assuming that r is a constant and integrating Eqn. 1.16, to give

$$(A^\circ(t)) = ((A^\circ(0)) - (A^\circ_{ss}))\exp(-ft/m) + (A^\circ_{ss}). \qquad 1.18$$

The difference between $(A^\circ(t))$ and its steady state values will decay with a decay constant of f/m, which is the reciprocal of length of time to flow one reactor volume through the system. If the rate of reaction is not constant, and is decreasing with time, (*i.e.* if the rate of reaction in a solution containing $(A^\circ(0))$ is greater than in the steady state solution) system will tend to steady state more rapidly than this.

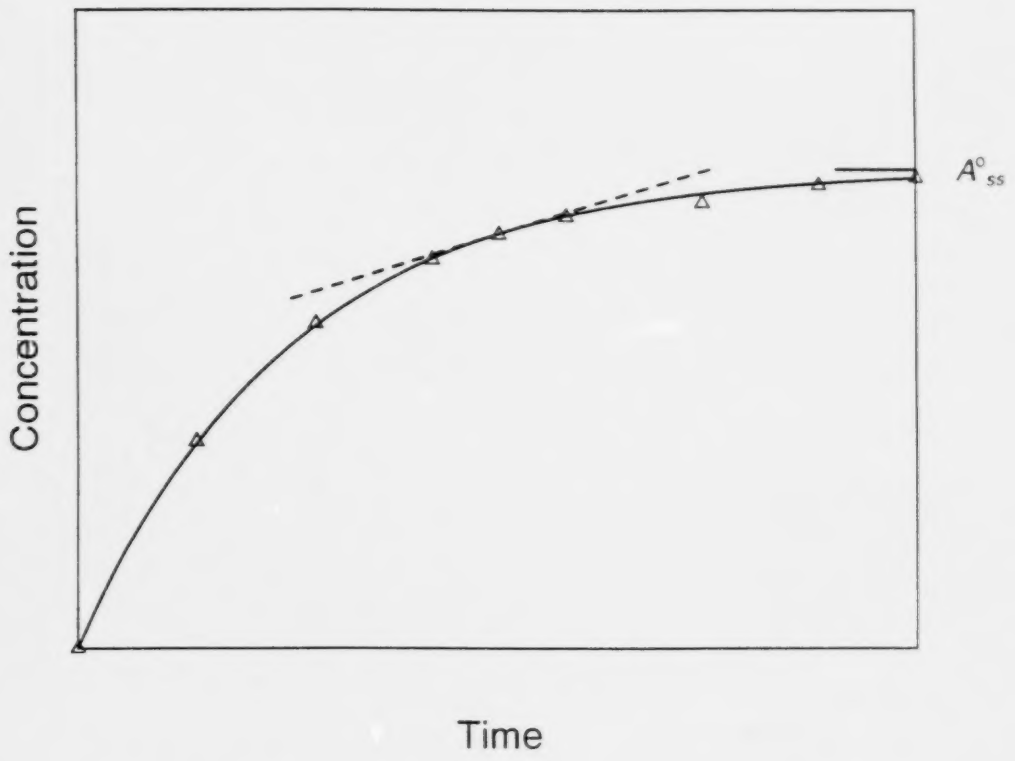

Figure 1.2: Simulated data from an open reactor. The composition of the solution within the reactor is evaluated at various times ($\triangle$) and the steady state composition (A°_{ss}) found. An empirical expression (solid line) can be fit to the data and its derivative (dashed line) can be used in Eqn. 1.19.

Equation 1.16 shows that, in contrast to closed reactors, stirred flow reactors yield direct rate information about the rate of dissolution in a solution with the steady state composition. Eqn. 1.15 can be rearranged to

$$r = \frac{1}{A}\left(\frac{d(\mathrm{A}_o^\circ)}{dt} + f((\mathrm{A}_o^\circ) - (\mathrm{A}_i^\circ))\right), \qquad 1.19$$

from which rates of dissolution in a continuous range of solution compositions can be calculated, given an accurate representation of $d(\mathrm{A}_o^\circ)/dt$.

In this study a stirred flow reactor was used to measure the rate of dolomite dissolution, since low temperature kinetic studies by Busenberg and Plummer (1982) demonstrate a change in reaction mechanism at temperatures above 45°C. This implies that any low temperature rate expressions may not be valid at higher temperatures.

Chapter 2

Experimental Designs

2.1 Introduction

The paucity of high temperature kinetic data is due, at least in part, to the relative difficulty of the required experiments. Low temperature dissolution studies rely on ion selective electrodes (*e.g.* Morse, 1974) which are, as yet, not readily available for higher temperature applications (Bourcier *et al.*, 1987). Dissolution studies also are facilitated if the hydrodynamic conditions within the reactor are known. Several experimental designs, such as a rotating disk (*e.g.* Lund *et al.*, 1975) and a slot flow cell (*e.g.* Compton *et al.*, 1989), that incorporate a known flow geometry have been developed. Space restrictions in the autoclaves limit the utility of rotating disk experiments; slot flow reactors may prove useful in future high temperature rate studies. A further problem is that the autoclaves are opaque, so that it is difficult to determine if conditions change within the reactor (*e.g.* fracture of the sample). Samples taken from the reactors must be cooled before they are analyzed, which may result in the precipitation of solids. Carbonates have retrograde solubility so this is not a concern; however, there may be degassing of dissolved CO_2 associated with the pressure drop on sampling. A final difficulty associated with high temperature rate studies is that there is a general reduction in accuracy in physical-chemical constants, specifically in the transport and thermodynamic properties, at elevated temperatures.

The vessels used in this study are stirred Parr 316 stainless steel and Hastelloy C autoclaves with 4 and 0.5 L capacity respectively. They are both rated to 5000 psi at 350°C. Figure 2.1 is a schematic drawing of these autoclaves. The diagram is of the configuration used for batch calcite experiments, but is very similar to that used for the dolomite runs. There was no crystal positioner in the autoclave used in the dolomite runs; the sample holder was simply fastened to the thermocouple well. The vapour phase was also absent in the dolomite experiments.

2.2 Calcite Experiments

2.2.1 Reactants

Optical quality cleavage rhombs of Iceland spar weighing between about 1 and 13 grams from Chihuahua, Mexico (Wards Chemical of Rochester, New York) were lightly etched in dilute HCl to clean the surfaces. A sample was dissolved in nitric acid. The resulting solution was analysed by ICP and the composition of the calcite was calculated (Table 2.1). Magnesium, at about 100 ppm, was the principal impurity. The surface area was calculated from the rhomb geometry, assuming the crystal was a perfect calcite rhombohedron. The dimensions of each crystal were measured using vernier calipers. SEM photomicrographs of a pre-run and post-run calcite surface is given in Talman *et al.* (1990). Three samples were chosen: a freshly fractured crystal, a crystal that was fractured and subsequently etched in 0.01N HCl for five minutes, and a crystal that had been used in a dissolution experiment. The fractured surfaces showed some surface roughness, which disappeared upon etching of the crystal. The surface of the dissolution experiment crystal appears unchanged from the etched crystal, with the exception of contamination by dust particles. A freshly cleaved surface was also examined on a Dektak II profilometer. Line profile scans of the crystal were made over several horizontal distances to see if the surface roughness varied with resolution. A typical tracing is shown in Fig. 2.2. The average slope at each scan length was approximately 0.05 from the horizontal. The greatest

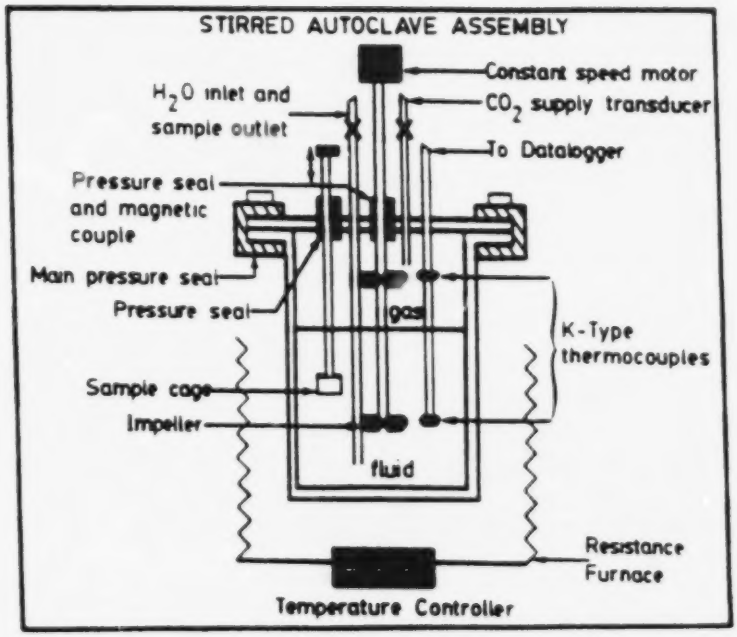

Figure 2.1: Schematic drawing of the autoclave used in the calcite dissolution experiments. The sample cage is mounted on a moveable rod to allow repositioning of the calcite during the run. With the exception of the moveable rod, the autoclave is essentially identical to that used in the dolomite experiments.

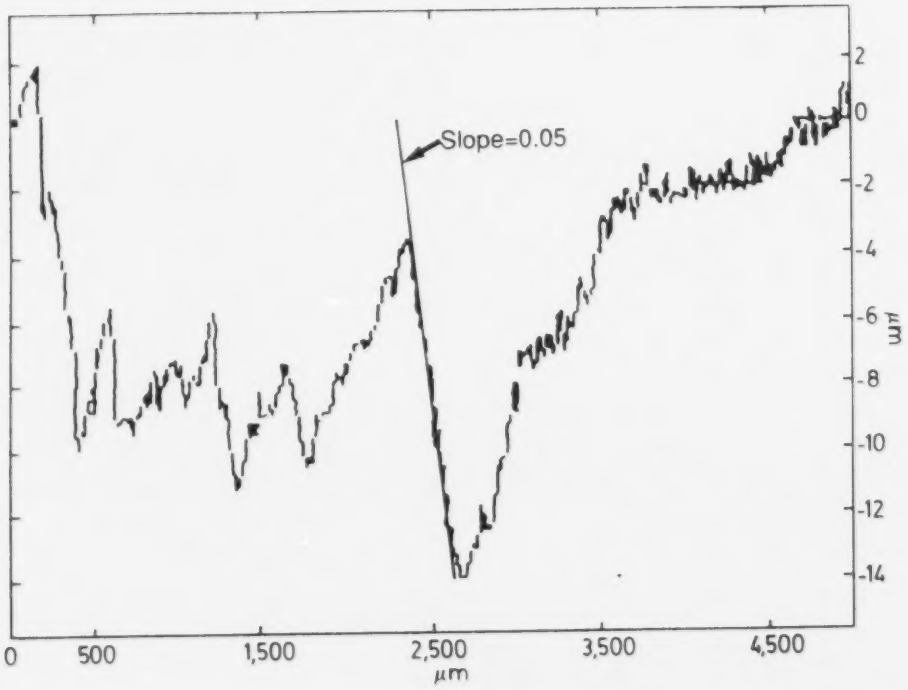

Figure 2.2: Line profile scans of Iceland Spar used in dissolution experiments produced with a Dektak II profilometer. A typical tangent to the surface and its slope are shown. Note the difference in the horizontal and vertical scales for the two scan lengths.

slope seen was 0.1. If the surface of the crystal were composed of peaks and valleys bounded by planes of slope 0.1, the surface area would only be increased by 1% compared to a perfectly flat surface; therefore, no corrections for surface roughness need be considered.

The autoclave was precharged with CO_2 and 2.0 kg of deionized water were added. A small floating piston accumulator (1 L capacity) was charged with CO_2 and water to so that an amount of CO_2 and water, equivalent to the amount removed during sampling, could be replaced in the autoclave.

2.2.2 Experimental details

The experiments were performed in a four litre Parr stirred stainless steel autoclave. Impellers affect stirring in both the gas and liquid phases (Fig. 2.1). A schematic diagram of the reactor system is shown in Fig. 2.3. Two types of crystal holder were used. Initial runs used a cage holder that surrounded the crystal, and consequently restricted the circulation of the solution near the crystal. Later runs used a holder consisting of two stainless steel wires, which reduces the interference with the fluid flow near the sample. A screw device allows the crystal to be raised or lowered during a run. Run conditions were achieved while the crystal was in the vapour. At the start of a dissolution experiment, the crystal was lowered into the aqueous phase. Samples of the solution (50 mL) in the autoclave were taken regularly through floating piston sample tubes. The floating piston ensures that there is no great pressure drop at the dip tube where the sample is removed from the autoclave, and hence no boiling. The temperature was maintained at the run temperature $\pm$ 0.2°C, except immediately after sampling, when the temperature would drop by about 2°C. A summary of the run conditions is given in Table 2.2.

The concentration of carbonic acid at run conditions could not be calculated from the initial charge of CO_2 since a small thermal gradient in the vapour made the partitioning of CO_2 difficult to predict. Consequently two samples were taken at each time interval. One sample was made basic with a 0.2 N NaOH solution to

Element	*Conc.(ppm)*	*Element*	*Conc.(ppm)*
Li	< 1.	Mn	< 1.
Na	25.	Fe	24.
K	< 3.	Al	< 6.
Mg	106.	Si	39.
Sr	37.	B	< 1.
Ba	< 1.	S	< 3.
P	22.		

Table 2.1: Chemical analysis of Iceland spar (Chihuahua, Mexico)

Experiment	t °C	Initial TIC mmoles/kg	Stirring Rate (rpm)	Surface Area cm^2	Crystal Mass (g)	Remarks
W130587	210	31.	500	4.35	1.014	crystal 1
W150987	210	38.	750	3.99	0.895	"
W271087	210	39.	750	3.80	0.774	"
W011287	210	32.	300	3.6†	0.654	"
W150288	210	36.	500	4.61	1.518	crystal 2
W250288	210	100.	500	4.40	1.396	"
W140388	210	39.	500	2.88	0.417	crystal 1
W160588	210	5.0	500	4.09	1.208	crystal 2
W310588	210	38.	750	3.92	1.145	"
W251088	150	7.1	500	17.5	13.243	crystal 3
W141288	150	7.3	350	17.5	13.042	"
W020389	100	0.	500	17.5	12848	"
W200389	100	16.5	500	17.4	12.790	"
W040489	100	0.	500	17.3	12.230	"
						0.002 molal HCl

Runs W130587 and W150987 used cage crystal holder, all other runs used wire holder.
Solution mass 2.0 kg for all the runs
† Estimated

Table 2.2: Summary of conditions for calcite experiments.

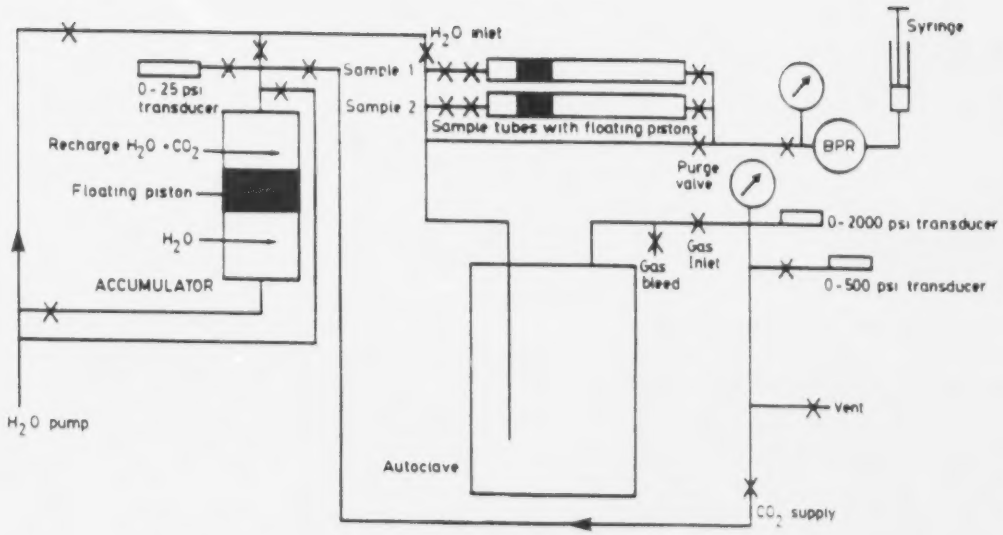

Figure 2.3: Schematic diagram of the stirred reactor system used in the calcite experiments. The back pressure regulator is denoted BPR.

fix the dissolved carbonate in solution as CO_3^{2-}. This sample was analysed for TIC (total inorganic carbon). The other sample was split. One portion was acidified and analysed for cations by ICP, and the pH and TIC were measured on the other portion after it had stabilized with respect to loss of CO_2.

2.3 Dolomite Experiments

2.3.1 Reactants

The dolomite crystals used in the study were optically clear crystals from Navarre, Spain (Wards Chemicals). The compositions of several of the dolomites were determined by dissolving them in nitric acid and analysing the resultant solution by ICP. These compositions are presented in Table 2.3.

The crystals were cleaved to remove any visible impurities and fractures. The surface areas of the resulting crystals were between about 4 and 10 cm^2. These were etched in concentrated HCl for several minutes to remove any surface features that might display anomalously high rates of dissolution.

The input solution was stored in a 10 L piston accumulator (initially 316 stainless steel, subsequently Teflonlined). The accumulator was either initially charged with a known pressure of CO_2 or volume of stock HCl solution, and subsequently filled with degassed, deionized water or else filled with deionized water, degassed and than charged with CO_2 or HCl (see Appendix).

2.3.1 Experimental details

A stirred flow reactor was constructed to study the dolomite dissolution kinetics. A schematic diagram of the system is shown in Fig. 2.3. As with the calcite experiments a Parr stirred reactor was used, but with a smaller volume. The conditions of the dolomite experiments are given in Table 2.3.

Steady state within the reactor is reached only after several reactor volumes of solution have passed through the reactor, so a relatively low volume reactor (500

Element	*Conc.*(%)	*Element*	*Conc.*(%)	*Element*	*Conc.*(%)
Mg	50.	Mg	52.	Mg	50.
Ca	48.	Ca	48.	Ca	49.
Fe	1.	Fe	$< .6$	Fe	0.7
Mn	0.1	Mn	0.1	Mn	0.1

Table 2.3: Chemical analysis of three dolomites (Navarre, Spain).

Experiment	t/°C	CO_2	HCl	Stir	Surface	Crystal
190790	150	$\surd$	•	100	4.90	crystal 1
051090	100	•	$\surd$	*nr*	3.32	"
31290	100	$\surd$	$\surd$	115	3.24	"
131290	100	$\surd$	•	*nr*	3.05	crystal 2
181290	100	•	$\surd$	100	3.01	"
290191	150	$\surd$	•	*var*	2.36	crystal 1
120291	200	$\surd$	•	*var*	2.941	crystal 2
200291	150	$\surd$	•	500	2.94	"
270291	100	$\surd$	•	*var*	2.53	"
270391	200	$\surd$	•	550	2.77	"
110591	150	*var*	•	*var*	8.4*	crystal 3
240691	200	*var*	•	500	8.00	"
90791	100	*var*	•	500	7.60	"
200991	100	•	*var*	*var*	7.68	"

Table 2.4: Summary of conditions for dolomite experiments. The run pressure was 400 psig for all 100 and 150°C experiments, and 600 psig for the 200 °C runs. * area not measured, estimated from area 240691. A $\surd$ in the column under an acid means that the input solution contained that acid, a • means that the acid was absent. A *var* in these columns means that the concentration of these acids was varied over the course of the run. *nr* – not recorded (assumed to be 100 rpm).

mL) reactor was used for these experiments. Heat losses are great in flow systems; in order to maintain a constant temperature the input solution was first warmed by the output solution in a coaxial heat exchanger. The heat exchanger consists of a piece of 0.25 in. tubing running through a $\approx$ 5 ft. length of half in. tubing that is swaged at each end by a T fitting and a drilled out half to quarter inch reducer. A description of the fittings required for such a heat exchanger is given by Callahan (1974). Also, a second autoclave was used as a preheater to further heat the input solution. With this configuration the temperature in the reactor vessel was stable to within less than 1°C, except when the flow rate was changed. Generally, any perturbations to the temperature were less than 3°C and lasted for less than one hour. A schematic diagram of the reactor system is presented in Fig. 2.4.

The crystals were suspended in the solution from the thermocouple well by a titanium or stainless steel wire sample holder similar to the second holder used in the calcite experiments.

The reactant solution was displaced from the accumulator at a constant flow rate by a positive displacement pump. A single pump with 1 L capacity was used for some early runs, but this required frequent interruptions of flow while the pump was refilled. Subsequently, a second 2 L pump was used in conjunction with the 1 L pump which resulted in a much more continuous flow. Most experiments involved keeping all experimental conditions constant except the flow rate which was changed after steady state samples were taken. The last few experiments involved changing the input solution while keeping the flow rate roughly constant. In these experiments the input composition of the solution was changed by connecting what is essentially a pistonless sample tube (PST) containing a known amount of gaseous CO_2 (quantity determined by weight) or HCl (known volume of known concentration) to the accumulator and circulating its contents through the accumulator at near system pressure with a rapid flow gear pump. The flow goes from the bottom of the accumulator up a nylon dip tube, through the pump and the PST and back to the top of the accumulator. This flow mixes the solution within the accumulator. The composition of the input solution

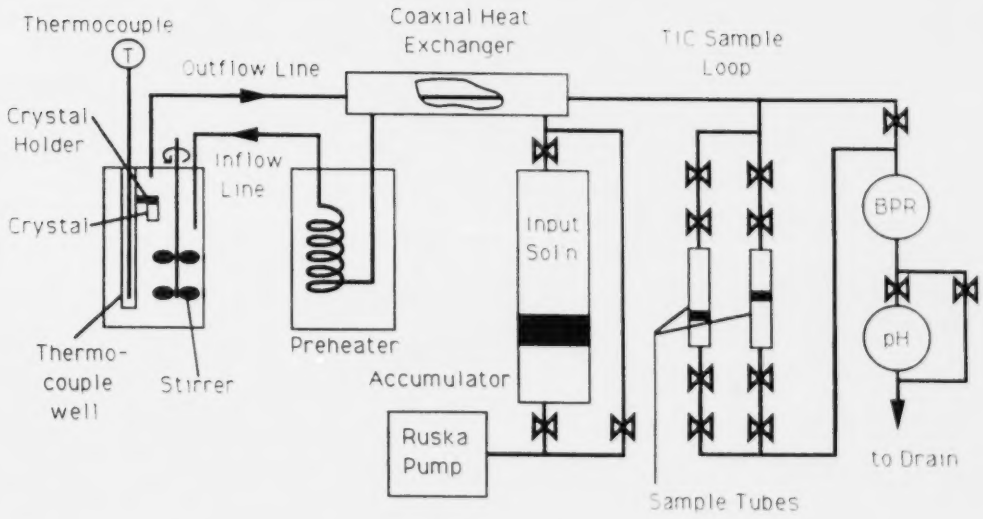

Figure 2.4: Schematic diagram of the stirred reactor system used in the dolomite experiments. The coaxial heat exchanger is shown with a cut-away section.

was determined by analysing the contents of the PST after this mixing.

A pH meter was placed on line, just after the back pressure regulator to provide a continuous monitor of the solution. There was some CO_2 evolution, the bubbles causing some noise in the pH measurement. There was no temperature correction on the pH meter.Generally the temperature was between 22 and 27°C. The attainment of steady state was assessed by the stability of the pH measurement. Samples from the outflow were taken for cation analysis by ICP. Carbonate samples were taken in the same manner as described in section 2.2.2. Further experimental details are given in the second section of the Appendix.

Chapter 3

Experimental Study of Calcite Dissolution Kinetics under Hydrothermal Conditions

3.1 Introduction

The kinetics of dissolution and precipitation of calcite have been studied extensively below 100°C. Reviews are presented by Plummer *et al.* (1979), Morse (1983), and Inskeep and Bloom (1985). These rate studies used several different experimental setups, each chosen to elucidate separate aspects of the dissolution reaction. In the simple Ca–CO_2–H_2O system at temperatures below 80°C, calcite dissolution kinetics has been found to be dependent on pH, p_{CO_2} and on the transport conditions in the reaction vessel (PWP; Herman, 1982; Rickard and Sjöberg, 1983; Compton and Daly, 1984). Several rate laws have been used to interpret the kinetic data; House (1981), Morse (1983) and Compton and Daly (1987) discuss the relative merits of these equations.

There are no rate data for calcite at temperatures above 100°C. Rates of dissolution of calcite were measured in a batch reactor at 100, 150 and 210°C at a variety of partial pressures of CO_2. Since there are several expressions which describe calcite dissolution rates at lower temperatures, the integrated rate data obtained from a batch reactor can be utilised (see Section 1.2.5). Integrated forms of the low temperature rate expressions can be fit to the experimental data obtained from a batch

reactor to test the validity of the expression. The batch reactor described in Chapter 2 was used for these experiments.

3.2 Experimental Results

A summary of the experimental conditions was given in Table 2.3. The raw data collected are presented in the first section of the Appendix (Table A.1). Plots of calcium *vs.* elapsed time for these experiments are shown in Fig. 3.1. As expected, the aqueous calcium concentration increases steadily with time, reaching a maximum value as equilibrium is approached. The curves in Fig. 3.1 will be discussed later (Sec. 3.3.2).

3.2.1 Solution Composition

The concentrations of calcium and carbon in the solution were used to calculate the distribution of species and the saturation index (Ω ($= [Ca^{2+}][CO_3^{2-}]\ /K_{sp}$)) at run conditions. The calculation involves solving the mass balance equations for Ca and TIC, subject to mass action and charge balance constraints. The dissociation constants (*e.g.* K_{AX} =[A][X]/[AX]) for the aqueous complexes and the solubility product of calcite were taken from the SOLMINEQ.88 data base (Kharaka *et al.*, 1988; Table 3.1).

The pH values of some quenched samples were measured. This pH was not stable since significant quantities of CO_2 evolved continuously from these samples. Eventually the pH would stabilize, after which the solution was made basic and analysed for TIC. The pH of a solution containing this measured (low) TIC and Ca could be calculated and compared with the measured pH, using charge balance as a restriction. The calculated and measured pH values were generally in agreement. However, in the case of disagreement, the results obtained from the quenched sample were generally disregarded, since it was felt there was a greater potential for errors associated with this sample.

A possible error in all calculations which use the charge balance equation arises from incomplete solution analyses. In the results presented here no cations other than Ca^{2+} and H^+ were used in the charge balance calculation; however, these were the dominant cations in virtually all of the samples. Some of the initial samples had relatively high iron contents (see Appendix), which quickly plated out on the autoclave.

3.2.2 Solubility Product of Calcite

The dissociation constant of the complex $CaHCO_3^+$ was reduced from the value in the SOLMINEQ.88 data base. If it was not decreased, the calculated saturation index, Ω, was still considerably less than 1.0 at the end of the experimental run. Reducing the value of $K_{CaHCO_3^+}$ frees up some of the complexed calcium and increases Ω at the end of the experimental run to near one. Thus, these results suggest that the complex $CaHCO_3^+$ is less stable in hydrothermal solutions than reported in the SOLMINEQ.88 data base. Plummer and Busenberg (1982) present low temperature solubility data of calcium carbonates that are more consistent with a lower value of $K_{CaHCO_3^+}$ than is in the SOLMINEQ.88 data base. Fein and Walther (1987) also concluded this complex was not very stable in supercritical H_2O – CO_2 solutions. Values of the ion activity product Q ($= K_{sp}\Omega$) calculated from the data collected at the end of the 210°C runs varied between 2.7×10^{-12} and 3.8×10^{-12}, and were, on average only slightly higher (3.3×10^{-12}) than the value of K_{sp} in the SOLMINEQ.88 data base of 2.9×10^{-12}.

Initial runs (not reported here) were performed without replacing the solution lost from the system during sampling, which caused CO_2 to evolve into the, increasingly large, vapour filled volume. Consequently, the solution was depleted in CO_2 through the run, which lead to calcite precipitation late in the run. In one run, dissolved calcium and TIC decreased by 7% and 25% respectively; however, Q maintained a near constant value between the previously mentioned limits. This demonstrates that calcite is stable in a solution at 210°C when $[Ca^{2+}][CO_3^{2-}]$ is near 3×10^{-12}.

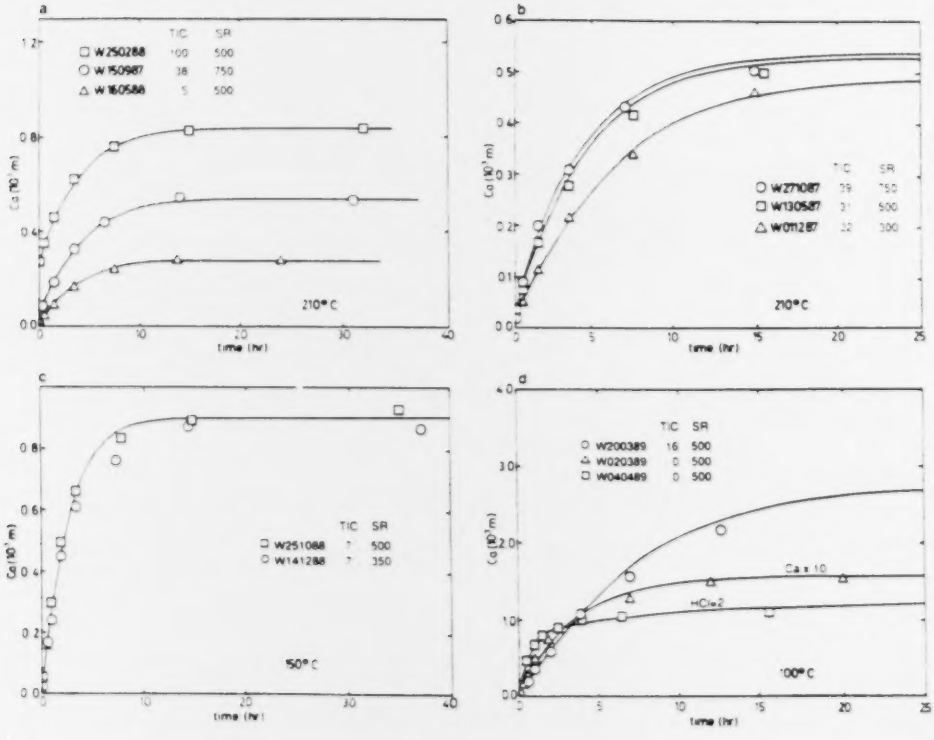

Figure 3.1: Aqueous calcium concentration (millimoles/kg) versus elapsed time (hours) for dissolution experiments at 100, 150 and 210°C. Curves were fit according to the rate expression of Plummer *et al.* (1978) using the rate constants listed in Table 3.2 with the exception of the upper and lower curves in (b) where values of $\log(k_1^C)$ used differ from the value in Table 3.2 by 0.15 and -0.58 respectively. The run conditions are shown in the figure, stirring rate is abbreviated as SR and concentration units of TIC and HCl are millimoles/kg.

3.3 Data Reduction

3.3.1 Rate Laws

Several empirical rate laws have been fit to calcite dissolution data (see Morse, 1983). Most of the rate laws are based on Ω, and are of the form:

$$r = k(1 - \Omega^n)^m$$

where n and m are fit parameters. To test this rate law, the reaction rate was evaluated by numerically differentiating the calcium concentration *vs.* time curve using a second degree interpolating polynomial. The rate was plotted in Fig. 3.2 as a function of Ω for runs at 210°C and three different p_{CO_2}'s. Errors associated with the calculated initial rate are about 10% . The uncertainty in Ω is large; as discussed earlier, the average value of the solubility product calculated here is 15% greater than the value of K_{sp} used to calculate Ω. Ω is the product $[Ca^{2+}]$, which is calculated by SOLMINEQ.88 from the input solution composition, and $[CO_3^{2-}]$, which is not measured but calculated from a charge balance equation. As a consequence $[CO_3^{2-}]$ is sensitive to errors in both the measured TIC and Ca, and the error in $[CO_3^{2-}]$ will be in the same sense as the error in Ca (*i.e.* if the concentration of Ca is over–estimated the calculated $[CO_3^{2-}]$ will also be over–estimated). Therefore, the error in Ω is likely $\pm$ 15%. The apparent dissolution of calcite in supersaturated solutions is a consequence of these errors. All the data should fall along the same curve if the rate is dependent solely on Ω. Although the errors are relatively large, this is clearly not the case; therefore, any rate law simply based on Ω is inadequate. Figure 3.2 demonstrates a dependence of the rate on p_{CO_2} that cannot be described solely in terms of Ω.

The stirring rate dependence of the rate of calcite dissolution is well documented (Lund *et al.*, 1975; Plummer *et al.*, 1978; 1979; Compton and Daly, 1984, Chapter 4). Fig. 3.1 presents raw data, these data are not normalized to surface area. The surface areas associated with the various data sets are different, so the dissolution

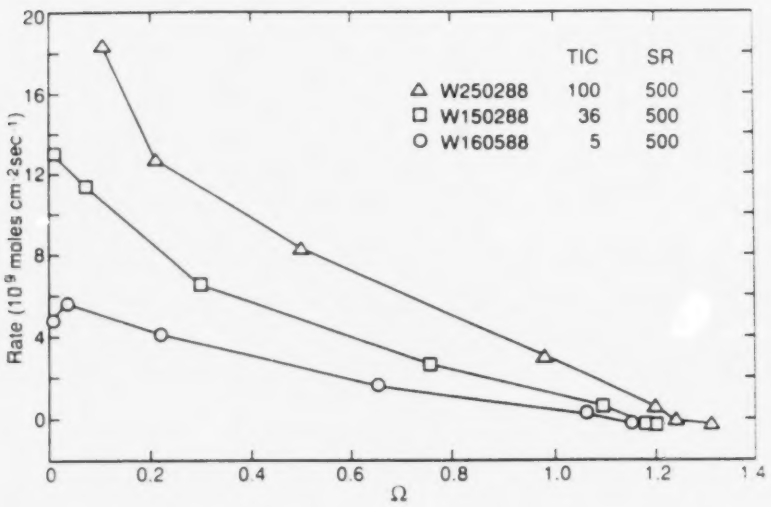

Figure 3.2: Dissolution rate (10^{-9}moles cm^{-2} s^{-1}) plotted against Ω for three runs at various values of p_{CO_2} at a constant stirring rate (SR).

rates between different runs cannot be directly from this plot without considering this normalization. Stirring rate dependence is demonstrated because the curves fit to the data are based on stirring rate dependent values of k_1^C (see below).

PWP separated the effects of both p_{CO_2} and H^+ on the rate of calcite dissolution. Their rate expression is

$$\frac{dCa}{dt} = k_1^C[H^+] + k_2^C[H_2CO_3] + k_3^C[H_2O] - k_4^C[Ca^{2+}][HCO_3^-] \qquad 3.1$$

in which k_1^C - k_4^C are rate constants. This rate law is developed by assuming that calcite dissolution proceeds by three simultaneous reactions:

$$CaCO_3 + H^+ \rightarrow Ca^{2+} + HCO_3^- \qquad 3.2$$

$$CaCO_3 + H_2CO_3 \rightarrow Ca^{2+} + 2HCO_3^- \qquad 3.3$$

and

$$CaCO_3 + H_2O \rightarrow Ca^{2+} + HCO_3^- + OH^-. \qquad 3.4$$

Plummer *et al.* (1978; 1979) derived Eqn. 3.1 from a mechanistic model of dissolution. The forward rate of reaction 3.2, $k_1^C[H^+]$, is limited by the rate of transport to the calcite surface, so that k_1^C is dependent on stirring rate. As the stirring rate is increased, k_1^C should increase until it reaches $K_{eq,1}$ / k_{-1}^C where $K_{eq,1}$ is the equilibrium constant for reaction 3.2, and k_{-1}^C is the rate constant for the back reaction. PWP grouped the rate for all three back reactions into one term involving k_4^C; however, in order to do this they had to introduce a p_{CO_2} dependence into k_4^C. Although this is not necessary since the forward and backward rate constants for elementary reactions are related to the equilibrium constant (see Lasaga, 1981), it is convenient for the retrieval of the rate constants. The expression PWP derived for k_4^C is

$$k_4^C = \frac{K_2}{K_{sp}}\left(k_1^{C\prime} + \frac{1}{[H_{(s)}^+]}\left[k_2^C[H_2CO_3] + k_3^C[H_2O]\right]\right) \qquad 3.5$$

where $k_1^{C\prime}$ is the limiting value of k_1^C at infinite stirring rate, and $[H_{(s)}{}^+]$ is the activity of hydronium at the crystal surface. An assumption made by PWP is that $[H_{(s)}^+]$ can

be approximated by the equilibrium value of $[H^+]$ in the system. In this case, its value is generally sufficiently small to ensure that $k_1^{C\prime}$ is negligible compared to the second term in the parentheses.

3.3.2 Evaluation of Rate Constants

The calculated speciation can be used to evaluate rate constants for the Plummer rate expression. Extracting the forward rate constants for reactions 3.2 - 3.4 from the batch reactor data requires either integrating the proposed rate expression or numerically calculating derivatives using the concentration data. The rate obtained by differentiation is very sensitive to errors in the solution analysis, so the rate law was integrated.

The complexity of the rate law requires that a simplification be introduced in order to make it possible to obtain a closed form solution to the rate equation. The activity of the aqueous species in Eqn. 3.1 (except Ca^{2+}) at any time, t, between sampling times t_1 and t_2 was estimated by a linear extrapolation of their activity, so that the various activity terms in Eqn. 3.1 can be written

$$[X(t)] = \frac{[X(t_2)] - [X(t_1)]}{t_2 - t_1}(t - t_1) + [X(t_1)], \qquad 3.6$$

in which $t_1 < t < t_2$. In this case Eqn. 3.1 becomes

$$rate = \frac{M}{A}\frac{dCa}{dt} = (C_1 + D_1 t)\,Ca + C_2 + D_2 t \qquad 3.7$$

where Ca is the concentration (molal) of calcium in solution, A and M are the surface area of the crystal and the solution mass respectively and

$$C_1 = k_4^C \left[f_{Ca}(t_1)\,[HCO_3^-(t_1)] - \frac{f_{Ca}(t_2)\,[HCO_3^-(t_2)] - f_{Ca}(t_1)\,[HCO_3^-(t_1)]}{t_2 - t_1} t_1 \right]$$

$$D_1 = k_4^C \left[\frac{f_{Ca}(t_2)\,[HCO_3^-(t_2)] - f_{Ca}(t_1)\,[HCO_3^-(t_1)]}{t_2 - t_1} \right]$$

$$C_2 = k_1^C \left[[H^+(t_1)] - \frac{[H^+(t_2)] - [H^+(t_1)]}{t_2 - t_1} t_1 \right]$$

$$+k_2^C\left[[\mathrm{H_2CO_3}(t_1)]-[\frac{\mathrm{H_2CO_3}(t_2)]-[\mathrm{H_2CO_3}(t_1)]}{t_2-t_1}t_1\right]$$
$$+k_3^C\left[[\mathrm{H_2O}(t_1)]-\frac{[\mathrm{H_2O}(t_2)]-[\mathrm{H_2O}(t_1)]}{t_2-t_1}t_1\right]$$

and

$$D_2 = k_1^C\frac{[\mathrm{H^+}(t_2)]-[\mathrm{H^+}(t_1)]}{t_2-t_1}+k_2^C\frac{[\mathrm{H_2CO_3}(t_2)]-[\mathrm{H_2CO_3}(t_1)]}{t_2-t_1}+$$
$$k_3^C\frac{[\mathrm{H_2O}(t_2)]-[\mathrm{H_2O}(t_1)]}{t_2-t_1}$$

and f_{Ca} relates the total dissolved Ca to $[\mathrm{Ca^{2+}}]$ (*i.e.* it incorporates both $\gamma_{\mathrm{Ca^{2+}}}$ and the distribution of Ca between the various Ca bearing species) and it is assumed to be the same for the fit and experimentally evaluated calcium concentration. Despite the approximations made in integrating the rate expression, it should be more accurate than the alternative approach of differentiating expressions fit to the concentration data, since it uses requires one less calculated quantity (dCa/dt).

Activity coefficients, γ_i were calculated using the expression

$$\log\gamma_i=\frac{-A(T)Z_i^2\sqrt{\mathrm{I}}}{1+\mathring{a}_i\,B(T)\sqrt{\mathrm{I}}}+B^{\bullet}(T)\mathrm{I} \qquad 3.8$$

(Helgeson, 1969), where I is the ionic strength, Z_i is the ionic charge, and $\mathring{a}$ is an ion size parameter. A and B are related to the density, ρ (g cc^{-1}), and dielectric constant, ϵ, of water by

$$A(T)=\frac{1.82\times10^6\sqrt{\rho}}{(\epsilon T)^{3/2}} \qquad 3.9$$

and

$$B(T)=\frac{50.3\times10^8\sqrt{\rho}}{\sqrt{\epsilon T}} \qquad 3.10$$

(Helgeson, 1969) and $B^{\bullet}$ is listed in Table 3.1. The contribution of the $B^{\bullet}$ term to the activity coefficient is small for all the samples. Based upon the linear approximation, Eqn. 3.1 can be integrated to give

$$\mathrm{Ca}(t) = \exp\left[-\frac{D_1}{2}\left(t_1^2-t^2\right)+C_1(t_1-t)\right]\left[\mathrm{Ca}(t_1)-\frac{D_2}{D_1}\right]+$$

$$\frac{D_2}{D_1} + \sqrt{\frac{2}{D_1}}\left(C_2 - \frac{D_2 C_1}{D_1}\right)\left[\mathrm{Daw}\left(\sqrt{\frac{D_1}{2}}t + \frac{C_1}{\sqrt{2D_1}}\right)\right.$$
$$\left. - \exp\left[-\frac{D_1}{2}\left(t_1^2 - t^2\right) + C_1\left(t_1 - t\right)\right]\mathrm{Daw}\left(\sqrt{\frac{D_1}{2}}t_1 + \frac{C_1}{\sqrt{2D_1}}\right)\right] \quad (3.11)$$

where Daw refers to the Dawson integral

$$\mathrm{Daw(x)} = \exp(-\mathrm{x}^2)\int_0^{\mathrm{x}} \exp(\mathrm{y}^2)\mathrm{dy}. \qquad 3.12$$

Equation 3.11 relates the concentration of calcium at time t_{i+1} to the concentration at time t_i (and, by recursion, to its initial concentration) and the activities of the other species appearing in 3.1. It is linear in C_2 and D_2 and non-linear in C_1 and D_1, and therefore, it is linear in the three constants k_1^C -k_3^C and non-linear in k_4^C. Consequently, given a k_4^C, values of k_1^C - k_3^C that minimize the expression $\sum_i(\mathrm{Ca}(t_i)' - \mathrm{Ca}(t_i))^2$, where $\mathrm{Ca}(t_i)'$ is the value from 3.11, can be calculated. Several values of k_4^C were tried in order to obtain the one that gave lowest deviation from the data. It is also possible to fit the entire curve with an additional constant, [Ca(0)]; however, with the approximations already made, it is unlikely to provide a superior fit. Values of k_1^C and k_4^C were in fair agreement for different runs at the same stirring rate and p_{CO_2}; however, values of k_2^C and k_3^C were not consistent. This is because neither $[H_2O]$ nor $[H_2CO_3]$ change very much during a given run, so these parameters are very sensitive to small changes in $[H_2CO_3]$ through the run (or random errors in the TIC data). However, the sum $(k_3^C + k_2^C[H_2CO_3])$ is relatively insensitive. Therefore, the values for k_2^C and k_3^C were evaluated from pairs of experiments at different carbonic acid activities ($[H_2CO_3]_{(1)}$ and $[H_2CO_3]_{(2)}$). The net contribution to the rate by water and carbonic acid $(k_3^C + k_2^C[H_2CO_3])$ should be the same with the new constants k_2^C and k_3^C as with the calculated values $k_{2,(1)}^C$, $k_{3,(1)}^C$, associated with $[H_2CO_3]_{(1)}$ and $k_{2,(2)}^C$ and $k_{3,(2)}^C$ associated with $[H_2CO_3]_{(2)}$, so that

$$k_3^C + k_2^C[H_2CO_3]_{(1)} = k_{3,(1)}^C + k_{2,(1)}^C[H_2CO_3]_{(1)}$$

and

$$k_3^C + k_2^C[H_2CO_3]_{(2)} = k_{3,(2)}^C + k_{2,(2)}^C[H_2CO_3]_{(2)}.$$

These equations are solved for k_2^C and k_3^C. Figure 3.1a demonstrates that the values calculated in this manner are consistent with data from a run at a third p_{CO_2}.

Figure 3.3 shows the solution compositions where the contributions from each of the three forward reactions are dominant at 210°C. The reason that the initial pH of the high p_{CO_2} run (W250288) is greater than the initial pH of the, lower p_{CO_2}, run W150288 is that there was a considerable reaction between the crystal and condensate in W250288 (see also Fig. 3.1). The values of the rate constants used to develop this plot and Fig. 3.1 are given in Table 3.2. As was noted earlier k_1^C is stirring rate dependent, the values of k_1^C in Table 3.2 are based on data obtained at a stirring rate of 500 rpm. The initial and final solution compositions of three runs at different p_{CO_2}'s are also shown in Fig. 3.3. Each of the three rate terms predominate for at least a portion of one of the runs. The confidence in the estimates of the rate constants is roughly related to the number of points in each area; the rate constant, k_1^C is the least well defined.

A single experiment was performed at 100°C with a starting solution containing 2 $\times 10^{-3}$ molal HCl, which defines the value of k_1^C very well at the run conditions. This experiment was not performed at other temperatures due to the corrosive nature of the initial solutions.

The curves in Fig 3.1 were calculated by numerically integrating Eqn. 3.1 using the rate constants in Table 3.2, except where noted in the figure caption. This integration requires the initial Ca concentration and, for those runs with an applied p_{CO_2}, the total dissolved carbonate in solution (approximately constant through the run). The total carbonate in the runs without an applied p_{CO_2} changed appreciably through the run, so a temperature dependent parameter, β (the ratio of H_2CO_3 in solution to the mass of CO_2 in the vapour), was introduced to simulate the partitioning of CO_2 between the solution and vapour, and a mass balance on carbonate was included in the calculations. A value of β that fit the measured TIC values was calculated. The input data (the initial conditions) defines the initial solution speciation and, from Eqn. 3.1, the initial rate of calcite dissolution. This rate is used to calculate

t/°C	$\log K_1$	$\log K_2$	$\log K_w$	$\log K_{CaCO_3^\circ}$	$\log K_{sp}$	B•
100.	−6.43	−10.16	−12.26	−4.17	−9.27	0.046
150.	−6.77	−10.39	−11.64	−4.67	−10.16	0.047
210.	−7.30	−10.87	−11.20	−5.60	−11.53	0.045

Table 3.1: Values of thermodynamic constants used in the calculations. K_1 and K_2 are the first and second dissociation constants of carbonic acid (*i.e.* $K_1 = [H^+][HCO^-]/[H_2CO_3]$, K_w is the dissociation constant of water, and $K_{CaCO_3^\circ}$ is the dissociation constant for $CaCO_3^\circ$. The dissociation constant for $CaHCO_3^+$ was set to −1.0 for all temperatures. The values of the dissociation constants were from the SOLMINEQ.88 data base (Kharaka *et al.*, 1988). $B^\bullet$ (Helgeson, 1969) is used in Eqn. 3.8.

	Rate constants (moles cm^{-2} s^{-1})					
	This work			Extrapolated		
t/°C	$\log k_1^C$	$\log k_2^C$	$\log k_3^C$	$\log k_1^{C,ext}$	$\log k_2^{C,ext}$	$\log k_3^{C,ext}$
100.	−4.8	−6.3	−9.0	−4.0	−6.0	−8.8
150.	−4.1	−6.2	−8.6	−3.9	−5.3	−8.2
210.	−3.3	−7.1	−8.2	−3.7	−4.7	−7.7

Table 3.2: Comparison of the results of this work with values extrapolated from the Arrhenius fit given by Plummer *et al.* (1978). These equations are $\log k_1^{C,ext}$ = -2.802 - 444/T, $\log k_2^{C,ext}$ = -0.16 -2177/T , and $\log k_3^{C,ext}$ = -4.10 - 1737/T.

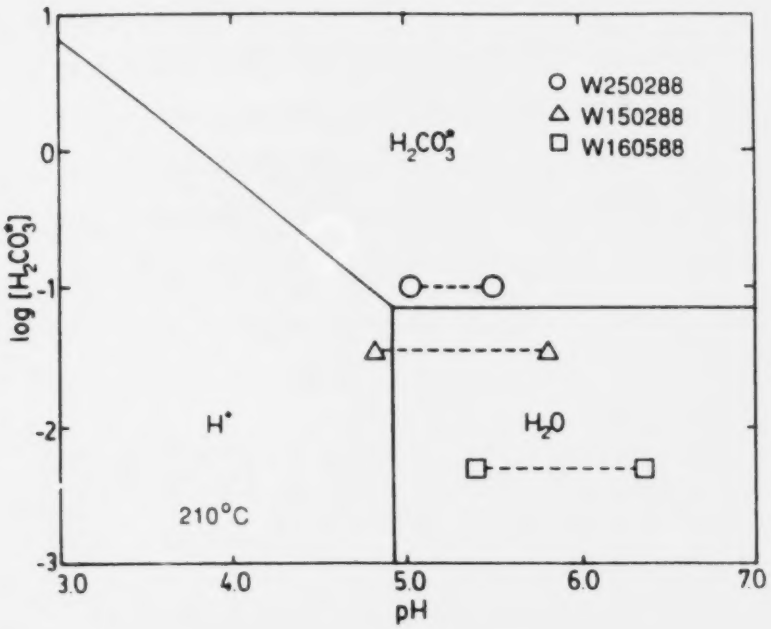

Figure 3.3: The initial and final solution hydronium and H_2CO_3 activities from three runs at 210°C and different p_{CO_2}'s are shown in this figure connected by dashed lines. The solid lines divide the plot into regions where each of the three forward reactions make the dominant contribution to the net forward rate at this temperature.

how much calcium will be added to the solution during a given time interval, after which the solution composition and dissolution rate are recalculated. This is repeated until the solution becomes saturated. The agreement between these curves and the data is very good, with the exception of some intermediate points in the two lower temperature runs; however, the fit in the region where the rate of the back reaction is small is much better. The discrepancy between the predicted and fit values may be due to an incorrect expression for the back reaction. A similar discrepancy between the observed rate and the rate predicted by Eqn. 3.1 in intermediate saturations was noted in batch reactor data presented in Compton and Daly (1987). Busenberg and Plummer (1986) and Chou *et al.* (1989) use a rate expression very similar to Eqn. 3.1 to describe the rate of dissolution of several single component carbonates, but with different expressions for the back reactions. Some factors affecting the expression for the back reaction will be discussed in Chapter 4.

Errors in the 210°C points were estimated by a Monte-Carlo type calculation in which the initial calcium and TIC values were varied by random errors of less than 5% . Two of the rate constants k_1^C, k_2^C, and k_3^C were held constant and the third constant and k_4^C were calculated using the regression calculation described previously. After about fifty calculations the mean and standard deviation of the k values were calculated. These standard deviations were generally within 15% of the mean.

3.3.3 Temperature Dependance

PWP studied calcite dissolution kinetics as a function of solution composition for temperatures between 0 and 60°C. They fit their measured rate constants with an Arrhenius relationship,

$$\log k_i^C = a_i - \frac{b_i}{T} \qquad 3.13$$

where T is the temperature in K. The values of a_i and b_i reported by PWP are also given in Table 3.2, and rate constants calculated from Eqn. 3.13 are also given at the run temperatures. The rate constants found in this study are shown on an Arrhenius plot in Fig. 3.4, together with the temperature dependence reported by PWP. The

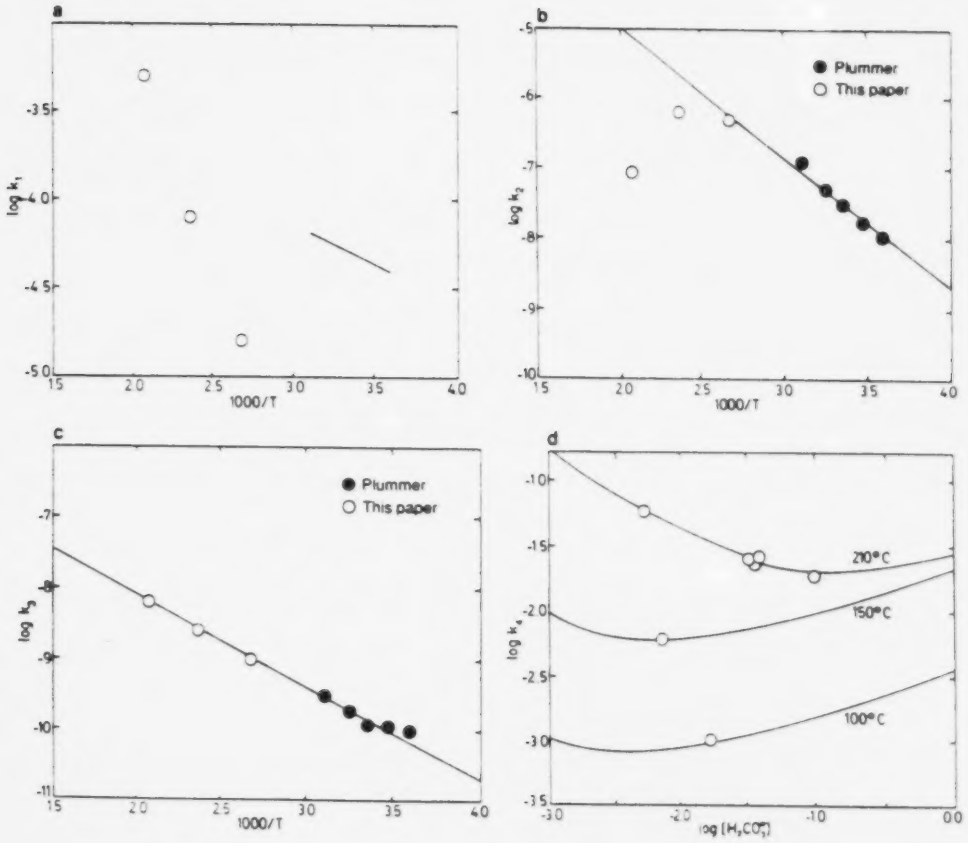

Figure 3.4: Arrhenius plots of the rate constants k_1^C, k_2^C and k_3^C (in moles cm^{-2} s^{-1} are shown in figures 7a, 7b, and 7c with Plummer's rate constants from 5 to 60°C and the rate constants reported here at 100, 150, and 210°C. Figure 7d shows the fit values of k_4^C from several runs. The curves show the values of k_4^C predicted by Eqn. 9.

logarithms of the rate constants k_2^C and k_3^C at 100°C presented here are about 0.25 lower than the extrapolated values; this discrepancy is not inconsistent with errors in surface area estimates or differences in defect densities (Schott *et al.*, 1989; Chou *et al.*, 1989; see also Chapter 4). Chou *et al.* (1989) also found discrepancies of a similar magnitude between their calcite dissolution rate data and those given by PWP. The expression by PWP for k_3^C above 25° extrapolates relatively well to the values reported here; however, the behavior of k_1^C and k_2^C with temperature is more complex. The value of k_2^C at 100°C is essentially co-linear with the low temperature data; however, the slope of the curve decreases as the temperature increases to such an extent that the slope of the curve is negative at 210°. The values of k_1^C obtained here show an irregular behaviour with temperature. For reasons described above, the value of k_1^C is the least well defined by these experiments, with the exception of the 100° datum. This value is considerably lower than the value fit from the low temperature data, even if the value is increased by a factor of two on the assumption that there is discrepancy due to surface area or crystal features. PWP observed variations in the value of k_1^C by a factor of about 1.5 by changing the stirring rate. The runs described here were done at lower stirring rates, but, perhaps more importantly, on a much bigger crystals. Flow across the surface of these larger crystals will be less turbulent than the flow across smaller grains used in the low temperature studies. Until it is possible to perform the higher temperature experiments in more acidic solutions under known hydrodynamic conditions, it will be difficult to evaluate k_1^C. Figure 3.4d plots the values of k_4^C evaluated here along with the values calculated from Eqn. 3.5 at the three run temperatures.

The decrease in k_2^C at temperatures above 150°C is almost certainly due to the decrease in calcite solubility with temperature. In Chapter 1 an expression for the rate dependence of a diffusion limited reaction (Eqn. 1.11) was developed

$$\frac{d \log r}{d(1/RT)} = -E_D + \Delta H^\circ.$$

The assumptions made in deriving Eqn. 1.11 are not valid for the case of calcite dissolution; however, the retrograde nature of the dissolution reaction must be, at

least partially, responsible for the anomalous behaviour of the rate constants. Further results dealing with the consequences of transport control on the reaction rate will be presented in the next chapter.

3.4 Conclusions

The rate of calcite dissolution from ambient to temperatures in excess of 200°C depends on temperature, flow rate, and pressure of CO_2 and is well described by the rate law proposed by PWP. The value of k_1^C is poorly constrained by these experiments except at 100°C at a stirring rate of 500 rpm where a quantity of acid was added at the start of the experiment. The temperature dependence of k_2^C is anomalous; it has a maximum near 150°C. This is a clear indication of a change in reaction mechanism, although the linear dependence of the rate on $[H_2CO_3]$ appears to remain. It is likely that both reactions 3.2 and 3.3 are diffusion limited at elevated temperatures, and the behaviour of k_2^C likely reflects the increased importance of transport properties in limiting the reaction rate. The variation of rate constant, k_3^C, with temperature is consistent with the variation noted at lower temperatures by PWP. The activation energy associated with k_3^C is about 24.7 kJ mole^{-1}.

Chapter 4

Mixed Kinetic Control of Calcite Dissolution

4.1 Introduction

This chapter explores the consequences of transport control in the rate expression proposed for calcite dissolution by PWP including a full treatment of the diffusion of solutes in the solution immediately adjacent to the dissolving grain. The model was developed to explore why the PWP model (which was developed using the assumption that the reaction is surface reaction controlled) works in a system that is, at least partially, transport controlled system. This treatment differs from others in the literature in including both the coupling of diffusion coefficients (see below) and an expression for the rate of the surface reaction driving the diffusive flux based on the observations presented by PWP. Many previously published models predict very large pH shifts around the dissolving grains (*e.g.* Sjöberg and Rickard, 1984a). If such shifts in pH occur it is surprising that the rate expression proposed by PWP should work, since such models predict that the solution chemistry adjacent to the grain is completely different than the composition used in the rate expression. Although the temperature dependence of the diffusion coefficients and stability constants of common ion pairs found in basic $CaCO_3$ solutions is poorly known at temperatures other than 25°C, calculations were also performed using estimated parameters to model calcite dissolution at 150°C.

Calcite dissolution kinetics is stirring rate dependent in most acidic solutions at 25°C (Sjöberg and Rickard, 1983); however, the reaction is not strictly limited by diffusion (see section 1.2.1) in the sense that the solution at the solid/solution interface is neither in equilibrium, nor close to equilibrium, with calcite. This has been demonstrated by: the variation of reaction rate with strain energy (see below); dissolution rates tend to be independent of stirring rate in solutions with high p_{CO_2} (PWP); and the formation of pits on etched calcite surfaces. The presence of etch pits is commonly cited as evidence that a reaction is not diffusion controlled (see Chapter 1). Furthermore, the morphology of etch pits formed on calcite surfaces in concentrated organic acid solutions is dependent on the type of acid used to etch the surface (Keith and Gilman, 1960) and the optical activity of the acid. This indicates that the driving force of the reaction is dependent on properties of the solution more complex than simply the degree of undersaturation. Finally, Schott *et al.* (1989; also Ferret *et al.*, 1987) demonstrate that, at least in solutions with a pH greater than 4.5, the increase in the rate of dissolution of calcite associated with an increase in the dislocation density of the crystal is greater than can be attributed simply to the increase in solubility associated with the strain energy.

Despite these observations it has been clearly demonstrated in series of papers by Sjöberg and Rickard (Sjöberg and Rickard, 1983; 1984a) that the rate of dissolution of calcite is proportional to the inverse square root of disc rotation rate in acidic solutions (pH < 4). Eqn. 1.4 ($J_D = \frac{D_{A^\circ}}{\delta}((A^\circ_s) - (A^\circ_b))$) relates the diffusive flux to a characteristic length, δ, which is related to the angular velocity of a rotating disc, ω, by:

$$\delta = 1.61 D^{1/3} \nu^{1/6} \omega^{-1/2}, \qquad 4.1$$

in which ν and D represent the kinematic viscosity of water and a diffusion coefficient (typically 10^{-5} cm^2 s^{-1}) respectively. An experimentally observed proportionality between dissolution rate and $\sqrt{\omega}$ is cited as evidence that a reaction is diffusion limited.

None of the previous models of calcite dissolution (*e.g.* PWP, Sjöberg and Rickard,

1984a) fully treat the transport terms of the reaction. The diffusion of electrolytes is strongly coupled (Lasaga, 1979; Anderson and Graf, 1976), a fact which has been neglected in most of the studies on calcite dissolution. An important exception is a recent paper by Lancia *et al.* (1991); however, they assume that the reaction is purely diffusion controlled. Leaist (1987) has explored the consequences of coupled diffusion in the dissolution of calcium hydroxide and found some non-intuitive consequences. For example, the dissolution of porous $Ca(OH)_2$ can lead to precipitation of $Ca(OH)_2$ within the pore structure.

4.2 Theory

4.2.1 Calcite Dissolution

The rate of dissolution is necessarily a function of the solution composition in the immediate vicinity of the solid. In the analysis of calcite dissolution kinetics this composition is estimated by either assuming pure transport or surface reaction control. The rate expression proposed by PWP is based on the bulk solution composition; however, some provisions for transport control are included in their model. Their expression for the forward rate of the reaction, r_f, includes three terms, which are first order in hydronium, carbonic acid and water activities;

$$r_f = k_1^C[H^+] + k_2^C[H_2CO_3] + k_3^C[H_2O]. \qquad 4.2$$

This rate expression suggests that calcite dissolution proceeds *via* the three independent elementary reactions (3.2 – 3.4). The stirring rate dependence was incorporated in the rate constant, k_1^C; the implication is that the transport of hydronium to the surface is rate limiting, at least in moderately acidic solutions. The rate constants associated with carbonic acid and water activities are stirring rate independent, which implies that the dissolution reaction associated with these reactants is surface controlled.

The value of the apparent rate constant k_1^C in the limit of an infinite stirring rate,

$k_1^C(0)$, is the rate constant for the elementary reaction (3.2); its value for an Iceland spar crystal was reported recently by Compton *et al.* (1989) to be 0.043±0.015 cm s^{-1}. The dimension of the rate constants $k_1^C - k_3^C$ differ by a factor of concentration depending on whether concentration or activity of the solute is used in Eqn. 4.1; however, their values are numerically equal if expressed in cm s^{-1} or mmole cm^{-2} s^{-1} (PWP). The experimental values of the apparent rate constant k_1^C reported by PWP ranged between 0.039 and 0.082 cm s^{-1}, which are very similar to the value of $k_1^C(0)$ determined by Compton *et al.* (1989). PWP suggested that their measured k_1^C was about an order of magnitude lower than $k_1^C(0)$. This indicates an inconsistency between the data of PWP and Compton *et al.* (1989).

Chou *et al.* (1989) found that the rate constants proposed by PWP overestimated their dissolution data by a factor of two to three which they attributed to an under-estimation by PWP of the surface area of their reactants or a difference in the defect density of their calcite. Work reported by Schott *et al.* (1989) suggests that the rate of Iceland spar dissolution is relatively independent of defect density, an increase in defect density of three orders of magnitude resulted in an increase in dissolution rate of only about a factor of three. Both PWP and Chou *et al.* (1989) used a geometric estimate of the surface area of their calcite. Ferret *et al.* (1987) found that the surface area of very finely ground calcite (2-20 μm grains) measured by BET was up to an order of magnitude greater than the geometric estimate. In light of these considerations, it is possible that PWP either under-estimated the surface area of their samples by a factor of about three, or used particularly reactive calcite grains in their studies. Consequently, it is conceivable that the rate constants reported in PWP are too high by a factor of about three. If this is accepted, the rate constant proposed by Compton *et al.* (1989) can be reconciled with the rate data of PWP.

PWP fit the back reaction to the expression

$$r_b = k_4^C[Ca^{2+}][HCO_3^-], \qquad 4.3$$

where k_4^C is a function of CO_2 pressure and the activities are those of the bulk solution. This expression is empirical and was obtained from correlations between the rate of

the back reaction (calculated from difference of the rate of the forward reaction given by 4.1 and the measured reaction rate) and various possible expressions for the back reaction. An alternative form r_b, which was used by Chou *et al.* (1989), is

$$r_b = [Ca^{2+}](k^C_{-1}[HCO_3^-] + k^C_{-2}[HCO_3^-]^2 + k^C_{-3}[CO_3^{2-}]) \qquad 4.4$$

where the rate constants k^C_{-i} are related to the rate constants k^C_i by $k^C_{-i} = k^C_i/K_i$ where K_i is the equilibrium constant of reaction (3. $i+1$). It should be noted that the activities in Eqn. 4.4 are those at the solid/solution interface.

A complicated reaction mechanism was developed by PWP to justify Eqn. 4.3 and to develop a relationship between k^C_4 and p_{CO_2}. It requires two assumptions: i) no appreciable concentration gradient between the surface and bulk solution develops in either H_2CO_3 or H_2O, and ii) the surface concentration of hydronium activity and other ions is maintained at calcite saturation. Despite the relative success of the model in describing their experimental data, the assumptions made are *ad hoc*, and are readily testable using a model of mixed reaction rate control.

4.2.2 Diffusion in electrolyte solutions

Treatment of the diffusion of electrolytes must include the fact that electrostatic forces couple the transport of different chemical species. The diffusional flux, J_i, of species i towards or from a solid surface is related to the concentration gradient in the solution by Fick's first law (assuming diffusion away (increasing x) from an infinite, flat plate)

$$J_i = -\sum_{j=1}^{n} D_{i,j}\frac{\partial c_j}{\partial x}, \qquad 4.5$$

where c_j is the molar concentration of the j^{th} solute, $D_{i,j}$ is the inter-diffusion coefficient (Lasaga, 1979), and there are n species with appreciable concentrations in solution. The coupling of diffusion between species is explicitly written into Eqn. 4.5, which can be re-written in matrix notation as

$$\vec{J} = \tilde{D}\vec{C}_x. \qquad 4.6$$

where $\vec{J}$ and $\vec{C}$ are column matrices (vectors) whose elements represent the fluxes and concentrations in solution, $\vec{C}_x$ is the derivative of $\vec{C}$ with respect to x and $\tilde{D}$ is the diffusion matrix. The $(i,j)^{th}$ element of $\tilde{D}$ can be estimated for dilute solutions (Lasaga, 1979) by

$$D_{i,j} = D_i^\circ \delta_{i,j} + \frac{z_i c_i D_i^\circ z_j D_j^\circ}{\sum_k z_k^2 c_k D_k^\circ}, \qquad 4.7$$

where D_i° is the tracer diffusion coefficient of the i^{th} species, z_i is the charge on species, i, and $\delta_{i,j}$ is equal to 0 unless $i = j$ in which case it is equal to 1.

4.3 Mixed reaction control

When diffusional processes limit the reaction rate to any extent, the (measurable) composition of the bulk solution will differ from the solution composition near the grain surface (not measurable). Although the solution composition at the crystal surface is not measurable, solution of the equation describing the diffusion of solutes around the grain can give a good indication of the solution composition adjacent to the grain. In order to formulate the problem, the rate law governing the dissolution, the relevant diffusion coefficients, and the hydrodynamics of flow around the solid must be known (or assumed). The hydrodynamic conditions are generally poorly known; a common assumption, which will also be used here, is that the solution is stagnant from the solid surface to a distance δ from the surface. The analysis is simplified if it is assumed that the volume of the solution in this stagnant film is much less than the total volume of the solution. In this case, the solution composition in the film will rapidly approach a steady state for a given bulk solution composition. This steady state solution is much more readily obtained than the time dependent solutions. It is safe to assume that the steady state criterion is met in most batch reactors; however, it is likely not met in most naturally occurring porous media. The steady state solution describing mixed reaction control will be developed below.

If δ is known for the dissolution experiments the analysis is simplified; without this constraint, the distance over which a compositional gradient is maintained in

the solution can be treated as a fitting parameter (Wallin and Bjerle, 1989). If it is assumed that this characteristic length, δ, is known, experimental results can be analysed as follows.

The steady state flux of an element, ϕ_i, from the calcite surface due to dissolution is a function, $F_{cc,i}$, of the solution composition at the solid-solution interface, $(\vec{C}(0))$, or

$$\vec{\phi} = \vec{F}_{cc}(\vec{C}(0)). \tag{4.8}$$

The flux of Ca and TIC from the dissolution of calcite is given by the difference of r_f and r_b (Eqn. 4.2 and Eqn. 4.3 or 4.4). The elemental flux, ϕ_i, is related, by simple mass balance, to the flux of the species in solution, $\vec{J}$, by

$$\phi_i = \sum_{j=1}^{n} \nu_{i,j} J_j, \tag{4.9}$$

where $\nu_{i,j}$ are stoichiometric coefficients. A steady state will only arise when the flux of solutes due to diffusion is balanced by the flux due to dissolution, or

$$\phi_i = -\sum_{j=1}^{n}\sum_{k=1}^{n} \nu_{i,j} D_{j,k} \frac{\partial c_k}{\partial x}. \tag{4.10}$$

Thus, the concentration gradients within the stagnant layer $(\frac{\partial c_k}{\partial x})$ can be related to the flux $\vec{\phi}$, or the solution composition at the solid/solution interface.

A further constraint on the solution composition within the stagnant layer arises since the solution speciation will change in response to concentration gradients within the layer. These changes can be treated if local equilibrium is assumed. By way of example, in the aqueous system HCl - CO_2 - $CaCO_3$, specifying total carbonate (TIC), Ca, and Cl concentrations will uniquely define the concentration of all the complexes present in the solution (assuming equilibrium). In order to treat the changes of speciation within the stagnant layer mass action equations must also be considered.

Within the solution, there may be appreciable concentrations of a host of solutes (*e.g.* Ca^{2+}, $CaCO_3^\circ$, $CaHCO_3^+$, H_2CO_3 HCO_3^-, CO_3^{2-}, H^+, OH^-, Cl^-, $CaCl^+$ and $CaCl_2^\circ$). Here we will only consider the first 9 of these species. In order to solve the

equations describing mass transfer in this system, the speciation must be calculated, and the manner in which each solute changes with distance must be described. The complete set of equations defining this system are a charge balance equation, three mass balance equations, five mass action equations. These can be differentiated to give:

$$\sum_{i=1}^{9} z_i \frac{dc_i}{dx} = 0 \tag{4.11}$$

$$\sum_{i=1}^{9} (D_{H_2CO_3,i} + D_{HCO_3^-,i} + D_{CO_3^{2-},i} + D_{CaCO_3^\circ,i} + D_{CaHCO_3^+,i}) \frac{dc_i}{dx} = r_b - r_f \tag{4.12}$$

$$\sum_{i=1}^{9} (D_{Ca^{2+},i} + D_{CaCO_3^\circ,i} + D_{CaHCO_3^+,i}) \frac{dc_i}{dx} = r_b - r_f \tag{4.13}$$

$$\sum_{i=1}^{9} (D_{Cl^-,i}) \frac{dc_i}{dx} = 0 \tag{4.14}$$

$$\frac{1}{[Ca^{2+}]} \frac{d[Ca^{2+}]}{dx} + \frac{1}{[CO_3^{2-}]} \frac{d[CO_3^{2-}]}{dx} = \frac{1}{[CaCO_3^\circ]} \frac{d[CaCO_3^\circ]}{dx} \tag{4.15}$$

$$\frac{1}{[Ca^{2+}]} \frac{d[Ca^{2+}]}{dx} + \frac{1}{[HCO_3^-]} \frac{d[HCO_3^-]}{dx} = \frac{1}{[CaHCO_3^+]} \frac{d[CaHCO_3^+]}{dx} \tag{4.16}$$

$$\frac{1}{[H^+]} \frac{d[H^+]}{dx} + \frac{1}{[HCO_3^-]} \frac{d[HCO_3^-]}{dx} = \frac{1}{[H_2CO_3]} \frac{d[H_2CO_3]}{dx} \tag{4.17}$$

$$\frac{1}{[H^+]} \frac{d[H^+]}{dx} + \frac{1}{[CO_3^{2-}]} \frac{d[CO_3^{2-}]}{dx} = \frac{1}{[HCO_3^-]} \frac{d[HCO_3^-]}{dx} \tag{4.18}$$

$$\frac{1}{[H^+]} \frac{d[H^+]}{dx} + \frac{1}{[OH^-]} \frac{d[OH^-]}{dx} = 0 \tag{4.19}$$

in which z_i is the ionic charge of the i^{th} species, r_f and r_b are given by Eqn. 4.2 and 4.4 respectively, and $D_{i,j}$ is given by Eqn. 4.7. Eqn. 4.11 is required by elecro-neutrality, and Eqn. 4.15 – 4.19 are required by the local equilibrium constraint. Eqns. 4.12 – 4.14 are expressions of conservation of mass, they relate the flux of each component from the crystal surface due to dissolution to the flux arising from diffusion. Eqn. 4.14 simply states that, since calcite is neither a source nor a sink of Cl, there should be no diffusive flux of Cl arising from its dissolution. This does not mean that there is necessarily no concentration gradient in Cl around a dissolving grain of calcite. The coupling of diffusion coefficients requires that such a gradient will develop. The

equations involving activities and derivatives of activities can be rewritten in terms of concentrations and derivatives of concentrations by the activity coefficient (Eqn. 3.7) and the resulting system of equations can be solved for dc_j/dx. The physical constants used in this model are given in Table 4.1.

This system of equations, or a related system, has been given by Plummer and Wigley (1976); Wallin and Bjerle (1989) and Dreybrodt and Buhmann (1991); Lancia *et al.* (1991); however, they did not simultaneously consider the ionic coupling during diffusion and the possibility that the solution immediately adjacent to the calcite surface is not saturated.

4.3.1 Numerical Scheme

Since the diffusional fluxes are coupled the equations needed to model mixed reaction kinetics must be solved numerically. Eqns. 4.11 – 4.19 were rewritten in terms of the logarithms of concentration for numerical stability. The transformed equations were integrated with a fourth order Runga-Kutta algorithm (Gerald, 1978) using double-precision arithmetic on a personal computer. Although the equations are first order, they cannot be integrated directly, since the term $r_f - r_b$ in equations 4.12 and 4.13 contain $\vec{C}(0)$ but the boundary condition (the bulk solution composition) is given at x= δ. Therefore, an iterative approach is required to match the boundary condition to a surface concentration. The concentration at the surface was calculated by guessing values for the three components ($\vec{N}(0)$), whose elements are the total calcium, total carbonate, and chloride concentrations at the surface and calculating the speciation of the solution ($\vec{C}(0)$). The equations were integrated from 0 to δ or until any element of the vector $\vec{C}$ became negative. In this case, new values for the three components that resulted in a lower rate of dissolution, were chosen and the calculations repeated. This eventually led to a solution for which all the elements of $\vec{C}(x)$ remained greater than 0.0 for all x less than δ. This value of $\vec{N}(0)$ provided an initial estimate for a Newton-Rapheson root finding algorithm. The increments in $\vec{N}(0)$ were halved if the concentration of any species vanished during the integration. The introduction

	$t = 25°C$		$t = 150°C$	
		Ref.		*Ref.*
$\log K_{H_2CO_3}$	-6.35	*a*	-6.77	*a*
$\log K_{HCO_3^-}$	-10.33	*a*	-10.39	*a*
$\log K_{H_2O}$	-14.0	*a*	-11.64	*a*
$\log K_{CaHCO_3^+}$	-1.11	*a*	-1.00	
$\log K_{CaCO_3^\circ}$	-3.22	*a*	-1.00	
$\log K_{sp}(CaCO_3)$	-8.48	*a*	-10.16	*a*
$k_1^C/10^{-2}$cm s^{-1}	4.3	*b*	14.	*c*
$k_2^C/10^{-5}$cm s^{-1}	1.1	*c*	500	*c*
$k_3^C/10^{-8}$cm s^{-1}	4.0	*c*	624	*c*
$D^\circ_{H_2CO_3^\circ}/10^{-5}$cm^2 s^{-1}	1.9	*d*	7.0	
$D^\circ_{HCO_3^-}/10^{-5}$cm^2 s^{-1}	1.18	*e*	9.30	*j*
$D^\circ_{CO_3^{2-}}/10^{-5}$cm^2 s^{-1}	0.92	*e*	3.9	
$D^\circ_{OH^-}/10^{-5}$cm^2 s^{-1}	5.28	*e*	21.5	*h*
$D^\circ_{H^+}/10^{-5}$cm^2 s^{-1}	9.3	*e*	28.3	*h*
$D^\circ_{Ca^{2+}}/10^{-5}$cm^2 s^{-1}	0.79	*e*	5.8	*h*
$D^\circ_{Cl^-}/10^{-5}$cm^2 s^{-1}	2.03	*e*	11.4	*h*
$D^\circ_{CaCO_3^\circ}/10^{-5}$cm^2 s^{-1}	0.6	*f*	0.6	*f*
$D^\circ_{CaHCO_3^+}/10^{-5}$cm^2 s^{-1}	0.6	*f*	0.6	*f*
$B^\bullet$	0.041	*a*	0.047	*a*
$\mathring{a}\,(H^+)$	9.	*k*		
$\mathring{a}\,(Ca^{2+})$	6.	*k*		
$\mathring{a}\,(CaHCO_3^+)$	6.			
$\mathring{a}\,(CaCO_3^\circ)$	0.			
$\mathring{a}\,(H_2CO_3^\circ)$	0.			
$\mathring{a}\,(OH^-)$	3.5	*k*		
$\mathring{a}\,(HCO_3^-)$	4.5	*k*		
$\mathring{a}\,(CO_3^{2-})$	4.5	*k*		
$\mathring{a}\,(Cl^-)$	3.0	*k*		
ϵ	78.5	*i*	43.9	*i*
ρ	1.00	*i*	0.92	*i*

Table 4.1: Values of physical parameters used in these calculations. The last 12 constants are needed for calculation of activity coefficients.
References - *a*) Kharaka *et al.* (1988); *b*) Compton *et al.* (1989); *c*) PWP with corrections for surface area (see text); *d*) Leaist (1985); *e*) Robinson and Stokes (1962); *f*) estimated; *h*) Oelkers and Helgeson (1988); *i*) Helgeson and Kirkham (1974); *j*) Bignold *et al.* (1971); *k*) Garrels and Christ (1965).

of activity coefficients, based on the Debye-Hückel expression, resulted in numerical results essentially identical to those obtained by treating the solution as ideal.

4.4 Results

Several computer simulations have been performed; the results are shown in a series of plots (Figs. 4.1 – 4.9). Figures 4.1 – 4.5 are plots of the calculated gradients in the solution composition in the case of highly undersaturated solutions with fixed bulk Ca, TIC and variable bulk Cl concentrations with $\delta = 7.0$ μm. This value of δ is representative of very vigorous agitation (see Sjöberg and Rickard; 1984a). Figure 4.3 shows that carbonic acid develops no appreciable concentration gradient in CO_2 rich solutions. The relative change in carbonic acid concentration between the surface and bulk increases with decreasing carbonic acid; however, its contribution to the total rate also diminishes. The relatively small gradient in carbonic acid is in agreement with the observation by PWP that their measured k_2^C is independent of the stirring rate (at least in solutions where the $k_2^C[H_2CO_3]$ term contributes appreciably to the total rate expression).

The plot of hydrogen concentration (Fig. 4.1) demonstrates that appreciable gradients exist; however, the surface concentration is proportional to the bulk concentration. This is demonstrated with Fig. 4.6 in which the surface H^+ activity is plotted as a function of its bulk value. There is a very good linear relationship shown (slope $\approx 1/3$), consequently, if $\delta = 7\mu$m, the term $k_1^C[H^+]$ in Eqn. 4.1 can be replaced by $3k_1^C[H_s^+]$. The apparent rate constant k_1^C can be related to the rate constant for the elementary reaction $k_1'^C$ by $k_1^C = k_1'^C/3$.

These calculations also suggest that, within the limitations of the model, calcite dissolution should be first order in H^+ activity over a wide concentration range, and that a deviation from first order kinetics will not arise due to the mixed reaction kinetics. Such non-unit slopes have been noted in experimental studies of calcite in concentrated solutions (*e.g.* Lund *et el.*, 1975). Factors which were not consid-

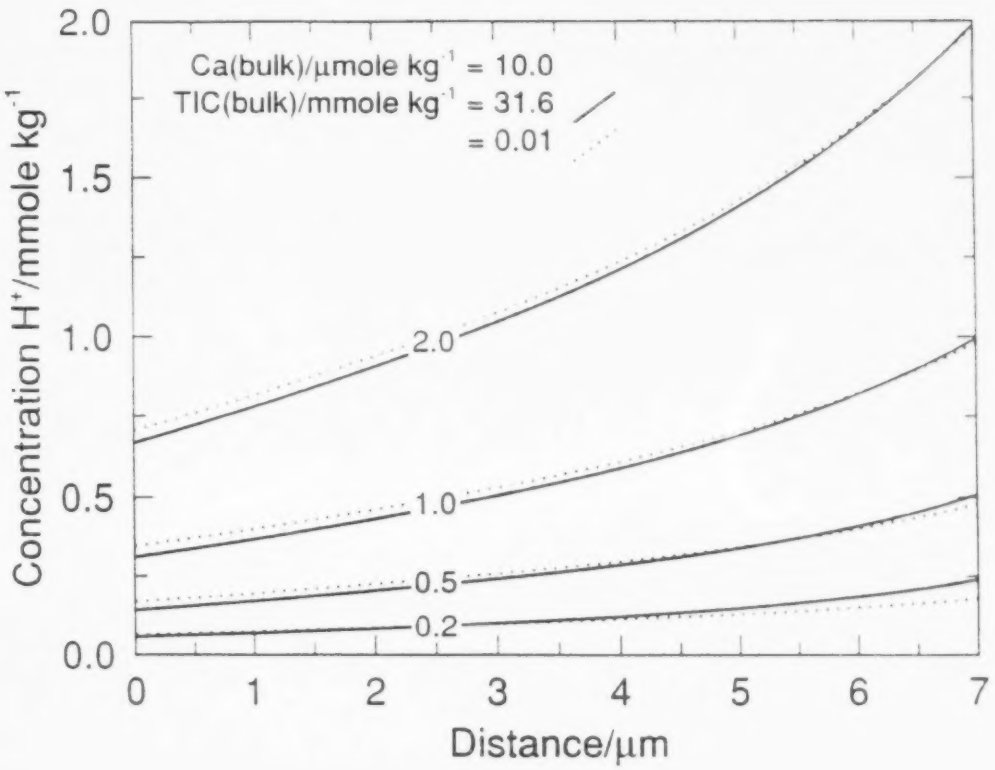

Figure 4.1: Calculated profiles of H^+ as a function of distance away from the calcite crystal surface for various bulk HCl concentrations and two values of TIC at 25°C. The concentration of Cl (mmole/kg) in the bulk solution is given on the curves. A value of 7.0 μm was used for δ.

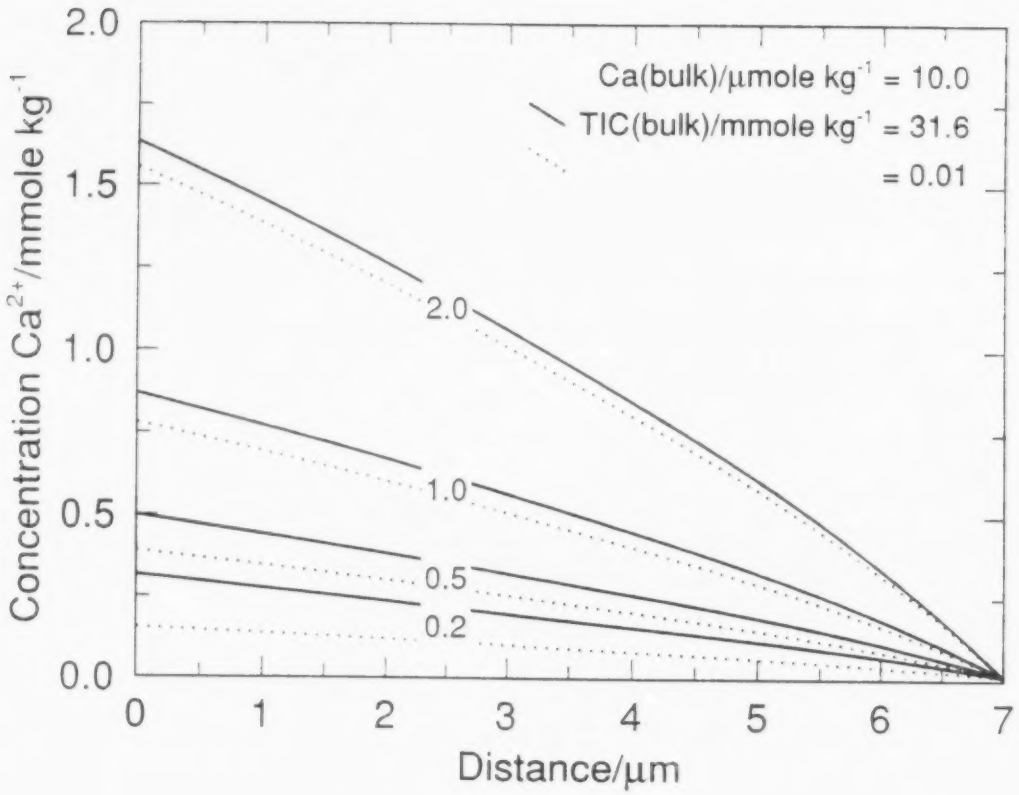

Figure 4.2: Calculated profiles of Ca^{2+} as a function of distance away from the calcite crystal surface for various bulk HCl and TIC concentrations. The conditions are the same as for Fig. 4.1.

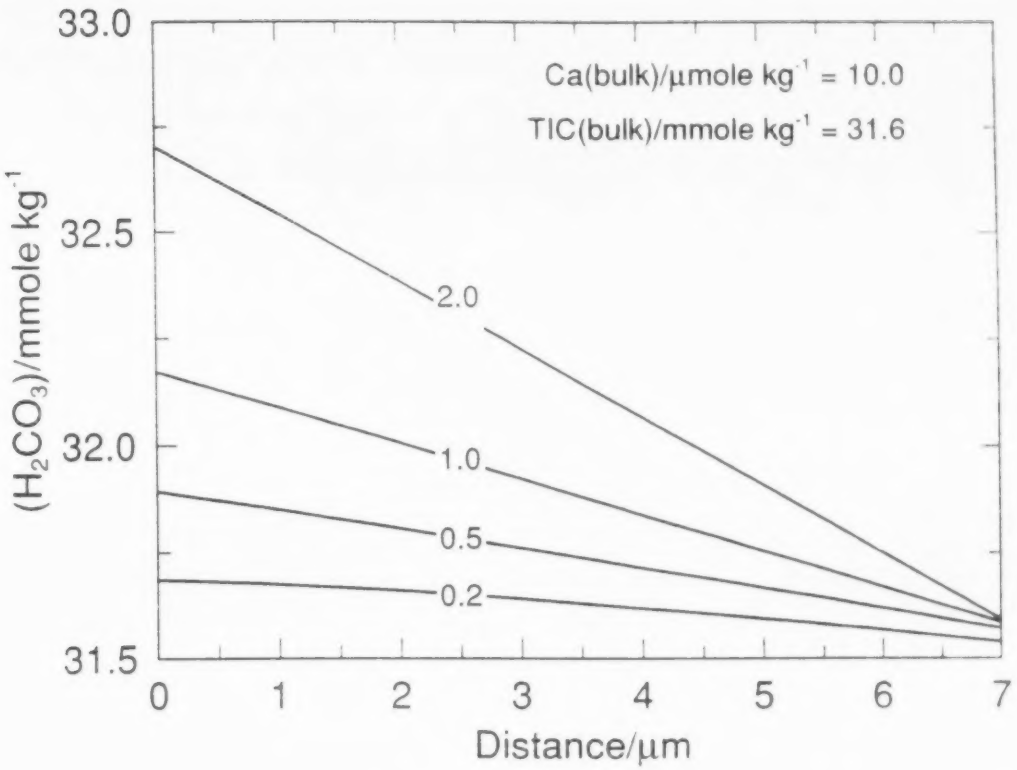

Figure 4.3: Calculated profiles of H_2CO_3 as a function of distance away from the calcite crystal surface for various bulk HCl concentrations. The conditions are the same as for Fig. 4.1. The lack of appreciable gradient in H_2CO_3 supports the claim by PWP that the rate constant k_2^C can be evaluated directly from the variation in dissolution rate with the bulk p_{CO_2}.

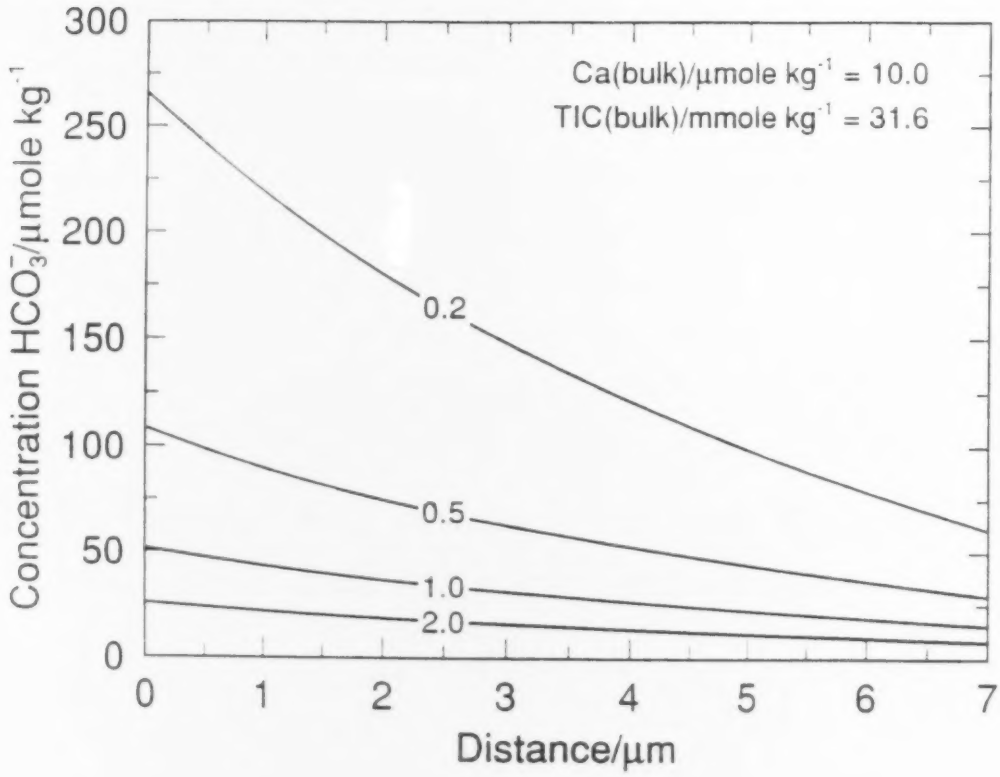

Figure 4.4: Calculated profiles of HCO_3^- as a function of distance away from the calcite crystal surface for various bulk HCl concentrations. The conditions are the same as for Fig. 4.1.

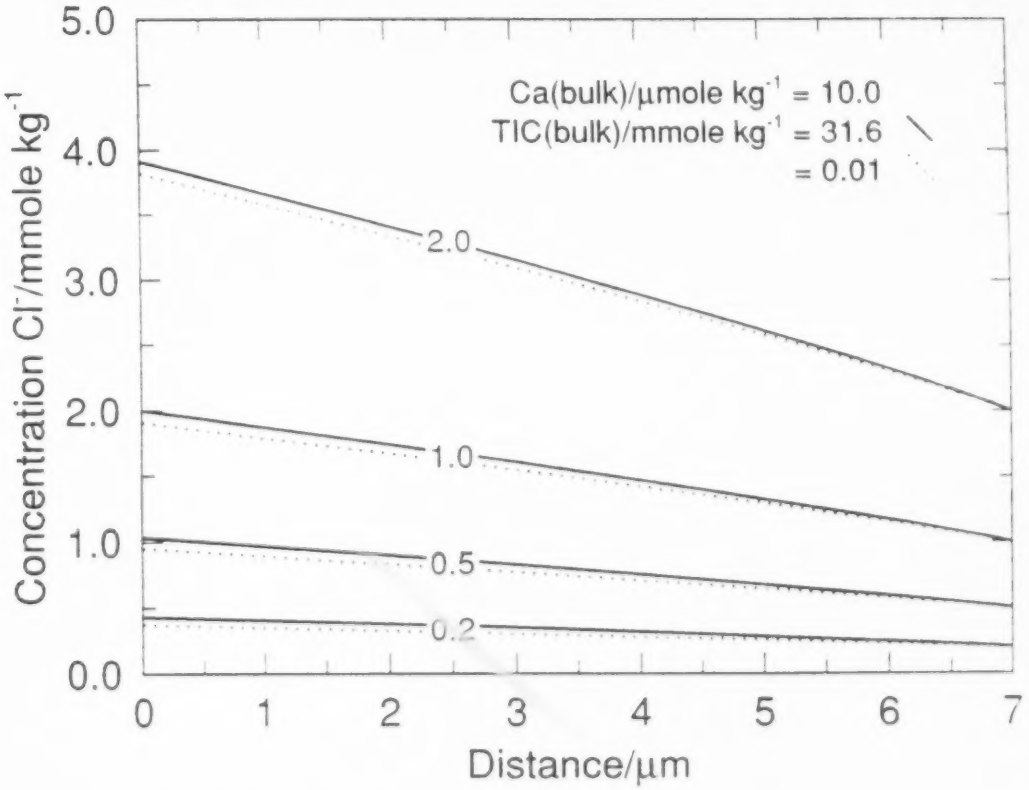

Figure 4.5: Calculated profiles of Cl^- as a function of distance away from the calcite crystal surface for various bulk HCl and TIC concentrations. The conditions are the same as for Fig. 4.1.

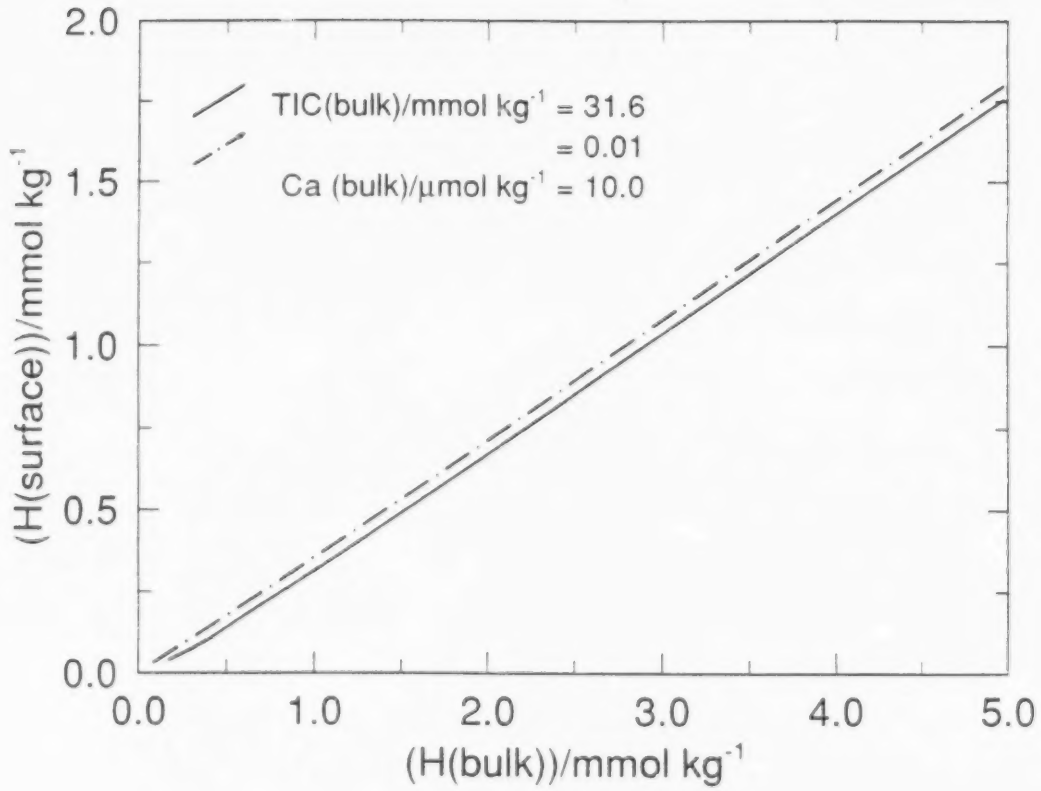

Figure 4.6: The calculated concentration of H^+ at the calcite surface plotted against the H^+ concentration in the bulk solution for the simulations described above. The plot is essentially a straight line, with a slope is about three. The slope of this line is dependent on δ. Were this plot not linear, the model predictions would be in disagreement with the experimental results of PWP. The slight curvature at the low H^+ concentrations is due to contributions from the second term in the forward rate expression.

ered here including density fluxes, more complex coupling of diffusion coefficients and solution composition, the presence of other supporting electrolytes, and other composition-activity relations may be responsible for these non-unit slopes.

These calculations do not support many of the assumptions and conclusions made by PWP with respect to the backwards reactions. The saturation index at the crystal surface is plotted as a function of δ in Fig. 4.7 for two bulk TIC concentrations. The saturation index of the bulk solution is the value at $\delta = 0$, which represents an infinite stirring rate. Although the saturation state at the crystal surface increases rapidly with small changes in δ, Fig. 4.7 shows that the solution at the interface remains well undersaturated at the crystal surface even in the case of relatively slow agitation (high values of δ), particularly in the higher TIC case. This is contrary to the assumption, made by PWP in their derivation of the form for the back reaction, that the solution at the crystal surface is saturated.

The form of the back reaction rate expression used by PWP cannot be reconciled with these calculations. Fig. 4.8 is a plot of the product of various ion concentration in the bulk solution *vs.* the back reaction rate (Eqn. 4.4). Since the quantities plotted differ by many orders of magnitude, factors are removed from the to facilitate the plotting. It also means that uncertainties in the association constant of the complex need not be considered. However, since the axes are linear, the form of any relationship between the back reaction rate and the bulk ion activity product (or bulk ion pair activity) is conserved. This plot shows noticeable curvature in the relation between the bulk $CaHCO_3^+$ activity and backwards reaction rate; although the results of PWP imply this line should be straight. In contrast, plots of both bulk $CaCO_3^\circ$ and $CaOH^-$ against the backwards rate are relatively straight. This relationship was not noticed by PWP, although Chou *et al.* (1989) did report a linear relation between bulk $CaCO_3^\circ$ and the back reaction rate. In order to make the back reaction rate appear to be linear in bulk $CaHCO_3^+$ an expression for the backwards reaction rate other than Eqn. 4.4 must be invoked.

The experimental observation that the rate of dissolution is proportional to δ^{-1}

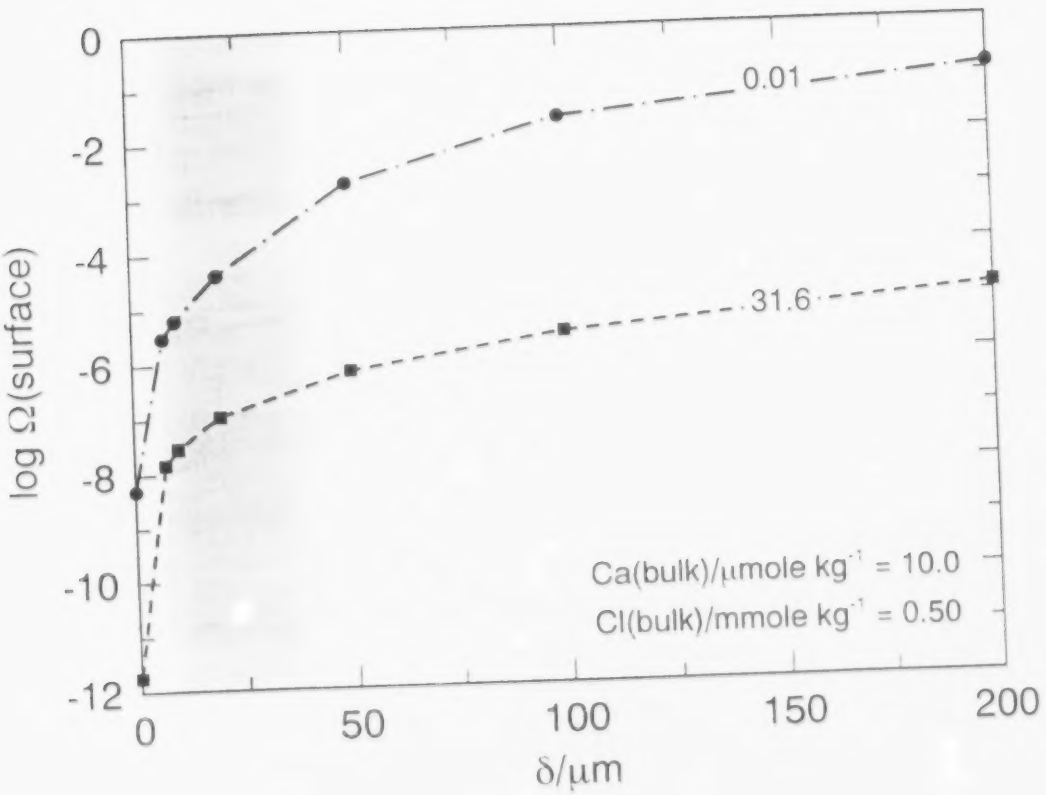

Figure 4.7: The logarithm of the calculated saturation index at the solution/mineral interface as a function of δ. The shaded area on the plot represents the values of δ typically achieved with a rotating disc. The solution remains several orders of magnitude undersaturated with respect to calcite, clearly demonstrating the mixed reaction control.

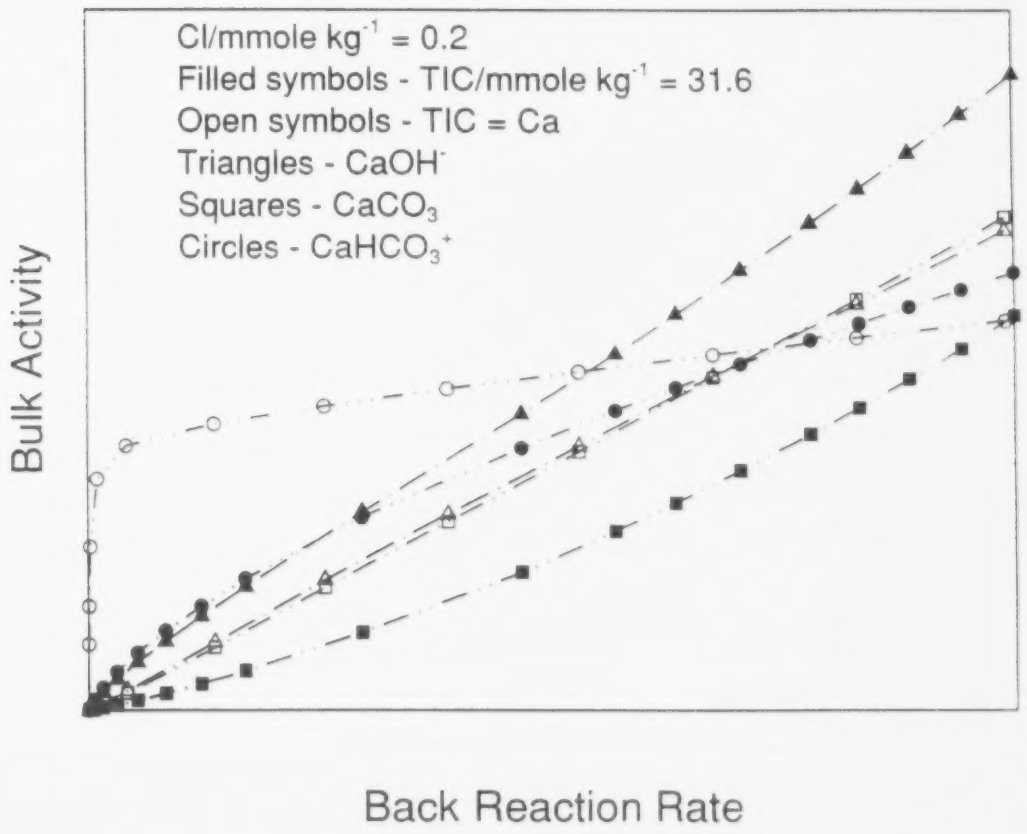

Figure 4.8: Various bulk solution activities ($CaCO_3$, $CaHCO_3^+$, and $CaOH^+$) plotted against the rate of the backwards reaction rate, calculated from Eqn. 4.4. The scale of the y-axis is different for each activity, calcite saturation is near the far right of the diagram. The TIC in the bulk solution is 31.6 mmole kg^{-1} for the filled symbols and equal to the bulk Ca concentration for the empty symbols. The plot of both $CaCO_3$ and $CaOH^+$ are, in both cases, less non-linear than the plots of $CaHCO_3^+$, whereas the analysis of PWP suggests the converse should be true.

can also be predicted with this model. Fig. 4.9 plots the surface H^+ concentration as a function of δ^{-1}. The values of δ used in these calculations are between 6 and 50 μm. The bulk solution used for these calculations is essentially a 10^{-3} mol/kg HCl solution. Under this condition the calcite surface is predicted to be well undersaturated (Fig. 4.7) for $\delta < 100\mu$m. Since the solution is well undersaturated, and since only the first term in the rate expression ($k_1'^C[H^+]$) makes an appreciable contribution to the total rate, the calculated surface $[H^+]$ concentration will be proportional to the dissolution rate. Figure 4.9 presents the calculated surface H^+ concentration plotted against δ^{-1}, and it demonstrates a strong linear trend. The slight non-linearity would almost certainly fall within the bounds of experimental error, and hence would be ignored in an experimental study.

Calculations similar to those presented here have been done on this system by other workers, although their work was based on different assumptions. If electrostatic interactions are ignored (uncoupled diffusion coefficients) there cannot be a concentration gradient in Cl^- by the dissolution. Similarly, the Ca^{2+} profile will be linear, although the gradients in species associated with the carbonate system (H_2CO_3, HCO_3^-, CO_3^{2-}, H^+, and OH^-) will show curvature. The absence of a Cl^- gradient will result in a more basic solution at the surface than was calculated here, and a higher degree of surface saturation. It has also been assumed by Sjöberg and Rickard (1984a), and Lancia *et al.*, (1991) that the dissolution reaction is strictly controlled by diffusion (*i.e.* the solution at the mineral surface is saturated with respect to calcite). This assumption led Sjöberg and Rickard (1984a) to conclude that the surface pH was more than 6 units greater than the bulk pH under conditions similar to those given here. Thus, the calculated solution composition near a dissolving calcite grain is highly dependent on the assumptions made in developing the model.

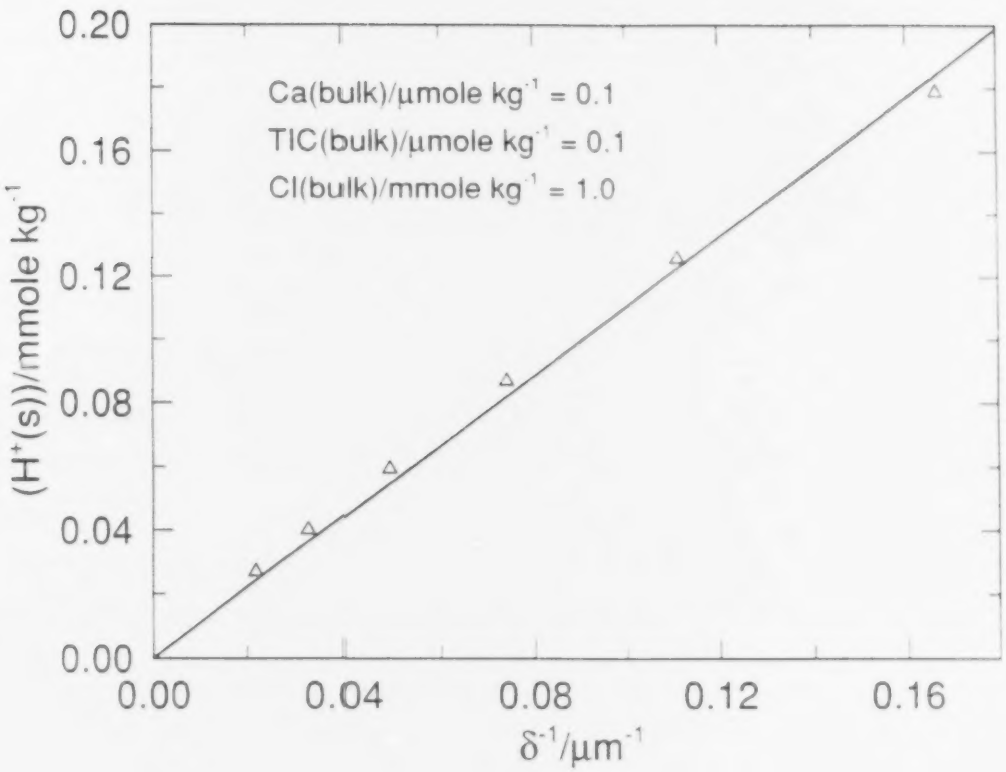

Figure 4.9: The calculated surface H^+ concentration plotted as a function of δ^{-1}. The composition of the bulk solution is given in the figure. The line is a best fit line to the data, constrained to pass through the origin.

4.5 Implications for High Temperature Results

The concentration gradients around a dissolving grain can affect experimental rate determinations in two ways. The first is, as is the case of calcite at 25°C, that the activity of a reactant which affects the reaction rate, is depleted at the solid/solution interface. This leads to a lower reaction rate than would be expected from the bulk solution composition. It was demonstrated that this will interpretation of the rate constants in the rate expression proposed by PWP, but that the form of rate expression will be relatively free of stirring rate dependence. The second, more complicated, case arises when the solution at the solid/solution interface becomes sufficiently concentrated that the back reaction rate at the interface becomes appreciable, yet remaining negligible in the bulk solution. In this case, changes in the stirring rate will change the concentration of both the reactants driving the dissolution reaction and the products driving the (appreciable) back reaction.

In Chapter 1 it was shown that diffusional processes become increasingly responsible for limiting the rate of dissolution of minerals with retrograde solubility as temperature increases. In Chapter 3 it was demonstrated that a rate law of the form proposed by PWP for lower temperatures will fit the higher temperature experimental data. This rate expression was developed using a mechanistic model; however, any concentration gradients present at 25°C will be amplified at higher temperatures. The model results at 25°C beg the question – Why does the PWP expression work at higher temperatures?

The model developed above cannot be confidently extrapolated to higher temperatures. As T increases, the degree of saturation at the surface will increase, as will the concentration of ion pairs whose physical properties are poorly constrained. Specifically, the diffusivities of the ion pairs $CaCO_3^\circ$ and $CaHCO_3^-$ and the carbonate ion are not known. Despite these limitations, modelling the system at higher temperatures may provide insights into the reason for the success of the PWP rate expression at higher temperatures. The stability constants and diffusivities of the Ca–carbonate species were maintained at their 25°C values. Consequently, the flux

δ/ μm	H_2CO_3/ $mmole\ kg^{-1}$	HCO_3^-/ $mmole\ kg^{-1}$	H^+/ $\mu mole\ kg^{-1}$	Ca^{2+}/ $mmole\ kg^{-1}$	Rate/ $mmoles$
	(b) – (s)	(b) – (s)	(b) – (s)	(b) – (s)	$cm^{-2}s^{-1}$
6.0	34.89 – 33.92	0.119 – 2.040	54.01 – 3.30	0.030 – 1.012	0.129
	34.77 – 33.79	0.227 – 2.108	27.48 – 3.19	0.100 – 1.045	0.124
	34.39 – 33.48	0.609 – 2.290	10.49 – 2.93	0.298 – 1.135	0.110
	33.00 – 32.54	1.99 – 2.822	3.29 – 2.34	0.986 – 1.397	0.054
15.	34.86 – 33.51	0.143 – 2.733	43.21 – 2.49	0.050 – 1.353	0.068
	34.77 – 33.44	0.227 – 2.751	27.48 – 2.47	0.100 – 1.362	0.066
	34.58 – 33.31	0.414 – 2.786	15.27 – 2.43	0.199 – 1.379	0.063
	33.99 – 32.97	1.002 – 2.885	6.45 – 2.33	0.496 – 1.428	0.049
	33.00 – 32.42	1.988 – 3.039	3.28 – 2.18	0.986 – 1.503	0.027
25.	34.89 – 33.43	0.114 – 2.937	54.01 – 2.32	0.030 – 1.454	0.045
	34.77 – 33.33	0.227 – 2.950	27.48 – 2.30	0.100 – 1.460	0.043
	34.58 – 33.21	0.414 – 2.969	15.27 – 2.28	0.199 – 1.469	0.040
	33.99 – 32.89	1.002 – 3.024	6.45 – 2.22	0.496 – 1.496	0.031
	33.00 – 32.38	1.988 – 3.112	3.28 – 2.13	0.986 – 1.539	0.007

Table 4.2: Bulk (b) and surface (s) concentration of the cations appearing in the PWP rate expression for calcite dissolution, and dissolution rate calculated at 150°C. The parameters used to generate this table are given in Table 4.1.

of these species will be trivial. The values of the surface reaction rate constants $k_1^C - k_3^C$ (denoted here $k_1^C(0) - k_3^C(0)$) were extrapolated using expressions given by PWP. The results, while tentative, should at least provide a qualitative description of the processes occurring at higher temperatures.

The results of several simulations are presented in Table 4.2. The bulk solution contained 35 mmole/kg TIC and the reaction rate was altered by varying the value of Ca in the solution. The input parameters used in the calculation at 150°C are given in Table 4.1. Three results are apparent from these calculations: the pH of the solution at the interface remains near the pK for the dissociation of carbonic acid (*i.e.* carbonic acid and bicarbonate are the dominant carbonate species); the concentration gradient in carbonic acid is small relative to the other reactants; and the back reaction rate is dependent on the stagnant layer thickness. This third point can be seen by comparing the rate of dissolution in two solutions that have nearly the same (H^+) and (H_2CO_3) at the surface (the same forward dissolution rate) but

δ	R	R_{fit}	$\%error$
6	0.129	0.138	−7
	0.124	0.121	3
	0.110	0.107	3
	0.054	0.061	−13
15	0.068	0.069	−1
	0.066	0.065	2
	0.063	0.061	3
	0.049	0.051	−5
	0.027	0.026	2
25	0.045	0.045	1
	0.043	0.042	2
	0.040	0.040	0
	0.031	0.032	−3
	0.007	0.007	−5

Table 4.3: Comparison of the calculated dissolution rate (Table 4.2) with values fit with the empirical expressions Eqns. 4.2 and 4.3.

a different value of δ. This is most easily noticed by comparing the last entries for $\delta = 15\mu$m and $\delta = 25\mu$m. The surface H_2CO_3 and H^+ concentrations differ by less than 3% but the net dissolution rate differs by 350%.

The calculated reaction rates were fitted to the bulk solution composition with the rate expressions 4.2 and 4.3, to get the empirical rate constants $k_1^C(\delta) - k_3^C(\delta)$. The results are given in Table 4.3 and 4.4. The actual rate constants used to produce the data (*i.e.* the $k_i^C(0)$'s) are given in Table 4.1, as well as in Table 4.4.

δ	$k_1^C(\delta)/10^{-3}$	$k_2^C(\delta)/10^{-6}$	$k_3^C(\delta)/10^{-9}$	$k_4^C(\delta)$
0.0	0.14	5.00	6.24	
6.0	0.628	2.81	6.24	20.545
15.0	0.257	1.50	6.24	15.330
25.0	0.096	0.97	6.24	15.928
$Exp'r$	0.079	0.63	2.5	

Table 4.4: Coefficients used in generating Table 4.3. The coefficients given for $\delta = 0$ are the rate constants used to relate the dissolution rate to the solution concentration at the solid/solution interface (Table 4.1). The values for $\delta = 0.0$ are extrapolated using equations given in PWP. The experimentally evaluated values (Chapter 3) of the rate constants are also given.

The contribution of the term $k_3^C(0)$ to the total rate was small, so the value of $k_3^C(\delta)$ was constrained to the extrapolated value, but it could also be neglected completely. If k_3^C was treated as variable parameter, the fitted values of the rate constants were often poorly constrained (*i.e.* there was a high probable error associated with their value) and often were less than zero. The value of $k_2^C(\delta)$ obtained from this regression is lower than $k_2^C(0)$ by a factor of about 2 for $\delta = 6\mu$m and factor of 5 for $\delta = 25\mu$m. The value of $k_2^C(\delta)$ is less sensitive to the stagnant film thickness than is $k_1^C(\delta)$. As well $k_1^C(\delta)$ calculated from the regression calculation was greater than $k_1^C(0)$ when $\delta =$ 6 μm and $\delta = 15\mu$m. Interestingly, although the calculations presented in this section are based on poorly constrained values for the rate constants and some diffusivities and stability constants, the values of the experimentally evaluated rate constants (with the exception of the negligible k_3^C) at 150°C are in reasonable agreement with the values given in Table 4.4 for 25 μm.

The model calculations are in agreement with the experimental observations that the rate of calcite dissolution can be related to the bulk solution composition with an expression of the form of Eqn. 3.1 at both temperatures. 150°C and comparable values of δ the solution composition at the interface is considerably more basic than the bulk solution. Nonetheless, an expression of the form of Eqn. 3.1 can reproduce, with reasonable accuracy, the calculated dissolution rates. The constants of proportionality in Eqn. 3.1 differ from the rate constants used to generate the concentration profiles in a manner similar to that observed experimentally.

Chapter 5

Dissolution Rate of Dolomite in Hydrothermal Solutions

5.1 Introduction and previous studies

The kinetics of dolomite dissolution has been studied by Lund *et al.* (1973), Busenberg and Plummer (1982), Herman and White (1985), and Chou *et al.* (1989). Rotating disks were used by Herman and White (1985) and Lund *et al.* (1973). Chou *et al.* (1989) and Herman and White (1985) restricted their work to low temperatures (0–25°C) while Lund *et al.* (1973) and Busenberg and Plummer (1982) worked at elevated temperatures (to 100°C and 65°C respectively). There is general agreement between these works that the rate of dissolution at 25°C is proportional to the square root of hydrogen ion concentration, and is nearly independent of stirring rate to 45°C. Herman and White (1985) found a weak, temperature dependent, stirring rate effect in their experiments; however, this may be an artifact arising from their experimental method (see below). There is also agreement that the rate of dissolution is too slow to measure at 25°C in many solutions that are well undersaturated with respect to dolomite. A low temperature rate law, proposed by Busenberg and Plummer (1982),

and confirmed by Chou *et al.* (1989), is

$$r_D = r_f^D - r_b^D \tag{5.1}$$

in which

$$r_f^D = k_1^D[\mathrm{H^+}]^{n_1} + k_2^D[\mathrm{H_2CO_3^*}]^{n_2} + k_3^D[\mathrm{H_2O}]^{n_3} \tag{5.2}$$

and

$$r_b^D = k_4^D[\mathrm{HCO_3^-}]. \tag{5.3}$$

This rate law is valid only in solutions far from equilibrium. The exponent, n_2, in Eqn. 5.2 was evaluated, by Busenberg and Plummer (1982), to be 0.5 for all temperatures. The value of n_1 is also 0.5 at temperatures below 45°C, but it increases with temperature and was found to be 0.85 by 100°C (Lund *et al.*, 1973; Busenberg and Plummer, 1982). In contrast, the less extensive study by Chou *et al.* (1989) concluded that both n_1 and n_2 are 0.75 at 25°C, and they found no need to invoke a back reaction (*i.e.* $k_4^D = 0.$). Busenberg and Plummer (1982) also noted breaks in their Arrhenius plots near about 45°C, which they attributed to changes in the reaction mechanism. Since $[\mathrm{H_2O}]$ remains near unity in the work reported here, the third term in Eqn. 5.2 can be replaced by k_3^D.

Although the form of the rate law used is common for dolomites from several diverse geologic settings, the rate constants and activation energies differed between samples (Busenberg and Plummer, 1982). Generally, cleavage fragments of hydrothermal dolomites showed lower values for the forward rate constants and higher apparent activation energies than sedimentary dolomites. The dissolution reaction was essentially congruent, although there was a very short initial period of a relatively rapid removal of Ca, which Busenberg and Plummer (1982) calculated to result in at most a few monolayers depletion in Ca.

The expression for r_b^D (Eqn. 5.3) is empirical as in the case of calcite (PWP; Chaps. 3; 4). The rate of the back reaction is calculated using Eqn. 1.12 ($r_b^D = r_f^D - r_D$). The term r_D is known from the experimental results, and the rate expression and rate constants needed to calculate r_f^D are evaluated from data obtained in the solutions

where the back reaction is most likely to be negligible. Expressions for the back reaction are obtained by trying to find relationships between r_5^D and the activities of various solutes. Eqns. 5.2 and 5.3 are of limited validity, since the rate of dissolution lacks explicit dependence on the Ca or Mg concentration, and consequently, there is no term which will cause the reaction rate to vanish at equilibrium. The rate law is only applicable in solutions which are relatively well removed from saturation (*i.e.* $\Omega \lesssim -3$). In solutions with higher degrees of saturation (*i.e.* $\Omega \gtrsim -3$) the rate of dolomite dissolution was found to be imperceptibly slow. The dissolution reaction cannot be cast in terms of reversible reactions since it does not proceed to equilibrium under the conditions studied by Busenberg and Plummer (1982), Instead, the reduction of reaction rate with reaction progress described by Eqn. 5.3 was interpreted by Busenberg and Plummer (1982) to result from inhibition of the reaction by adsorption of bicarbonate to the dolomite surface.

The initial rapid Ca release and the non-integral values of $n_1 - n_3$ were interpreted by Busenberg and Plummer (1982) as evidence of a complex, multi-step reaction mechanism. The first step is a rapid reaction of the $CaCO_3$ component with proton sources (i.e. H^+, H_2CO_3, H_2O) to yield adsorbed Ca^{2+} and HCO_3^-. The remaining substrate (an ill defined magnesian carbonate) reacts slowly with the same proton sources; this is the rate determining step. Busenberg and Plummer (1982) explain that the relationship between the reaction rate and the square root of the activity of the proton sources arises since "the forward rates are dependent on only half the total consumption of reactants for each mole of solid dissolved." Some complex reaction mechanism is required to achieve the fractional order, but the fractional order does not necessarily follow from the rate scheme proposed by Busenberg and Plummer (1982). In fact, Chou *et al.* (1989) demonstrate that the mechanism proposed by Busenberg and Plummer (1982) should result in a rate law that is first order in the activity of the reactants.

5.1.1 Stirring Dependence

In contrast to the results of Busenberg and Plummer (1982), Herman and White (1985) noted some variation of reaction rate with stirring rate at all temperatures between 0 and 25°C. W.B. White (personal communication) described the geometry of the rotating disk used in the experiments reported in Herman and White (1985) (see Fig. 5.1). The dolomite sample covers a large proportion of the disk face. The

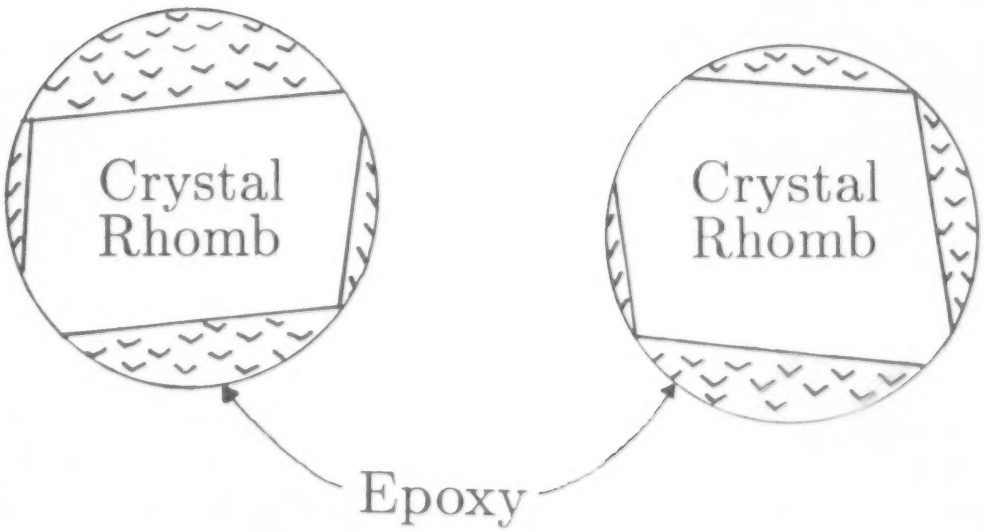

Figure 5.1: Traces of the rotating disks used by Herman and White (1985) in their study of dolomite dissolution kinetics (approx. 2X magnification).

equations describing the flow around the reacting surface are developed using the assumption that the reactive surface is much smaller than the surface of the entire

disk (Atkins, 1982). This assumption is made so that complications arising in the hydrodynamic equations near the perimeter of the disk (edge effects) can be ignored. Edge effects can give rise to turbulence and cavitation at the surface of the disk. The presence of turbulent conditions at the surface will likely increase the energy of interactions between the solid and solution, and, as a consequence, increase the dissolution rate. In order to reduce these edge effects most rotating disk electrodes are designed to be very thin near the perimeter of the disk. The electrodes used by Herman and White (1985) were not constructed with these considerations in mind; the low temperature transport dependence reported by Herman and White (1985) may result from a failure to properly control the hydrodynamics in their experimental design.

Although the evidence of stirring rate dependence is equivocal at low temperatures, Lund *et al.* (1973) reported a strong dependence of dissolution rate on stirring rate at 100°C. The appearance of stirring rate dependence may coincide with the change of reaction order (k_1^D) at temperatures above 45°C (Busenberg and Plummer, 1982). The transport control of dolomite dissolution will be explored in the next chapter.

5.2 Results

A summary of the experimental conditions is given in Table 2.4. The flow through reactor used for the experiments is described in Sec. 2.3.1. The experimental conditions were varied by changing the composition of the input solution, the stirring rate, and the flow rate through the reactor. Generally, the pH and the concentrations of Ca, Mg, and TIC in the outflow solutions were measured.

The full analysis described overdetermines the aqueous composition. The TIC and cations can be used to calculate the solution pH, a measured pH gives additional information, which may be contradictory. Two approaches were taken to resolve inconsistencies within the data set.

The first approach involved minimizing a sum of squares of the deviation between measured and estimated, charge balanced, solution composition. The charge balance was forced by using the method of Lagrange multipliers. As with all least squares minimizations, each measurement can be weighted based on the estimated accuracy of the measurement. There is no general way to assign these weights, and estimated compositions were quite sensitive to these weights. Furthermore, if the solution analysis is incomplete, charge balance need not be satisfied. A second approach was developed. This involved analysing each solution composition individually and determining the likely causes for the discrepancies within the data set. The results from each run are discussed individually in the second section of the Appendix. Any inconsistencies within the data were removed when possible and the modified data are presented in Tables 5.1 – 5.3. These, self-consistent, data are used as input to the program SOLMINEQ.88 (Kharaka *et al.*, 1988).

Results from three typical runs are presented in Fig. 5.2, which is a plot of the dissolution rate as a function of the flow rate. The composition of the input solution was constant during each of these runs, so the saturation state within the reactor should depend solely on the time that the solution is in contact with the crystal. It can be seen that the dissolution rate increases with flow rate (*i.e.* decreases with reaction progress) and decreases with stirring rate. The decrease in dissolution rate with flow rate is much more apparent in the 200°C data than in the other sets. Unlike the runs at the lower temperatures, by 200°C the dolomite dissolution reaction proceeded to near equilibrium at the lowest flow rates (the affinity ($-\Delta G$ in tables) of the dissolution reaction is given in Tables 5.4 – 5.6).

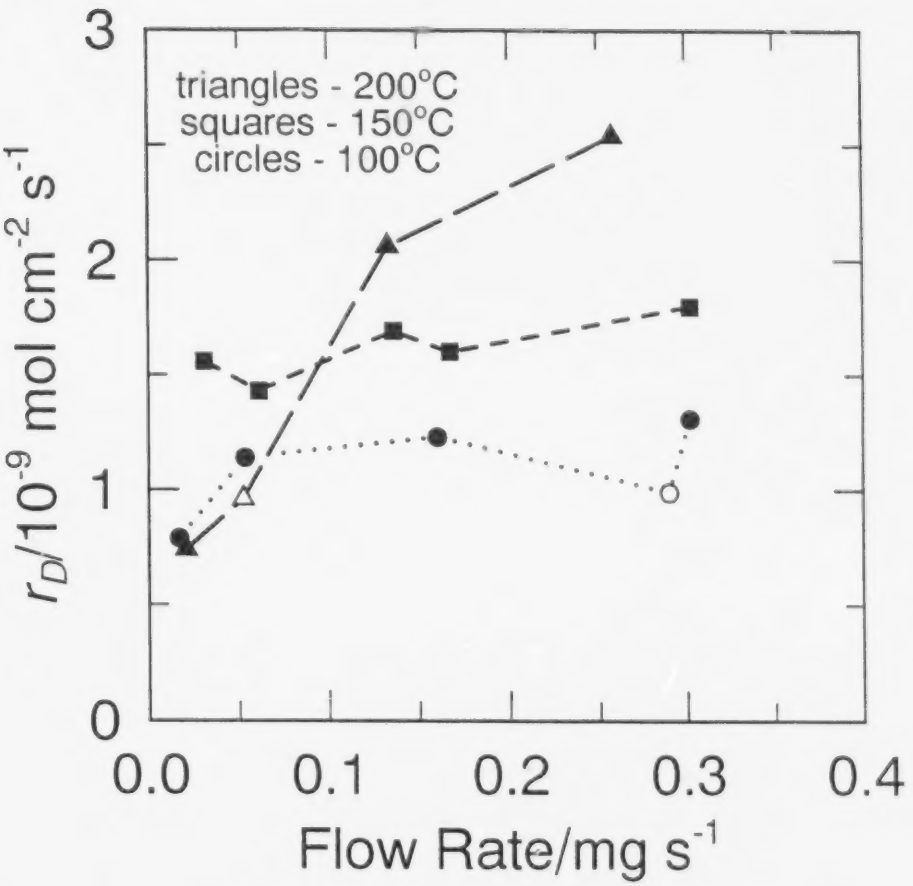

Figure 5.2: Measured rate of dissolution of dolomite (see Eqn. 1.17) as a function of flow rate for a run at each of 100, 150, and 200°C. The H_2CO_3 concentrations were, in order of increasing run temperature, 26 (run 270291), 21 (run 200291), and 15 mmole kg^{-1} (run 120291). The open symbols represent low stirring rates (170 rpm instead of 500 rpm).

Table 5.1: Table of internally consistent solution compositions (compare with Table A.4) from the 100°C runs. These compositions were used as input for the high temperature speciation calculations whose results are presented in Table 5.4. Note – * pH calculated at TIC = 0.028 moles kg^{-1} which is approximately the solubility carbon dioxide at ambient pressure. The pH of those solutions used in the SOLMINEQ input file was calculated based on the tabulated TIC.

Experiment $T = 100°C$

Sample	*Stirring rate/* rpm	*flow rate/* mg s^{-1}	Ca/ μmol kg^{-1}	Mg/ μmol kg^{-1}	pH	TIC/ mmol kg^{-1}	*Area/* cm^2	*Rate/* nmol $cm^{-2}s^{-1}$
051090	100	0.311	15.	16.	3.21	0.0	3.32	1.45
		0.178	23.	25.	3.23	0.0		1.29
		0.100	40.	41.	3.28	0.1		1.22
		.0333	70	70.	3.39	0.1		0.70
031290	100	0.311	25.	28.	3.36	38.0	3.24	2.54
		0.124	42.	45.	3.43	38.0		1.66
		.0533	72.	73.	3.56	38.0		1.19
		.0311	100.	98.	3.72	38.0		0.95
		.0178	137.	135.	3.95	38.0		0.75
131290	100	0.311	–	–	4.42	4.2	3.05	–
		0.124	8.	8.	4.57	4.2		0.32
		.0533	18.	17.	4.73	4.2		0.31
		.0311	35.	32.	4.94	4.2		0.34
181290	100	0.212	76.	76.	2.62	0.1	3.01	5.35
	600	0.212	96.	92.	2.64	0.08	0.2	6.62
	100	0.302	53.	49.	2.63	0.137		5.11
	600	0.302	68.	65.		0.162		6.67
270291	630	0.302	10.	12.	4.06	26.4	2.53	1.31
	210	0.290	8.	8.	4.03	26.4		0.99
	550	0.160	18.	21.	4.12	26.4		1.23
	550	.0167	120.	120.	4.64	26.4		0.79
	550	.0533	60.	49.	4.35	26.4		1.14
090791	500	0.156	13.	15.		0.0	7.60	0.29
	500	0.167	26.	25.	4.51	9.3		0.56
	500	0.156	42.	36.	4.39	18.2		0.80
	500	0.182	44.	31.	4.24	27.1		0.90
	500	0.182	46.	32.	4.22•	37.5		0.93
	500	0.182	56.	42.	4.28•	47.9		1.17
200991	100	0.160	12.	12.	4.50	0.1	7.68	0.23
	100	0.160	38.	39.	3.30	0.1		0.78
	500	0.160	75.	76.	3.46	0.2		1.52
	100	0.178	69.	70.	3.03	0.2		1.55
	500	0.222	126.	125.	3.15	0.3		3.54

Experiment $T = 150°C$								
Sample	*Stirring rate/* rpm	*flow rate/* mg s^{-1}	Ca/ μmol kg^{-1}	Mg/ μmol kg^{-1}	pH	TIC/ mmol kg^{-1}	*Area/* cm^2	*Rate/* nmol $cm^{-2}s^{-1}$
190790	100	0.311	40.	37.	3.80	110.	4.90	2.44
	100	0.186	65.	66.	3.90	110.		2.48
290191	100	.0700	16.	17.	4.63	4.8	2.355	0.49
	300	0.134	18.	17.	4.64	4.8		1.00
	300	0.284	9.	9.	4.50	4.8		1.08
	300	0.391	3.	3.	4.39	4.8		0.50
	300	.0222	44.	45.	4.96	4.8		0.42
200291	500	0.302	20.	13.	4.16	20.8	2.769	1.80
	500	0.136	44.	25.	4.32	20.8		1.69
	500	0.167	32.	21.	4.25	20.8		1.60
	500	.0306	145.	137.	4.80	20.8		1.56
	500	.0611	74.	56.	4.50	20.8		1.43
110591	500	0.116	32.5	24.6	10.35	0.0	8.4	0.39
	500	0.109	60.0	57.6	4.93	6.7		0.76
	500	0.076	110.	100.	4.96	11.0		0.94
	260	0.109	100.	98.7	4.67	20.0		1.30
	250	0.109	120.	111.	4.59*	32.0		1.50
	250	0.204	75.0	65.8	4.41*	40.0		1.71

Table 5.2: Table of internally consistent solution compositions (compare with Table A.5) from the 150°C runs. These compositions were used as input for the high temperature speciation calculations whose results are presented in Table 5.5. Notes – * pH calculated at TIC = 0.028 moles kg^{-1} which is approximately the solubility carbon dioxide at ambient pressure. The pH of those solutions used in the SOLMINEQ input file was calculated based on the given TIC.

Experiment $T = 200°C$								
Sample	*Stirring rate/* rpm	*flow rate/* mg s^{-1}	Ca/ μmol kg^{-1}	Mg/ μmol kg^{-1}	pH	TIC/ mmol kg^{-1}	*Area/* cm^2	*Rate/* nmol $cm^{-2}s^{-1}$
120291	160	.0522	54.	54.	4.57	15.5	2.941	0.96
	500	0.258	32.	26.	4.34	15.5		2.54
	500	0.133	49.	42.	4.50	15.5		2.06
	500	.0203	108.	108.	4.82	15.5		0.74
270391	550	0.133	58.	60.	4.35*	37.5	2.77	2.83
	550	0.222	40.	44.	4.26*	37.5		3.37
	550	.0233	108.	106.	4.57*	37.5		0.90
	550	.0555	72.	75.	4.43*	37.5		1.47
240691	180	0.182	23.	23.	–	0.0	8.00	0.52
	500	0.158	38.	36.	4.67	8.3		0.73
	500	0.160	48.	44.	4.45	17.5		0.92
	500	0.160	83.	71.	4.47	26.4		1.54
	500	0.160	82.	69.	4.44*	34.3		1.51
	500	0.196	80.	68.	4.43*	44.0		1.81

Table 5.3: Table of internally consistent solution compositions (compare with Table A.6) from the 200°C runs. These compositions were used as input for the high temperature speciation calculations whose results are presented in Table 5.6. Notes – * pH calculated at TIC = 0.028 moles kg^{-1} which is approximately the solubility carbon dioxide at ambient pressure. The pH of those solutions used in the SOLMINEQ input file was calculated based on the given TIC.

5.2.1 Stoichiometry of dissolution

Busenberg and Plummer (1982) reported that stoichiometric dissolution of dolomite proceeds only after a period of non-stoichiometric dissolution in which Ca is released preferentially to Mg. They calculated that the excess Ca released would lead to a Ca depleted layer at the dolomite surface of only about a single atomic layer. A reacted dolomite was sent to be analysed by J. Price using the SIMS at the University of Western Ontario. No cation depleted zone was detected (Price, personal communication). With the exception of some samples from runs 240691 (200°C) and 090791

(100°C), there was no systematic trend to suggest non-stoichiometric dissolution. The exceptional data were collected at high CO_2 pressures, and demonstrated a consistent enrichment of Ca over Mg in the outflow. The analyses seems to be good; the dissolution was stoichiometric for the low CO_2 pressure samples from the same runs, and the low standard submitted along with the samples agreed to within 3% with the expected value. If, in fact, a Mg enriched phase was formed in the autoclave, it must be unstable, since there is no evidence of Mg rich samples from the following run using the same crystal. There may be a retrograde reaction to remove this putative Mg rich phase during the quench or the start up of the next run. In contrast, data from 110591 (150°C), which were collected under similar conditions, did not clearly demonstrate an enrichment of Ca relative to Mg in the output solution. It seems likely that if the dissolution reaction is non-stoichiometric it is only so at relatively high CO_2 pressures.

5.2.2 Determination of Rate Constants

The rate law (Eqns. 5.1 – 5.3) contains 6 unknown parameters, k_1^D – k_4^D, n_1, and n_2. In addition to Eqn. 5.3, other expressions for r_b^D are possible, particularly at 200°C where the reaction seems to be reversible (the reaction affinity approaches 0.). Expressions for the back reaction should include terms based on possible back reactions. Processes which can possibly reduce the reaction rate are: the adsorption of HCO_3^- (the k_4^D term, Busenberg and Plummer, 1982), the adsorption of CO_3^{2-} (the k_5^D term), a reaction between the Ca or Mg and CO_3^{2+} (the k_6^D term), a mechanism similar to that proposed by PWP for calcite (the k_7^D term), and a reaction between Ca or Mg and two bicarbonate ions (the k_8 term). The non-linear least squares minimization program MLSQQ was run to test the rate data against a rate law of the form

$$r = k_1^D[H^+]^{n_1} + k_2^D[H_2CO_3]^{n_2} + k_3^D + k_4^D[HCO_3^-] + k_5^D[HCO_3^-]/[H^+] + ([Ca^{2+}] + [Mg^{2+}])(k_6^D[HCO_3^-]/[H^+] + k_7^D[HCO_3^-] + k_8^D[HCO_3^-]^2). \quad (5.4)$$

In any calculation each of the parameters k_1^D – k_8^D, n_1, and n_2 could be constrained to a fixed value.

At all temperatures, the calculated values of k_4^D – k_8^D were often the wrong sign (they represent back reactions, they should be less than 0) and the probable error associated with these values was invariably greater than the value itself. Consequently, it is impossible to distinguish any form for an expression for the back reaction from these data. In addition, the presence of stirring rate dependence indicates that concentration gradients exist around the dolomite crystal, which suggests that any rate expression need not be simply related to the bulk solution composition.

Results at 100°C

Table 5.4 presents the activity at 100°C of each of the solutes appearing in Eqns. 5.2 and 5.3 as calculated by SOLMINEQ. The solution composition from which these activities are derived are given in Table 5.1. The activities in Table 5.4, and corresponding rates, were used as input to the non-linear least squares regression calculation described above. Results of these calculations suggest that the rate constant k_1 is dependent on stirring rate, while k_2 and k_3 vary between dolomites. If the exponent, n_1, was not constrained, its value varied between 0.9 and 1.1 depending on the data set or the form of the rate expression used. The best-fit value of n_2 varied near about 0.4, but in light of the low temperature results, its value was constrained to 0.5.

The results of these calculations are shown in Fig. 5.3, which is a plot of the measured reaction rate less a term proportional (proportionality constant k_2) to the square root of the carbonic acid concentration as a function of the hydrogen ion activity from the 100°C runs. Data obtained at a high stirring rate (500 rpm) are shown with a solid symbol, those from low stirring rate runs (100 rpm) are shown with open symbols. Three separate crystals were used in the experiments. Different values of k_2 were used for the different crystals. A single value of k_2 ($k_2 = 3.54 \times 10^{-9}$ moles cm^{-2} s^{-1}) was found to fit the rate data obtained from the two crystals described in Table 2.4 as crystal 2 and 3. These data are marked in Fig. 5.3 with squares. The

Table 5.4: Activities of various solutes at run temperature, measured, and calculated rates, from the 100°C runs. The equations used to calculate the rates are: [1] *rate calc*/10^{-9} moles cm^{-2} s^{-1} 2170 $[H^+]$ + 2.06 $\sqrt{[H_2CO_3]}$ + 0.15 (crystal 1, low stirring rate): [2] *rate calc*/10^{-9} moles cm^{-2} s^{-1} = 2870 $[H^+]$ + 2.06 $\sqrt{[H_2CO_3]}$ + 0.15 (crystal 1, high stirring rate): [3] *rate calc*/10^{-9} moles cm^{-2} s^{-1} = 2820 $[H^+]$ + 3.54 $\sqrt{[H_2CO_3]}$ + 0.26 (crystals 2 and 3, high stirring rate): [4] *rate calc*/10^{-9} moles cm^{-2} s^{-1} = 1250 $[H^+]$ + 3.54 $\sqrt{[H_2CO_3]}$ + 0.26 (crystals 2 and 3, low stirring rate).

$[Ca^{2+}]$	$[Mg^{2+}]$	$[H^+]$	$[H_2CO_3]$	$[HCO_3^-]$	ΔG	*rate*	*rate calc*
12.7	13.7	6.13×10^{-4}	3.10×10^{-5}	2.01×10^{-8}	-31.8	$1.45 \pm 15\%$	1.49[1]
19.5	21.4	5.86×10^{-4}	4.80×10^{-5}	3.26×10^{-8}	-30.4	$1.29 \pm 10\%$	1.43[1]
33.8	35.0	5.22×10^{-4}	8.09×10^{-5}	6.17×10^{-8}	-28.5	$1.22 \pm 7\%$	1.30[1]
59.0	59.5	4.05×10^{-4}	1.40×10^{-4}	1.37×10^{-7}	-26.1	$0.70 \pm 4\%$	1.05[1]
21.8	24.6	4.30×10^{-4}	3.80×10^{-2}	3.51×10^{-5}	-19.4	$2.54 \pm 10\%$	1.48[1]
36.6	39.4	3.65×10^{-4}	3.80×10^{-2}	4.14×10^{-5}	-18.2	$1.66 \pm 7\%$	1.34[1]
62.2	63.5	2.69×10^{-4}	3.80×10^{-2}	5.62×10^{-5}	-16.5	$1.19 \pm 4\%$	1.13[1]
85.7	84.7	1.85×10^{-4}	3.79×10^{-2}	8.15×10^{-5}	-14.9	$0.95 \pm 3\%$	0.95[1]
116.	115.	1.06×10^{-4}	3.79×10^{-2}	1.43×10^{-4}	-12.8	$0.75 \pm 3\%$	0.78[1]
0.	0.	3.55×10^{-5}	4.15×10^{-3}	4.66×10^{-5}		–	–
7.58	7.60	2.47×10^{-5}	4.13×10^{-3}	6.65×10^{-5}	-15.8	$0.32 \pm 20\%$	0.34[1]
16.8	15.9	1.69×10^{-5}	4.10×10^{-3}	9.66×10^{-5}	-13.6	$0.31 \pm 8\%$	0.32[1]
32.1	29.5	1.03×10^{-5}	4.04×10^{-3}	1.56×10^{-4}	-11.2	$0.34 \pm 4\%$	0.30[1]
57.1	58.6	2.38×10^{-3}	1.60×10^{-4}	2.68×10^{-8}	-31.2	$5.35 \pm 3\%$	5.33[1]
72.1	70.8	2.27×10^{-3}	2.10×10^{-4}	3.68×10^{-8}	-30.3	$6.62 \pm 3\%$	6.72[2]
40.0	38.0	2.32×10^{-3}	1.37×10^{-4}	2.35×10^{-8}	-31.9	$5.11 \pm 4\%$	5.21[1]
51.4	50.3	2.22×10^{-3}	1.62×10^{-4}	2.91×10^{-8}	-31.2	$6.67 \pm 3\%$	6.57[2]
9.31	11.2	8.10×10^{-5}	2.63×10^{-2}	1.29×10^{-4}	-16.2	$1.31 \pm 20\%$	1.07[3]
7.47	7.49	8.70×10^{-5}	2.63×10^{-2}	1.20×10^{-4}	-16.8	$0.99 \pm 20\%$	0.94[4]
16.6	19.4	7.09×10^{-5}	2.62×10^{-2}	1.47×10^{-4}	-14.9	$1.23 \pm 20\%$	1.04[3]
102.	103.	2.06×10^{-5}	2.51×10^{-2}	4.99×10^{-4}	-8.7	$0.79 \pm 3\%$	0.90[3]
53.7	44.1	4.06×10^{-5}	2.61×10^{-2}	2.57×10^{-4}	-11.8	$1.14 \pm 3\%$	0.95[3]
12.3	14.2	4.67×10^{-7}	6.44×10^{-5}	5.49×10^{-5}	-9.4	$0.29 \pm 15\%$	0.29[3]
24.0	23.2	2.81×10^{-5}	9.17×10^{-3}	1.30×10^{-4}	-13.4	$0.56 \pm 8\%$	0.68[3]
38.2	32.9	3.70×10^{-5}	1.80×10^{-2}	1.94×10^{-4}	-12.6	$0.80 \pm 5\%$	0.84[3]
39.9	28.2	5.23×10^{-5}	2.69×10^{-2}	2.05×10^{-4}	-13.1	$0.92 \pm 3\%$	0.99[3]
41.6	29.1	6.79×10^{-5}	3.73×10^{-2}	2.18×10^{-4}	-13.3	$0.93 \pm 3\%$	1.14[3]
50.0	37.8	7.10×10^{-5}	4.76×10^{-2}	2.67×10^{-4}	-12.8	$1.17 \pm 3\%$	1.24[3]
10.8	11.6	6.30×10^{-5}	2.26×10^{-5}	1.43×10^{-7}	-25.8	$0.23 \pm 15\%$	0.36[4]
33.0	34.0	4.99×10^{-4}	7.74×10^{-5}	6.18×10^{-8}	-28.4	$0.78 \pm 5\%$	0.91[4]
64.3	65.6	3.45×10^{-4}	1.59×10^{-4}	1.83×10^{-7}	-25.3	$1.52 \pm 3\%$	1.24[3]
56.4	57.8	9.27×10^{-4}	1.39×10^{-4}	5.97×10^{-8}	-28.6	$1.55 \pm 3\%$	1.46[4]
102.	104.	7.03×10^{-4}	2.52×10^{-4}	1.43×10^{-7}	-26.0	$3.54 \pm 3\%$	2.26[3]

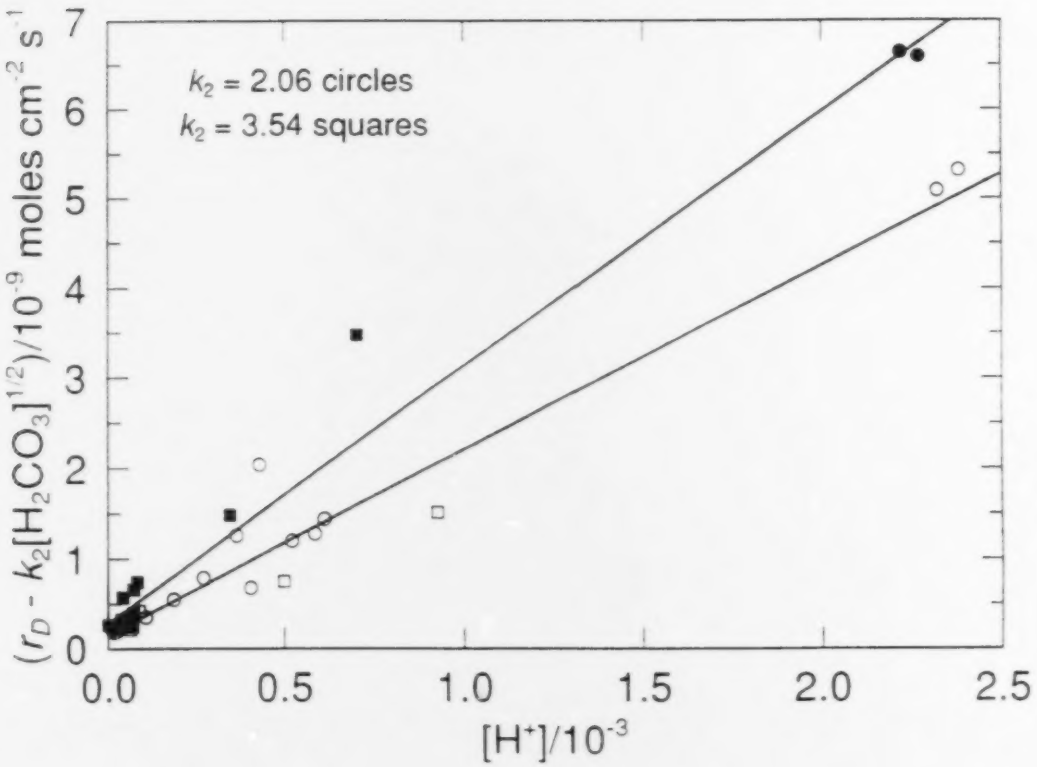

Figure 5.3: Rate of dolomite dissolution at 100°C, less the contribution from the term $k_2[H_2CO_3]^{1/2}$ as a function of $[H^+]$. The data marked with open symbols are from low stirring rate runs, closed symbols represent high stirring rate runs.

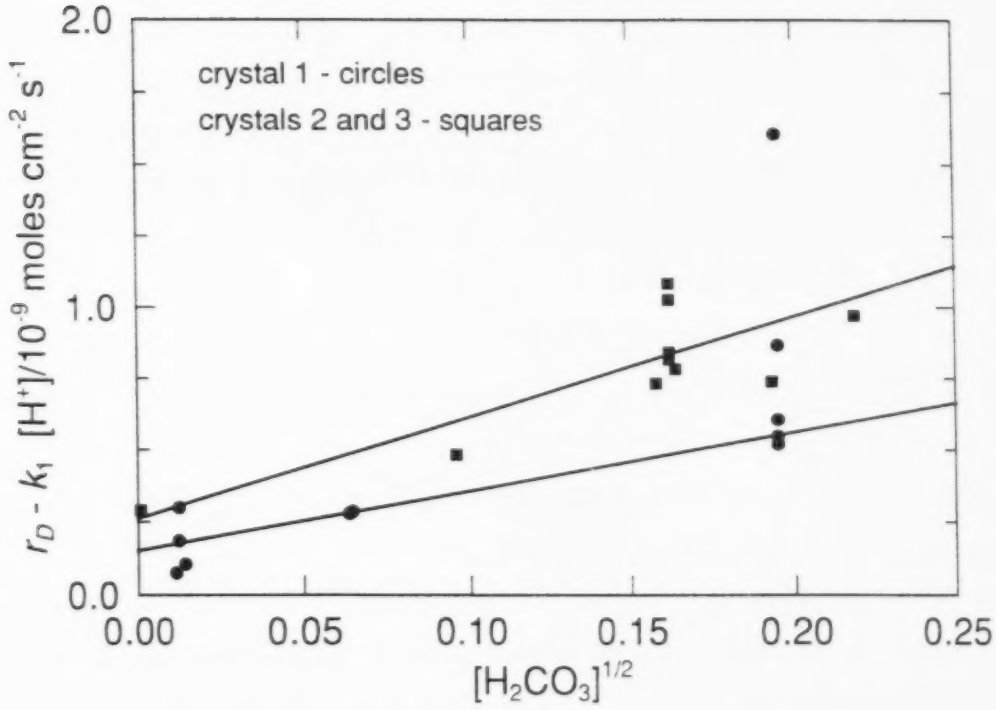

Figure 5.4: Rate of dolomite dissolution at 100°C, less the contribution from the term k_1 [H^+] as a function of [H_2CO_3]$^{1/2}$.

value of k_2 used for crystal 1 was 2.06 $\times 10^{-9}$ moles cm^{-2} s^{-1} and the results from this crystal are shown with circles. The data from the high stirring rate runs tend to fall along one straight line, while the behaviour of the low stirring rate data is more erratic. Generally, the data from crystal 1 tend to define a greater slope than the data from crystals 2 and 3. In any event, there is no need to invoke a back reaction to fit the rate expression to the data. The data representing the low stirring rate runs tend to fall along a line whose slope is a factor of about 1.4 times (crystal 1) or 2.2 times (crystal 2 and 3) smaller than that defining the high stirring rate data. This indicates a stirring dependence in the reaction through the rate constant k_1. This is similar to the behaviour demonstrated by calcite at lower temperatures (Plummer *et al.*, 1978). The variation in k_2^D and k_3^D between crystals was about a factor of two, and is small compared to the variability noted by Busenberg and Plummer (1982).

Fig. 5.4 presents a plot similar to Fig. 5.3 but instead of plotting the difference of the measured rate and the k_2^D term against $[H^+]$ the difference between the measured rate and the k_1^D term is plotted against $[H_2CO_3]$. The plot shows a good deal of scatter, but it does demonstrate that the values of k_2^D are required to fit the data from different crystals. The five circles at about $\sqrt{[H_2CO_3]} = 0.2$ are from run 031290.

The major discrepancies between the fit and measured rates are in the first two samples in the second run (031290) and the high stirring rate data from the last run (200991). The difficulties associated with the data from 031290 may be, at least in part, due to a failure to properly resolve the inconsistencies in the data (see Appendix). The discrepancies in the data from 200991 cannot be resolved.

Results at 150°C

The 150°C data were treated in the manner described above. The activities of those solutes appearing in Eqns. 5.2 and 5.3 at run temperature are given in Table 5.5.

Fits to the 150°C data (at 100, 300, and 500 rpm) found that k_1 increases in proportion to the stirring rate (SR) raised to the 0.82 power. This variation with stirring rate is much greater than was seen at 100°C, where the exponent is less

$[Ca^{2+}]$ $/10^{-6}$	$[Mg^{2+}]$ $/10^{-6}$	$[H^+]$	$[H_2CO_3]$ $/10^{-3}$	$[HCO_3]$ $/10^{-4}$	ΔG $/kJ\ mol^{-1}$	*rate*	*rate calc*
35.0	32.9	8.61×10^{-5}	110.	2.43	−50.2	2.44	2.56
55.4	57.4	6.41×10^{-5}	110.	3.26	−42.7	2.48	2.46
14.9	15.9	1.16×10^{-5}	4.7	0.77	−49.8	0.49	0.68
16.7	15.8	1.13×10^{-5}	4.7	0.80	−59.4	1.00	0.78
8.5	8.5	1.73×10^{-5}	4.7	0.52	−49.0	1.08	0.85
2.9	2.9	2.50×10^{-5}	4.8	0.36	−72.4	0.50	0.94
39.1	40.4	4.91×10^{-6}	4.6	1.79	−31.4	0.42	0.70
18.4	12.0	3.84×10^{-5}	20.7	1.03	−56.5	1.80	1.82
39.4	22.6	2.36×10^{-5}	20.6	1.66	−44.8	1.69	1.56
29.0	19.2	2.90×10^{-5}	20.7	1.36	−49.4	1.60	1.66
115.	112.	5.99×10^{-6}	20.1	6.40	−16.3	1.56	1.24
63.9	49.1	1.46×10^{-5}	20.5	2.68	−33.5	1.43	1.40
28.3	12.1	9.16×10^{-9}	0.0	0.52	−0.8	0.39	0.23
52.3	50.9	5.24×10^{-6}	6.4	2.35	−28.0	0.76	0.83
91.1	84.8	4.85×10^{-6}	10.6	4.15	−19.7	0.94	0.97
83.3	84.1	9.60×10^{-6}	19.6	3.89	−25.1	1.30	1.30
98.2	93.3	1.30×10^{-5}	31.5	4.61	−25.1	1.50	1.45
64.1	57.3	2.50×10^{-5}	39.7	3.03	−39.7	1.71	1.71

Table 5.4: Activities of various solutes at run temperature, measured, and calculated rates, from the 150°C runs. The equation used to calculate the rates are; $rate\ calc/10^{-9}$ moles cm^{-2} s^{-1} = 4620 $[H^+]$ $(SR/100rpm)^{0.82}$ + 5.9 $\sqrt{[H_2CO_3]}(SR/100rpm)^{0.13}$ + 0.22.

than 0.2. As well, greater improvement in the quality of the fits was obtained if the parameter k_2 was allowed to vary slightly with stirring rate (*i.e.* its value increased in proportion to $SR^{0.13}$) than if it was allowed to vary between crystals (which was invoked to fit the 100°C data). The variation of dissolution rate with $[H_2CO_3]^{1/2}$ is shown in Fig. 5.5 which presents the results of the four 150°C runs. The rate of dissolution less 4.62×10^{-3} (SR/100 rpm $)^{0.82}$ $[H^+]$ is plotted against the square root of the carbonic acid activity. While the results of the regression calculation suggested that there was a stirring rate dependence in k_2^D at 150°C, the considerable scatter in Fig. 5.5 makes it difficult to justify such a stirring rate dependence. Fits to the data, in which the exponents n_1 and n_2 were allowed to vary, were slightly better than if n_1 and n_2 were constrained to be 1.0 and 0.5 respectively; however, there are insufficient data to justify changing them.

Results at 200°C

The data collected at 200°C could not be satisfactorily fit to any expressions of the form of Eqn. 5.4. Tabulated data from these runs are given in Table A.6. The stirring rate was 500 or 550 rpm for all but 2 samples (the first and ninth rows) for which it was 170 rpm. It can be seen that the ΔG of the dissolution reaction is approaching 0.0, indicating that there is a significant back reaction. With the exception of a rate determination made using pure water as the input solution, the maximum ΔG reached in any of the 150°C runs was -16.3 kJ mole^{-1}. The likelihood of a significant back reaction, and the presence of substantial concentration gradients around the crystal, make it reasonable to expect that simple rate expressions based on bulk solution analysis, such as Eqns. 5.4, will not describe the dissolution reaction.

Temperature Dependence of Rate Constants

Busenberg and Plummer (1982) noted a sharp break in plots of the logarithm of their measured rate constants against $1/T$ at about 50°C. This temperature also corresponds to the temperature where deviations from $n_1 = 0.5$ were noted. Busenberg

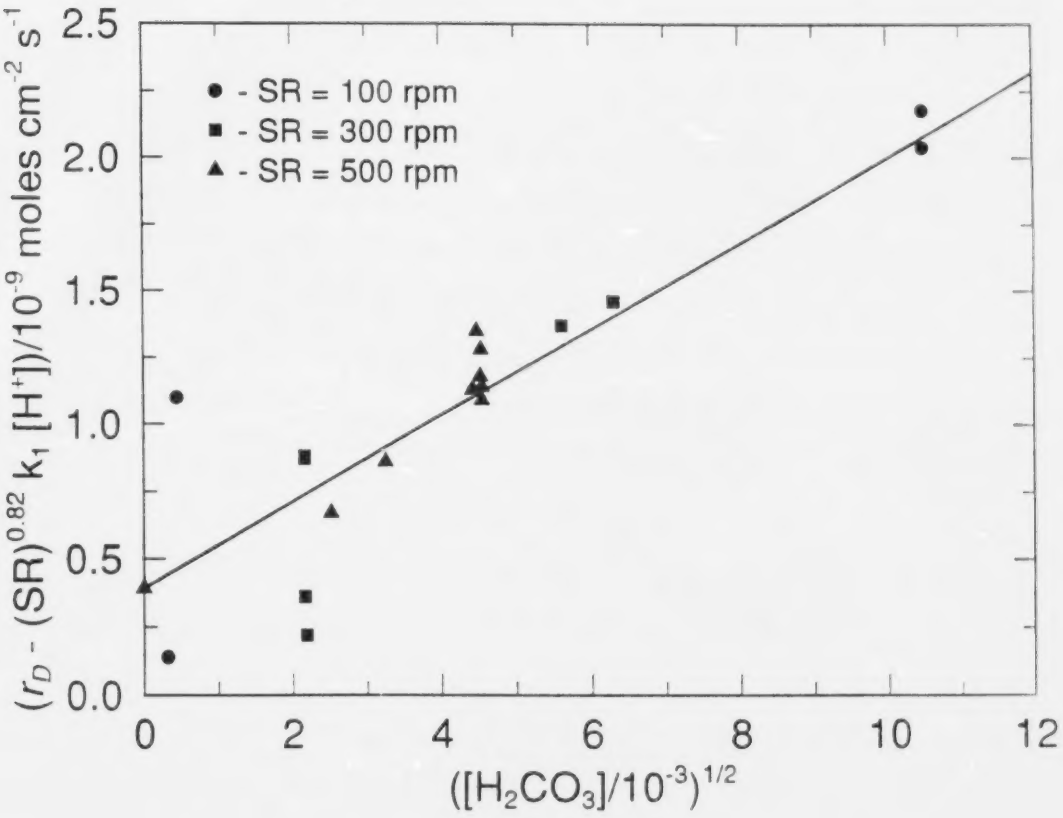

Figure 5.5: Rate of dolomite dissolution at 150°C less the contribution from the term $k_1(SR)$ [H^+] as a function of [H_2CO_3]$^{1/2}$.

and Plummer (1982) associated the break with a probable change in the reaction mechanism. At temperatures above the break the rate constants k_2^D and k_3^D became nearly temperature independent (*i.e.* the associated activation energy essentially vanished). The rate constants varied considerably between crystals; at 65°C $\log(k_2^D/10^{-9}$ moles cm^{-2} $s^{-1})$ varied between 0.1 and 0.35, and the values of $\log(k_3^D/10^{-9}$moles cm^{-2} $s^{-1})$ were between -2.0 and -1.6. The values of $\log(k_3^D/10^{-9}$ moles cm^{-2} $s^{-1})$ presented here were -0.82 and -0.58 at 100°C and -0.66 at 150°C. The values of $\log(k_2^D/10^{-9}$ moles cm^{-2} $s^{-1})$ evaluated at 100°C were 0.31 and 0.55. Since the expression for k_1^D, and k_2^D at 150°C, are stirring rate dependent, means that no comparison can be made between their values as a function of temperature; however, if the 150°C data were fit without considering any stirring rate dependence the value of $\log(k_2^D/10^{-9}$moles cm^{-2} $s^{-1})$ would be about 0.8.

The logarithm of the rate constants k_2 and k_3 report by Busenberg and Plummer (1982) for dolomite from Navarro, Spain are plotted against $1000/T$ along with the values evaluated here in Figs. 5.6 and 5.7. The data from Busenberg and Plummer (1982) are shown as solid circles; the open circles are those reported here. Figure 5.6 demonstrates that, while there seems to be a change in the activation energy near 50°C, it is not as extreme as the results of Busenberg and Plummer (1982) suggest. Figure 5.7 also demonstrates a break in behaviour of k_3^D with temperature, although not until about 100°C.

5.3 Conclusions

The results of this study support the observation of Busenberg and Plummer (1982) that the rate of dolomite dissolution above about 50°C become progressively more limited by diffusional processes as temperature is increased. Evidence for this is the break in the Arrhenius plots for k_2^D and k_3^D at about 50°C and 100°C respectively, and the gradual increase in n_1 with temperature. The value of n_1 changes from the value of 0.5, which describes the surface reaction, to 1.0, which is expected for the

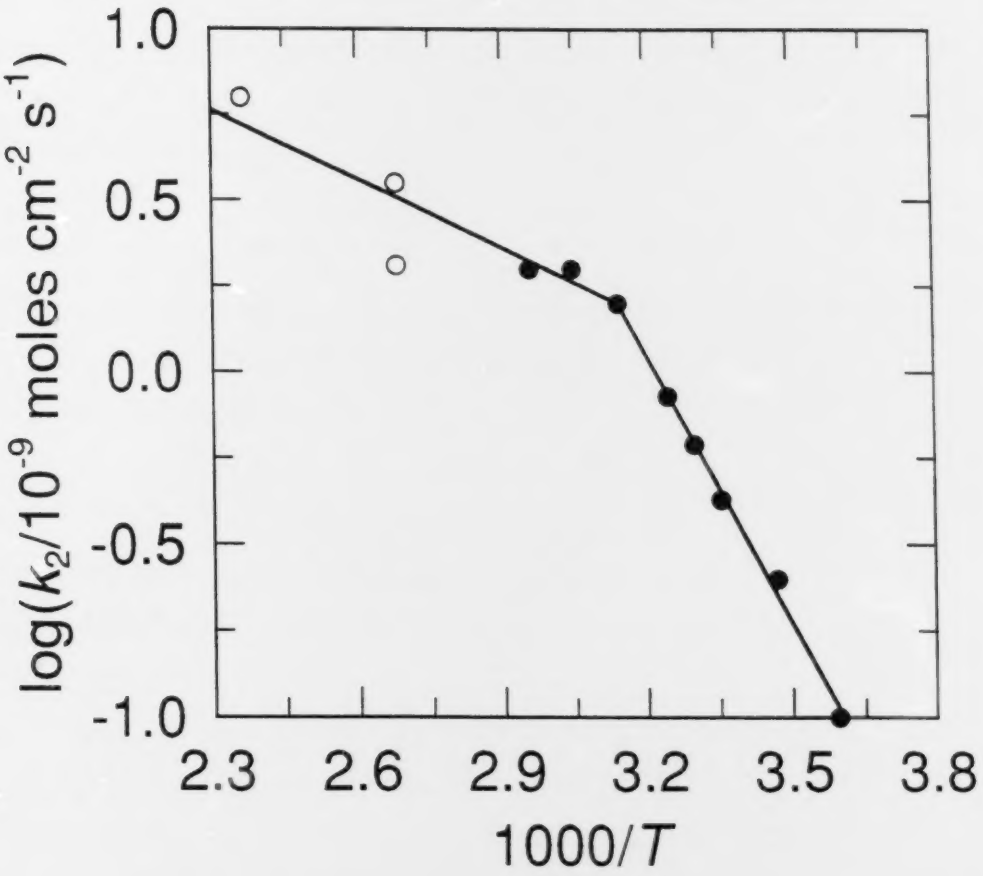

Figure 5.6: The variation of $\log(k_2^D)$ as a function of $1000/T$. Data from Busenberg and Plummer (1982) are marked with a solid circle.

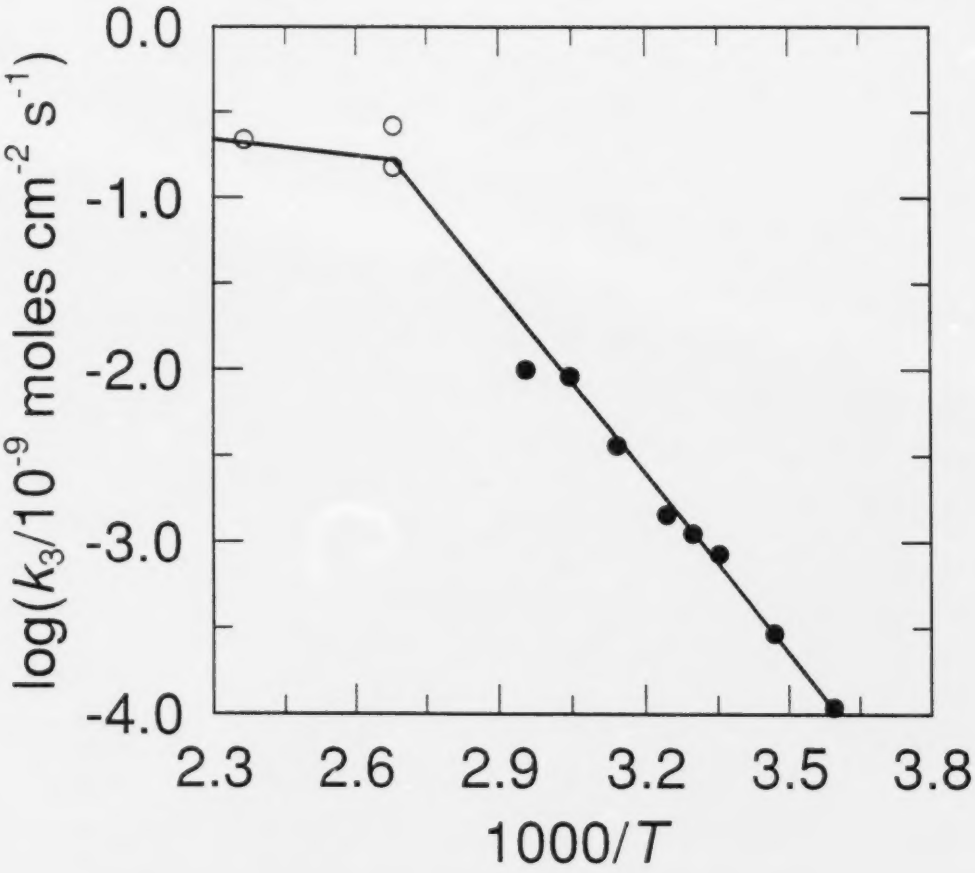

Figure 5.7: The variation of $\log(k_3^D)$ as a function of $1000/T$. Data from Busenberg and Plummer (1982) are marked with a solid circle.

diffusion limited case. The analysis presented in the previous chapter suggested that, if the surface reaction was first order, the reaction remains first order after the onset of transport control. In the case of dolomite, where the surface reaction is likely order 1/2, the situation is more complex. The change of n_1 from 1/2 at 25°C to 1.0 at 100°C most likely indicates a switch to some diffusional limiting step. At about 100°C the rate constant k_1 becomes dependent on the stirring rate. The solution composition immediately adjacent to the dissolving grains becomes more basic than the bulk (measurable) solution, and the measured solution composition becomes less representative of the conditions near the grain. Further increases in temperature increase the sensitivity of the dissolution rate to the stirring rate. This can be seen by noting that at 150°C the difference between k_1^D for crystal 1 at 100 rpm and 500 rpm is about 2.7 times larger than at 100°C. As well, the rate constant k_2^D is more sensitive to the dolomite specimen at 100°C than at 150°C. This suggests that solubility, rather than the surface defects, controls the dissolution rate. The increased variation of k_1^D (a factor of 2.2 increase between 100 and 500 rpm) with stirring rate seen in crystal 2 and 3 (actually the value is based almost exclusively on data from crystal 3) at 100°C may be due to the fact that the third crystal was considerably larger than the first. As such, the stagnant film corresponding to a particular stirring rate may be greater for the third crystal. At higher stirring rates the hydrodynamic conditions near the surface may be sufficiently erratic to obscure this difference. It must also be noted that the 150°C data can be reasonably well described without invoking any size variation in k_1^D.

By 200°C it is likely that the concentration gradients surrounding the dolomite crystal are so great as to make any analysis without consideration of a back reaction meaningless. The lack of a mechanistic model of the back reaction at lower temperatures makes it highly speculative to try to fit the data presented here with any expression for the back reaction. In order to fit rate data with a mechanistic rate expression better control of the hydrodynamics in the solution surrounding the grain is required. Without this control, neither the solution composition at the surface nor

the form of the forward rate expression can be predicted. It is clear, though, that by 200°C the inhibition of dolomite dissolution by HCO_3^-, which is seen at lower temperatures, does not prevent the dissolution reaction from proceeding to equilibrium.

$[Ca^{2+}]$ $/10^{-6}$	$[Mg^{2+}]$ $/10^{-6}$	$[H^+]$ $/10^{-3}$	$[H_2CO_3]$	$[HCO_3^-]$	ΔG	*rate*
45.5	46.4	0.211	1.53×10^{-2}	4.67×10^{-6}	−3.8	0.96
28.3	23.3	0.119	1.54×10^{-2}	8.33×10^{-6}	−7.0	2.54
41.8	36.5	0.185	1.53×10^{-2}	5.33×10^{-6}	−4.6	2.06
90.9	86.3	0.430	1.50×10^{-2}	2.26×10^{-6}	0.2	0.74
48.3	51.4	0.236	3.73×10^{-2}	1.02×10^{-5}	−4.9	2.83
34.3	38.6	0.181	3.73×10^{-2}	1.33×10^{-5}	−6.4	3.37
83.7	86.1	0.418	3.71×10^{-2}	5.72×10^{-6}	−1.7	0.90
58.5	63.1	0.291	3.72×10^{-2}	8.26×10^{-6}	−3.7	1.47
21.1	16.2	0.130	3.26×10^{-5}	1.62×10^{-7}	−4.4	0.52
33.1	31.6	0.147	8.15×10^{-3}	3.57×10^{-6}	−4.6	0.73
41.0	38.3	0.184	1.73×10^{-2}	6.08×10^{-6}	−4.8	0.92
67.3	59.5	0.304	2.61×10^{-2}	5.54×10^{-6}	−2.8	1.54
66.4	57.8	0.303	3.40×10^{-2}	7.24×10^{-6}	−3.3	1.51
64.8	57.1	0.301	4.37×10^{-2}	9.37×10^{-6}	−3.9	1.81

Table 5.5: Activities of various solutes at run temperature and measured rates ($/10^{-9}$ moles cm^{-2} s^{-1}) , from the 200°C runs.

Chapter 6

Mixed Kinetics of Dolomite Dissolution

6.1 Introduction

It was demonstrated in Chapter 1 that at elevated temperatures diffusion tends to limit the rate of dissolution of minerals with retrograde solubility. In Chapter 5 arguments were presented that the rate of dolomite dissolution becomes increasingly dependent on stirring rate above 100°C. This dependence of rate on stirring rate was also noted at 100°C (Lund *et al.*, 1973). Any stirring rate dependence indicates, at least some, transport control of the reaction (Dibble and Tiller, 1981, Chapter 1).

A temperature dependence of the reaction order associated with the consumption of a proton (n_1 in Eqn. 1.13) has been observed by both Busenberg and Plummer (1982) and Lund *et al.* (1973). Lund *et al.* (1973) suggested, based on this observation, that the rate limiting step in the dissolution of dolomite involved a reaction between adsorbed hydrogen and the dolomite matrix. They further assumed that the adsorption is described by a Freundlich isotherm; the change in the reaction order is due to an increase in adsorbed hydrogen with temperature. Similar adsorption based models have been used to describe albite dissolution (Chou and Wollast, 1985) and minerals in general (Wieland *et al.*, 1988).

An alternative explanation is possible. The change in n_1 in Eqn. 1.13 from 0.5 to near 1.0 between 25 and 100°C suggests that, at the higher temperature, the

dissolution reaction consumes H^+ so rapidly that the first order transport reaction begins to limit the reaction. The gradual change in n_1 may reflect the transition from surface controlled to mixed reaction kinetics. Analysis of the dissolution of dolomite with the model of mixed kinetics developed in Chapter 4 may give insight as to the extent that diffusional processes limit the rate of dissolution of dolomite.

Busenberg and Plummer (1982) investigated the rate of dissolution as a function of temperature and of stirring rate from 1.5 to 65°C; Figs. 6.1 and 6.2 present some results from this study. Fig. 6.1 demonstrates the dependence of dissolution rate (at low CO_2 pressures) on pH as a function of temperature. The slope of the lines on this log–log plot give the reaction order n_1; above 45° C it clearly increases with temperature. Fig. 6.2 is a plot of the logarithm of the dissolution rate as a function of stirring rate at 45°C. There is no detectable dependence of dissolution rate on stirring rate. The experiments of Busenberg and Plummer (1982) used a suspended dolomite sample, much the same as described Chapter 2. The hydrodynamics of this setup are poorly defined; however, there is evidence that the effective stagnant boundary layer is small. In a study of calcite dissolution Busenberg and Plummer (1986) reported a value of k_1^C (Eqn. 3.1) for calcite dissolution at a stirring rate of 260 rpm. of $10^{-2.061}$ which is about a factor of 5 less than the limiting rate constant $k_1^{C\prime}$ reported for Iceland spar by Compton *et al.* (1989). Calculations presented in Chapter 4 (Fig. 4.9) suggest that a stagnant film thickness of about 6 μm ($\delta^{-1} = 0.17$) leads to an apparent k_1^C which is about a factor of five less than $k_1^{C\prime}$. The lowest stirring rate that Busenberg and Plummer (1982) report dolomite dissolution rates for is 260 rpm, so their data likely corresponds to stagnant film thickness of 6 μm and less. So although they varied the stirring rate within their reactor by an order of magnitude, it is quite likely that they failed to work under conditions where any stirring rate dependence would be detectable. In other words, the stagnant surface film was too thin, even at their lowest stirring rate, for diffusional processes to limit the reaction rate appreciably. The slower rate of dolomite dissolution accounts for the difficulty in detecting the stirring rate dependence.

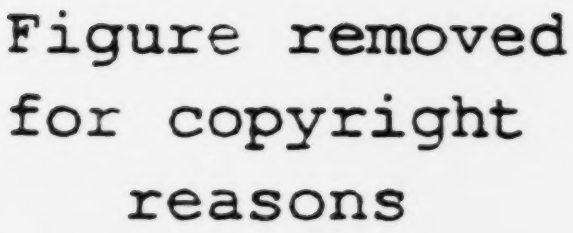

Figure 6.1: Dissolution rates of dolomites as a function of pH and T at $pCO_2 = 0$. (after Busenberg and Plummer, 1982).

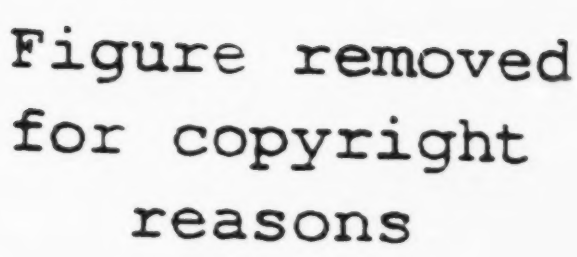

Figure 6.2: Dissolution rates of dolomites as a function of stirring rate for three bulk solution compositions at 45°C (after Busenberg and Plummer, 1982).

6.2 Theory

The only differences between the treatment of dolomite dissolution kinetics and the treatment of calcite presented in Chapter 4 is that the surface rate law is given by Eqn. 5.2 (with both n_1 and n_2 equal to 0.5)

$$r_f^D = k_1^D[\mathrm{H^+}]^{1/2} + k_2^D[\mathrm{H_2CO_3}]^{1/2} + k_3^D$$

instead of Eqn. 3.1, and that the diffusion of another component (Mg) must be considered. The treatment of the back reaction is also different. The expression proposed by Busenberg and Plummer (1982) for the rate of the back reaction is simply (Eqn 5.3),

$$r_b = k_4^D[\mathrm{HCO_3^-}].$$

The form of this expression suggests that $\mathrm{HCO_3^-}$ adsorption on the surface of the dolomite is responsible for the reduction of reaction rate with reaction progress. Given the empirical nature of the expression for the back reaction, it was ignored in these calculations. Since the calculations were done exclusively in acidic, Ca, Mg poor solutions (in order to simplify the model calculations by neglecting $\mathrm{OH^-}$, $\mathrm{CO_3^{2-}}$, and various ion pairs), failure to consider a back reaction should have very little impact on the calculation. However, at higher temperatures, or greater values of δ, a higher surface saturation state is expected and the calculations may overestimate the dissolution rate.

Since dolomite dissolution is less rapid than calcite dissolution, and since the 25°C calculations presented in Chapter 4 imply that, in acidic solutions, the bulk and surface $[\mathrm{H^+}]$ are at least of the same order of magnitude, assumptions about the speciation can be made which were not made in Chapter 4. These are: the concentrations of $\mathrm{CO_3^{2-}}$ and $\mathrm{OH^-}$ are negligible, and no ion pairs of Ca or Mg form. This simplifies the set of equations that must be solved to:

$$\sum_{i=1}^{6} z_i \frac{dc_i}{dx} = 0 \qquad 6.1$$

$$\sum_{i=1}^{6} (D_{\mathrm{H_2CO_3},i} + D_{\mathrm{HCO_3^-},i}) \frac{dc_i}{dx} = -2r_f^D \qquad 6.2$$

$$\sum_{i=1}^{6}(D_{Cl^-,i})\frac{dc_i}{dx} = 0 \qquad 6.3$$

$$\sum_{i=1}^{6}(D_{Ca^{2+},i})\frac{dc_i}{dx} = -r_f^D \qquad 6.4$$

$$\sum_{i=1}^{6}(D_{Mg^{2+},i})\frac{dc_i}{dx} = -r_f^D \qquad 6.5$$

$$\frac{1}{[H^+]}\frac{d[H^+]}{dx} + \frac{1}{[HCO_3^-]}\frac{d[HCO_3^-]}{dx} = \frac{1}{[H_2CO_3]}\frac{d[H_2CO_3]}{dx}. \qquad 6.6$$

Values of r_f^D are given by Eqn. 5.2. Eqns. 6.1–6.6 were solved using an algorithm similar to that was used in Chapter 4, although, the transport of a fourth component, Mg, is included. The temperature dependence of the constants in Eqns. 6.1 - 6.6 were all extrapolated using

$$\log k_i^D = a_i + \frac{b_i}{T}. \qquad 6.7$$

The low temperature rate expression (Eqn. 5.2, both n_1 and n_2 equal to 0.5) was used for all the temperatures.

6.3 Numerical Results

Calculated profiles of the ion distribution in the vicinity of the dolomite surface, similar to Figs. 4.1 – 4.5 are presented in Figs. 6.3 – 6.10. The bulk solution was assumed to contain 10^{-3} molar HCl with no appreciable TIC, Ca, or Mg. The physical parameters used in the calculations, with the exception of Cl_b^-, are given in Table 6.1. Cl_b^- can be read off the Cl^- *vs.* distance plot for the profile of interest. The concentration of TIC is sufficiently low in the solution that the contribution of H_2CO_3 to the dissolution rate will be negligible in comparison to the contribution from H^+. It is apparent that the rate of reaction will be stirring rate independent (*i.e.* there are no appreciable gradients in those species (specifically H^+) that directly influence the reaction rate) at 25°C (Fig. 6.3, 6.4), some gradients form at 45°C (Fig. 6.5, Fig. 6.6), and the gradients are most noticeable for δ= 25 μm. By 65 and 100°C the solution chemistry changes around the dissolving grain (Fig 6.7 – 6.10), indicating a shift to mixed reaction control.

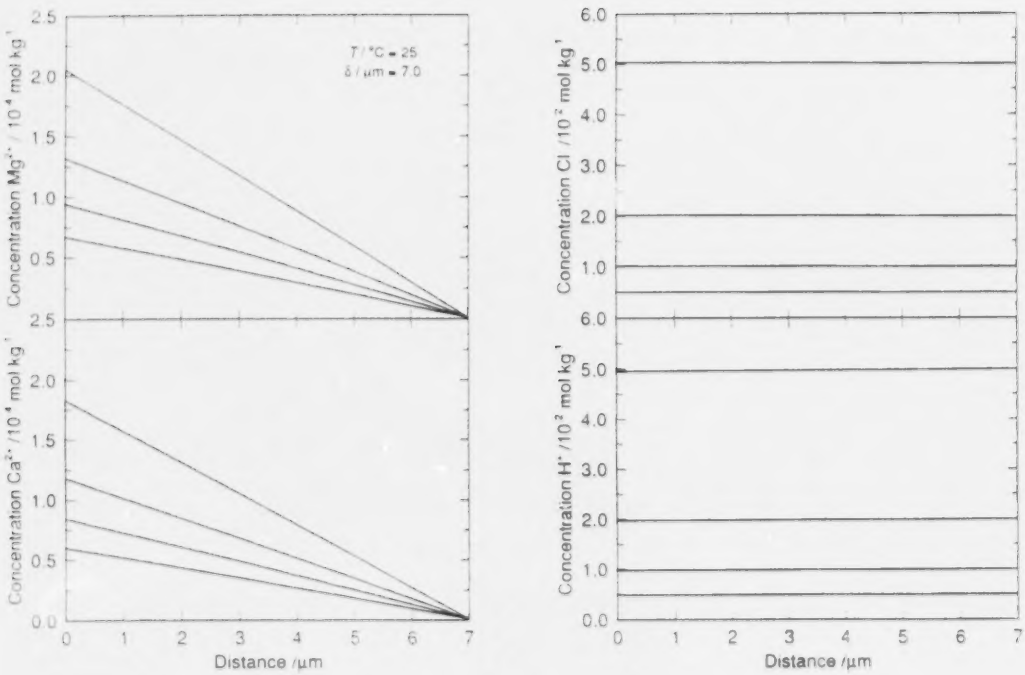
T / °C = 25
δ / μm = 7.0
Concentration Mg2+ / 10-4 mol kg-1
Concentration Ca2+ /10-4 mol kg-1
Concentration Cl- /10-2 mol kg-1
Concentration H+ /10-2 mol kg-1
Distance /μm
Distance /μm

Figure 6.3: Calculated solute concentrations as a function of the distance away from a dolomite crystal at 25°C at $\delta = 7.0$ μm. Profiles are presented for four bulk HCl concentrations (0.5, 1.0, 2.0, and 5.0 mmoles/kg).

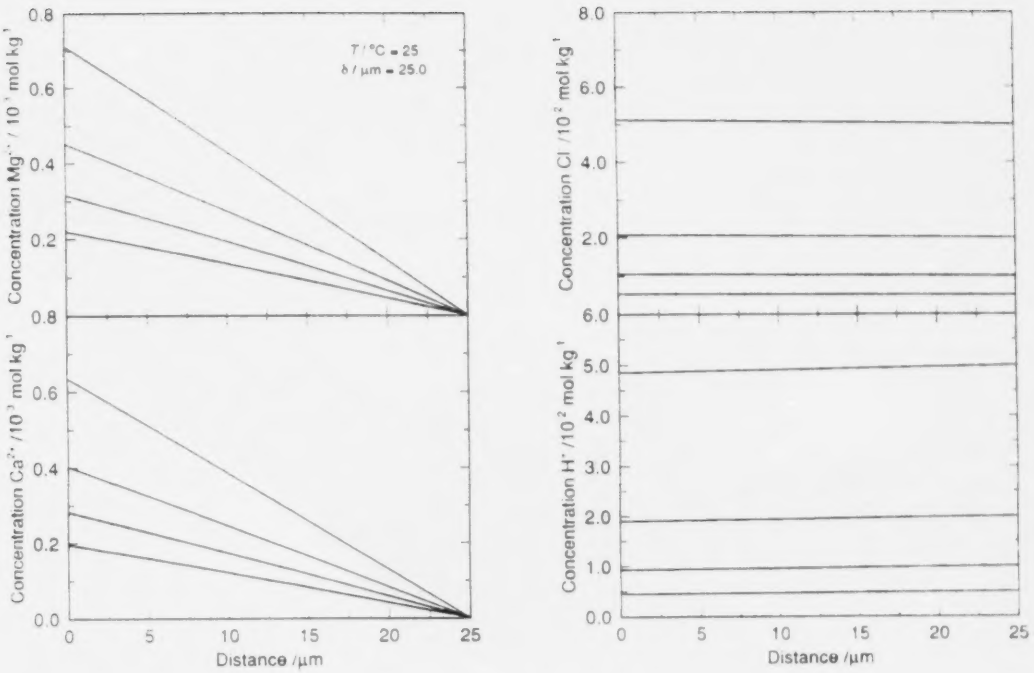
T / °C = 25
δ / μm = 25.0
Concentration Mg2+ / 10-1 mol kg-1
Concentration Ca2+ /10-1 mol kg-1
Concentration Cl- /10-2 mol kg-1
Concentration H+ /10-2 mol kg-1
Distance /μm
Distance /μm

Figure 6.4: Calculated solute concentrations as a function of the distance away from a dolomite crystal at 25°C at $\delta = 25.0$ μm. Profiles are presented for four bulk HCl concentrations (0.5, 1.0, 2.0, and 5.0 mmoles/kg).

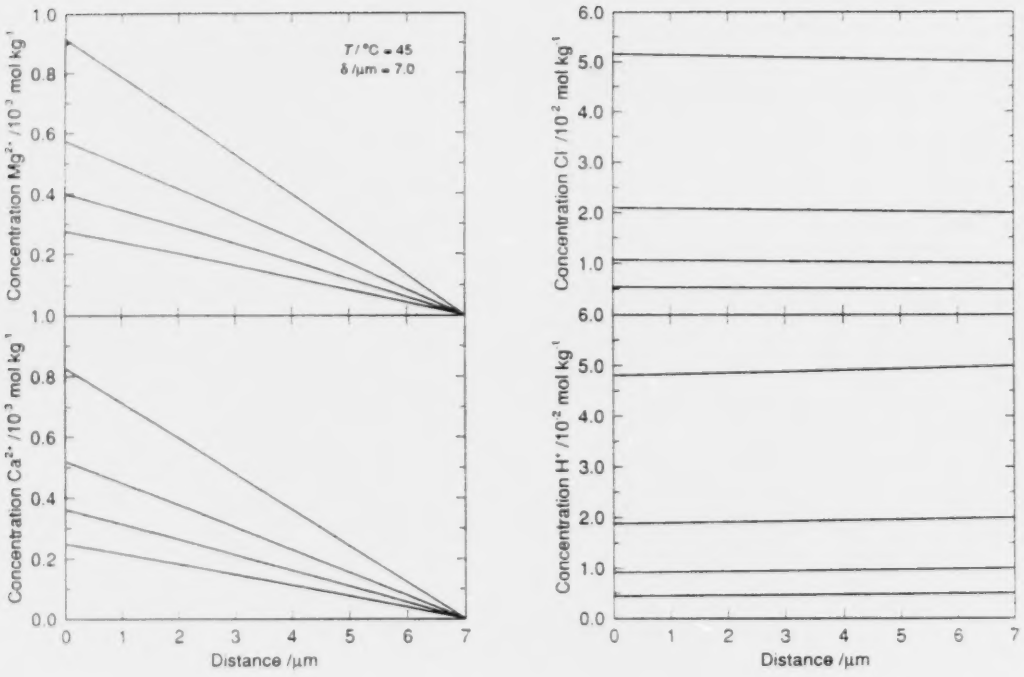
T / °C = 45
δ /μm = 7.0
Concentration Mg2+ /10-3 mol kg-1
Concentration Ca2+ /10-3 mol kg-1
Concentration Cl- /10-2 mol kg-1
Concentration H+ /10-2 mol kg-1
Distance /μm
Distance /μm

Figure 6.5: Calculated solute concentrations as a function of the distance away from a dolomite crystal at 45°C at $\delta = 7.0$ μm. Profiles are presented for four bulk HCl concentrations (0.5, 1.0, 2.0, and 5.0 mmoles/kg).

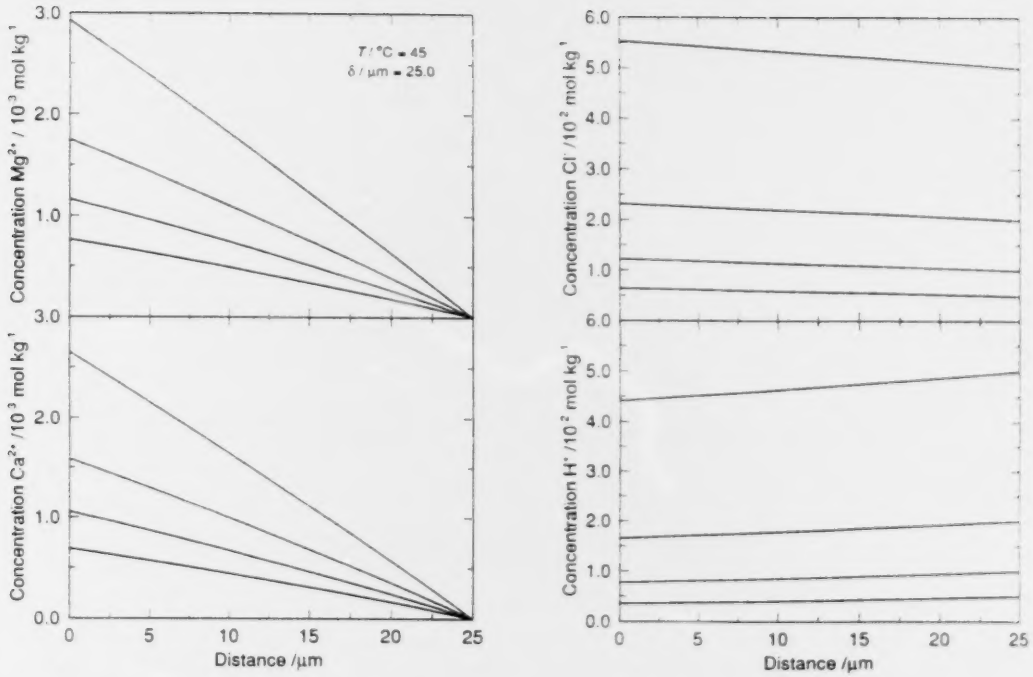
T / °C = 45
δ / μm = 25.0
Concentration Mg2+ / 10-3 mol kg-1
Concentration Ca2+ /10-3 mol kg-1
Concentration Cl- /10-2 mol kg-1
Concentration H+ /10-2 mol kg-1
Distance /μm
Distance /μm

Figure 6.6: Calculated solute concentrations as a function of the distance away from a dolomite crystal at 45°C at $\delta = 25.0$ μm. Profiles are presented for four bulk HCl concentrations (0.5, 1.0, 2.0, and 5.0 mmoles/kg).

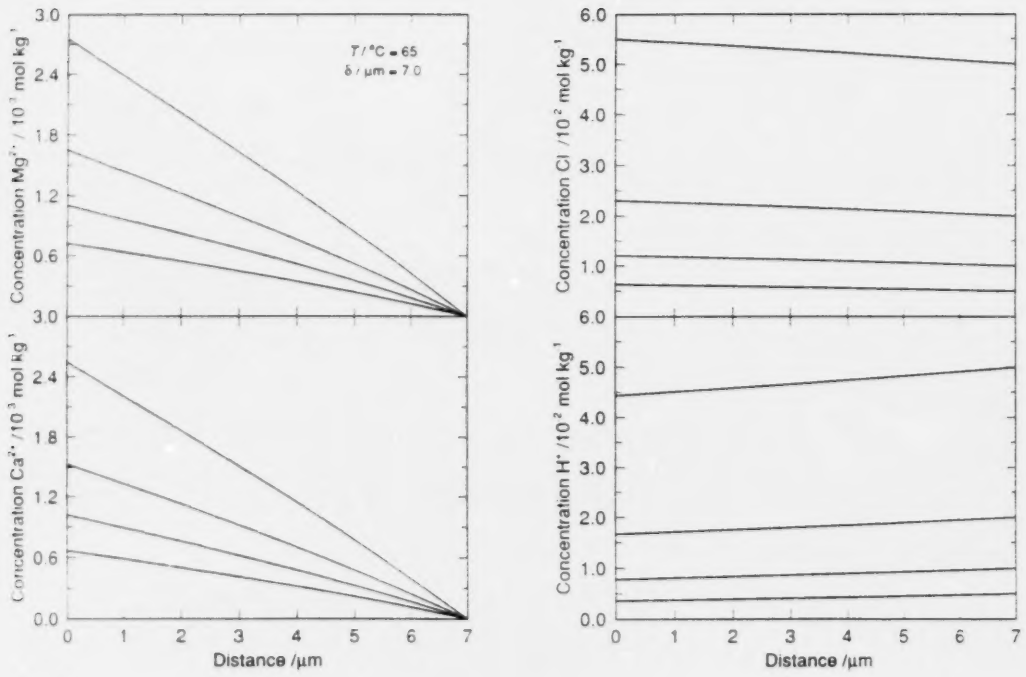
T/°C = 65
δ / μm = 7.0
Concentration Mg2+ / 10-1 mol kg-1
Concentration Ca2+ /10-3 mol kg-1
Concentration Cl- /10-2 mol kg-1
Concentration H+ /10-2 mol kg-1
Distance /μm
Distance /μm

Figure 6.7: Calculated solute concentrations as a function of the distance away from a dolomite crystal at 65°C at $\delta = 7.0$ μm. Profiles are presented for four bulk HCl concentrations (0.5, 1.0, 2.0, and 5.0 mmoles/kg).

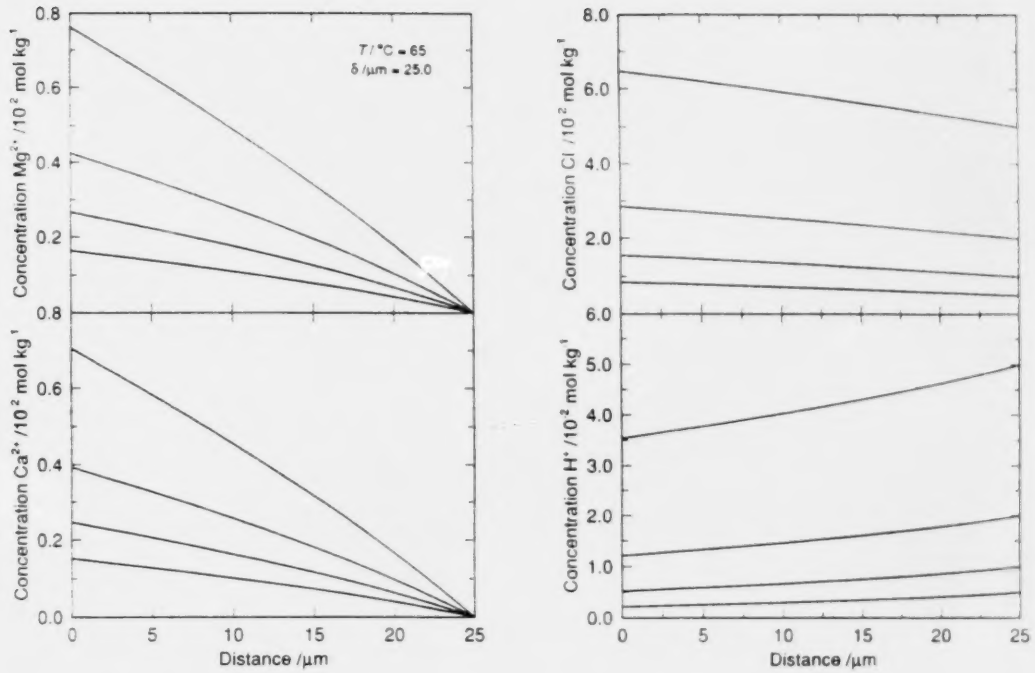
T / °C = 65
δ /μm = 25.0
Concentration Mg2+ /10-2 mol kg-1
Concentration Ca2+ /10-2 mol kg-1
Concentration Cl- /10-2 mol kg-1
Concentration H+ /10-2 mol kg-1
Distance /μm
Distance /μm

Figure 6.8: Calculated solute concentrations as a function of the distance away from a dolomite crystal at 65°C at $\delta = 25.0$ μm. Profiles are presented for four bulk HCl concentrations (0.5, 1.0, 2.0, and 5.0 mmoles/kg).

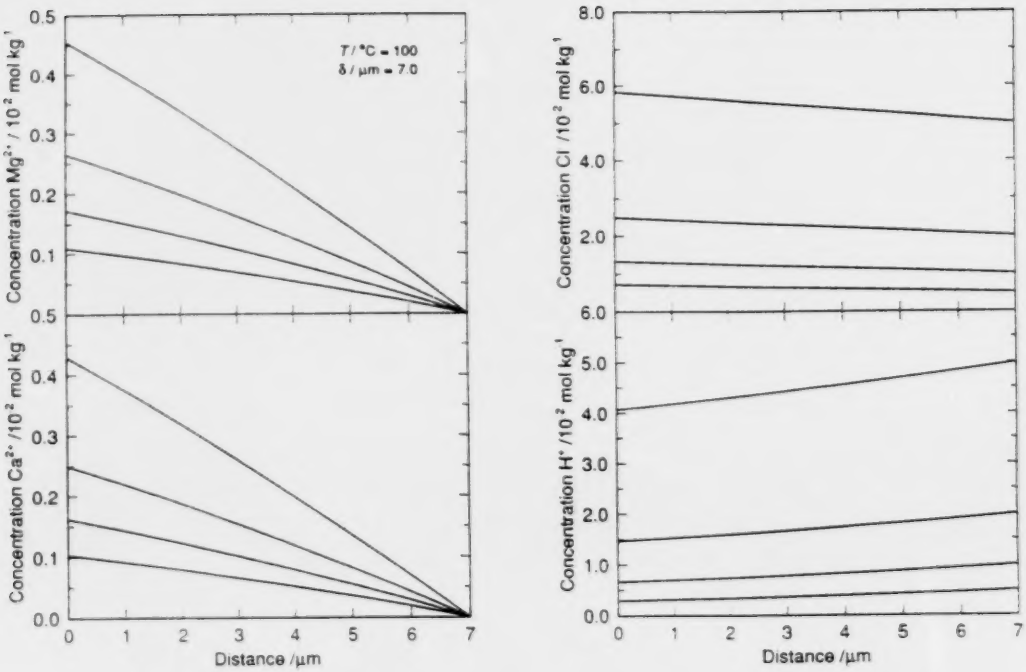
T / °C = 100
δ / μm = 7.0
Concentration Mg2+ / 10-2 mol kg-1
Concentration Ca2+ /10-2 mol kg-1
Concentration Cl /10-2 mol kg-1
Concentration H+ /10-2 mol kg-1
Distance /μm
Distance /μm

Figure 6.9: Calculated solute concentrations as a function of the distance away from a dolomite crystal at 100°C at $\delta = 7.0$ μm. Profiles are presented for four bulk HCl concentrations (0.5, 1.0, 2.0, and 5.0 mmoles/kg).

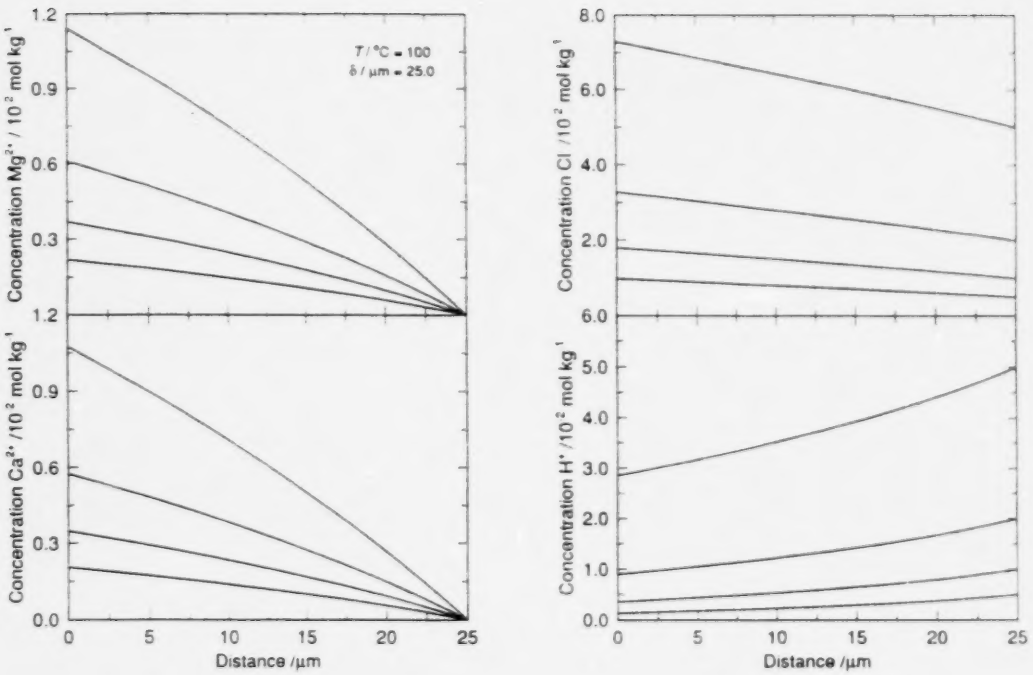
T / °C = 100
δ / μm = 25.0
Concentration Mg2+ / 10-2 mol kg-1
Concentration Ca2+ /10-2 mol kg-1
Concentration Cl /10-2 mol kg-1
Concentration H+ /10-2 mol kg-1
Distance /μm
Distance /μm

Figure 6.10: Calculated solute concentrations as a function of the distance away from a dolomite crystal at 100°C at $\delta = 25.0$ μm. Profiles are presented for four bulk HCl concentrations (0.5, 1.0, 2.0, and 5.0 mmoles/kg).

Equations 6.1 - 6.6 will only give an adequate description of the system in acidic media. These equations were only solved for HCl rich solutions; these solutions are the most likely to result in a transport limited reaction. Since the solutions are all acidic and H_2CO_3 poor, the rate of dolomite dissolution, r^D, can be written, to a good approximation as

$$r^D = k_1^D \sqrt{H^+(s)}. \tag{6.7}$$

If log H^+(s) is a linear function of log H^+(b), then

$$\log H^+(s) = c + m \log H^+(b) \tag{6.8}$$

and

$$\log r^D = \log k_1^D + c + \frac{m}{2} \log H^+(b) \tag{6.9}.$$

Fig. 6.11a is a plot of calculated log (H^+(b)) as a function of log (H^+(s)) at 25°C for 4 values of δ (7, 10, 15 and 25 μm). There is essentially no difference between any of these lines and the line that represents a pure surface controlled reaction (log (H^+(s))= log (H^+(b)). The same calculations were repeated for 45°C, 65°C, and 100°C, and the results presented in Figs. 6.11b, 6.11c, and 6.11d. These clearly demonstrate a marked departure from the case of pure surface reaction control, and the extent of the departure increases with the temperature. Although there is curvature in the plots, it is slight, and would be obscured by the noise in experimental data. In contrast to the results at 25°C, the calculations at 45°C predict that a departure from a surface controlled reaction should be apparent, at least for low stirring rates ($\delta = 25\mu$m). The departure from pure surface reaction control is slight when $\delta = 10\mu$m or less (the slopes of best fit lines through the upper two curves in Fig. 11b are 1.050 ($\delta = 7\mu$m) and 1.066 ($\delta = 10\mu$m). The continued increase of temperature, to 65 and 100°C, leads to an increase in the transport dependence of the reaction. By 65°C, the slope of best fit lines through the curves have increased to 1.123 ($\delta = 7$ μm) and 1.156 ($\delta = 10$ μm). These slopes correspond to an apparent order of about 0.57 ($=m/2$ see Eqn. 6.9), which is lower than the observed 0.7^{th} order rate dependence. The transport control is even more noticeable in Fig. 11d.

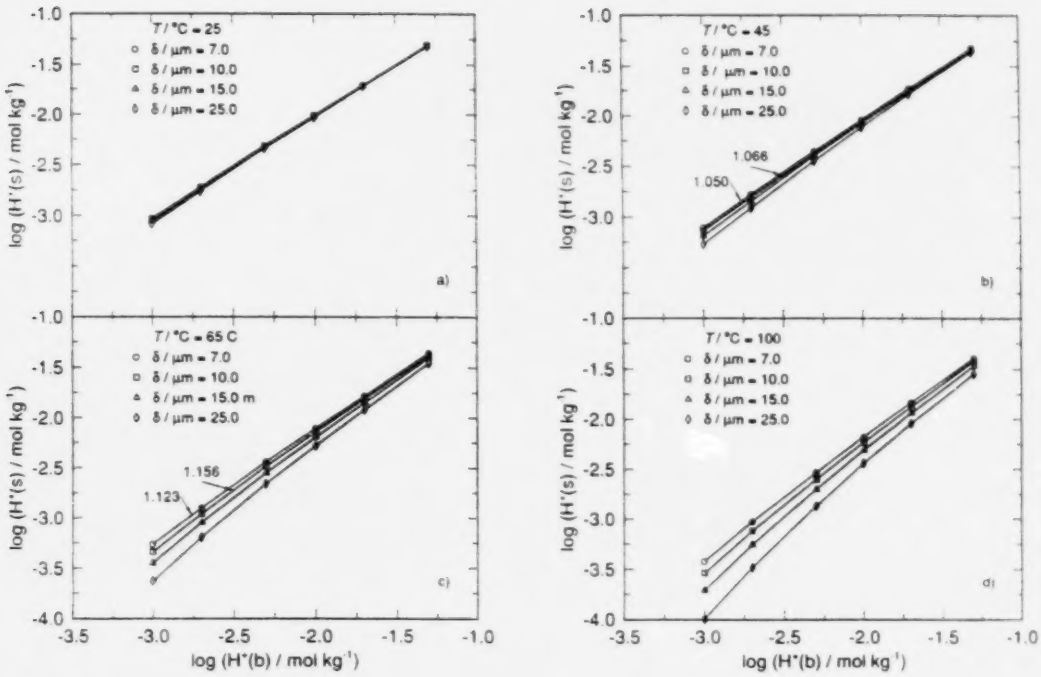
T / °C = 25
δ / μm = 7.0
δ / μm = 10.0
δ / μm = 15.0
δ / μm = 25.0
a)
T / °C = 45
δ / μm = 7.0
δ / μm = 10.0
δ / μm = 15.0
δ / μm = 25.0
1.066
1.050
b)
T / °C = 65 C
δ / μm = 7.0
δ / μm = 10.0
δ / μm = 15.0 m
δ / μm = 25.0
1.156
1.123
c)
T / °C = 100
δ / μm = 7.0
δ / μm = 10.0
δ / μm = 15.0
δ / μm = 25.0
d)
log (H+(s) / mol kg-1)
log (H+(b) / mol kg-1)

Figure 6.11: Calculated surface H^+ concentration plotted as a function of bulk H^+ concentration for stagnant film thicknesses of 7, 10, 15, and 25 μm.

This discrepancy between the reaction order predicted from the model calculations and experimental observations may arise from several factors. The input parameters may be wrong; if the activation energy associated with k_1^D were increased the reaction would be further transport limited (larger m). Increased values of δ (*e.g.* $> 25\mu$m) would result in such a high reaction order; however, in light of previous discussions (Chapter 4, sec. 6.1), this seems unlikely.

The model for dolomite dissolution kinetics proposed by Lund *et al.* (1973) offers a possible explanation for the discrepancy. They proposed that the rate of dissolution is proportional to the concentration of adsorbed protons, which is related to $[H^+]$ by the Freundlich isotherm

$$H(ads) = k_{ads}[H^+]^{nf}, \tag{6.10}$$

in which H(ads) is the concentration of adsorbed H and nf is a temperature dependent parameter. Lund *et al.* (1973) report that nf is related to T by

$$nf = \frac{RT}{(1 - aT)X_m}, \tag{6.11}$$

where a and X_m are essentially fit parameters.

A similar expression was obtained by Chou and Wollast (1985) in a model of the dissolution of albite. Their model assumes that the surface complex whose concentration governs the reaction rate (*i.e.* an adsorbed proton, denoted S—H) mixes non-ideally with the uncomplexed surface sites (in the case of albite S—Na). They further assume a regular solution model to obtain the form of the activity coefficients of these two surface complexes. This assumption leads to the result that the rate of dissolution should be related to the solution composition by

$$r_{albite} = k_{CW}[H^+]^{1/ncw}, \tag{6.12}$$

where

$$ncw = 1 - \frac{\omega}{2RT}. \tag{6.13}$$

The term ω in Eqn. 6.13 is the excess enthalpy of mixing. The reaction rate is dependent on $1/ncw$ which is

$$\frac{1}{ncw} = \frac{2RT}{2RT - \omega},$$

which is of similar form to nf, although nf is constrained by $nf \leq 1.0$ whereas, in general, $1/ncw \geq 1.0$ (Pitzer and Brewer, 1961). However, the similarity of form suggests that Eqn. 6.11 is a reasonable empirical expression with which to fit the temperature dependence of reaction orders.

Despite the predictions of both the models mentioned above, the reaction order, n_1, of the dolomite dissolution is sensibly temperature independent from 1.5 to 45°C (Busenberg and Plummer, 1982). The parameters in Eqn. 6.11 can be manipulated to force nf to be relatively temperature independent over this temperature range; however, in so doing nf will also be relatively constant up to 100°C. For example, if $nf(0°C)$ is constrained to 0.45 and $nf(45°C)$ is 0.55 than $nf(65°C)$ will only be about 0.6. It may be necessary to invoke both the model proposed by Lund *et al.* (1973), or some variation thereof, and the demonstrated increase in transport control described here, to account for the experimental observations. However, unless the dolomite dissolution experiments are performed under known hydrodynamics conditions, it will be difficult to develop a comprehensive model to describe the surface reaction.

6.4 Applications to higher temperatures

Difficulties arose in interpreting experimental dissolution rates using a rate expression of the form proposed by Busenberg and Plummer (1982) at 150 and 200°C. The 200°C could not be interpreted in terms of any rate expression. The rate data were tested against several possible rate laws, including various expressions for both the forward and back reactions.

Whether this failure to be able to describe the rate of dolomite dissolution in terms of bulk solution is due to the increased role of diffusion in limiting the reaction rate can be investigated with the model presented above. Values of the rate constants k_1^D - k_3^D were extrapolated to 150°C from the temperature dependence reported in Busenberg and Plummer (1982). The tracer diffusion coefficients used are given in Table 4.1 with the exception of the Mg^{2+} value which was 5.5×10^{-5} cm^2 s^{-1}. As with all the other

calculations presented in this chapter, no provision for a back reaction was included. A value of δ of 15μm was used, and the bulk solution was a well undersaturated, CO_2 rich solution; however, the calculated solution composition at the solid/solution interface was well oversaturated. This requires that a back reaction term must be included in the model, and demonstrates that the model assumptions are false. The model results do demonstrate the importance of diffusion in limiting the reaction rate. Until experiments can be performed under better defined hydrodynamic conditions, it will be very difficult to separate all the factors determining the rate of dolomite dissolution. If δ is known, the measured dissolution rate and the diffusion equation can be used to estimate the solution composition at the solid/solution interface, and hence, the surface reaction rate constants and an expression for the back reaction can be determined. This is in contrast to the case of calcite dissolution where an expression for the back reaction (Eqn. 4.4) can be assumed, since the dissolution reaction proceeds without any of the inhibition apparent in the case of dolomite dissolution. However, since δ is not known, the bulk solution is not a useful indicator of the solution composition at the solid/solution interface, and until experiments can be performed under better defined hydrodynamic conditions it will be very difficult to separate all the factors determining the rate of dolomite dissolution.

By way of summary, although the calculations demonstrate that transport processes become increasingly important in limiting the rate of dolomite dissolution at temperatures about 50°C, the calculated change in reaction order resulting from the transport control is less than observed experimentally. The reaction order is dependent on δ, so it is possible to match the temperature dependence with the experimental observations by fitting δ to match the observed reaction order. This will result in large values for the fit δ, larger than seems likely based on arguments presented here. The temperature dependence of the reaction order at temperatures below 100° is most likely a result of both a change in the sorption properties of $[H^+]$ to the dolomite surface and an increase in transport control. The relationship between reaction rate and bulk solution composition becomes progressively more difficult to

ascertain as temperature increases, due to the steady increase of transport control on the reaction rate.

Physical Parameters				
$T/°C$	25	45	65	100
$D°(Mg^{2+})/10^{-5}cm^2\ s^{-1}$	0.70	1.10	1.64	2.95
$D°(Ca^{2+})/10^{-5}cm^2\ s^{-1}$	0.79	1.22	1.77	3.13
$D°(Cl^-)/10^{-5}cm^2\ s^{-1}$	2.03	3.17	4.72	8.51
$D°(H^+)/10^{-5}cm^2\ s^{-1}$	9.30	13.1	17.7	27.8
$D°(H_2CO_3)/10^{-5}cm^2\ s^{-1}$	1.90	2.90	4.20	7.32
$D°(HCO_3^-)/10^{-5}cm^2\ s^{-1}$	1.18	1.88	2.82	5.20
$(pK(H_2CO_3)$	6.35	6.30	6.31	6.43
$k_1^D/10^{-5}$	1.00	7.35	36.3	121.
$k_2^D/10^{-6}$	0.93	1.36	4.04	12.8
$k_3^D/10^{-9}$	2.00	2.8	35.0	197.
$Ca(\delta)/\mu mol\ kg^{-1}$	1.0	1.0	1.0	1.0
$Mg(\delta)/\mu mol\ kg^{-1}$	1.0	1.0	1.0	1.0
$TIC(\delta)/\mu mol\ kg^{-1}$	2.0	2.0	2.0	2.0

Table 6.1: Values of physical parameters used in these calculations.

Chapter 7

Implications and Applications to other Systems

It is apparent from both experimental and theoretical considerations that carbonate reaction kinetics are controlled, at least partially, by diffusional processes at temperatures above 100°C. This diffusional control leads to the introduction of a parameter representing the length over which the diffusional flux is supported (δ), into the rate expression. The rate dependence on δ may be expressed either implicitly through stirring rate (see Table 3.2), or explicitly (Chap. 4).

7.1 Application to Industrial Problems

Carbonate scales are commonly found in boiler systems. These scales are generally removed by acid etching. In order to accurately predict the rates of scale removal by acid etching some knowledge of the flow conditions in the pipe must be known. The stagnant film thickness associated with a given flow condition can be either calculated from hydrodynamic models of flow through a roughened pipe, or by relating previously measured rates of scale removal to an empirical parameter equivalent to δ. The importance of the stagnant film thickness in determining the dissolution rate, at high temperatures, is demonstrated in section 4.5 and Table 4.4. A change in δ

from 25 μm to 6 μm will lead to 6 fold increase in the dissolution rate. Although, it is conceivable to present a complete set of differential equations to accurately describe the chemical changes in the etching solution throughout the pipe, it may not be practical to solve them. Some idea of the complexity of that approach is demonstrated below.

In two dimensional cartesian coordinates the diffusion-advection equation describing the evolution of the composition, C, of a solution flowing at a velocity, v, in the x direction is (Domenico and Schwartz, 1990)

$$D(\frac{\partial^2 C}{\partial x^2} + \frac{\partial^2 C}{\partial y}) + v\frac{\partial C}{\partial x} = \frac{\partial C}{\partial t}, \qquad 7.1$$

Equation 7.1 can be simplified by assuming that the term $\partial^2 C/\partial x^2$ is small (*i.e.* the diffusive flux in the flow direction is small relative to the flux due to advection) to

$$D\frac{\partial^2 C}{\partial y} + v\frac{\partial C}{\partial x} = \frac{\partial C}{\partial t}, \qquad 7.2$$

Assuming that the flow is between two parallel, infinite, dissolving planes, separated by $2L$, that the solution is saturated at the boundaries (pure diffusion control) and that the inflowing solution has composition C_o the boundary conditions are $C(x,0,t) = C(x,2L,t) = C_{sat}$ and $C(0,y,t) = C_o$ and the initial condition $C(x,y,0) = C_s$. The solution to eqn. 7.2 subject to these conditions is

$$C(x,y,t;t < x/v) = C_s + \frac{2(C_i - C_s)}{\pi}\sum_{l=1}^{\infty}\frac{\exp(-w_l^2 t)\sin(w_l y)}{w_l} \qquad 7.3$$

$$C(x,y,t;t > x/v) = C_s + \frac{2(C_o - C_s)}{\pi}\sum_{l=1}^{\infty}\frac{exp(-w_l^2\frac{x}{v})\sin(w_l y)}{w_l}, \qquad 7.4$$

in which $w_l = (2l-1)\pi\sqrt{D}/2L$. The derivation of this solution is similar to that presented in Murphy *et al.* (1989) for the case $v = 0$, and the extension to non-zero values of v is straight forward since diffusion in the flow direction is ignored. Analytical solutions also exist for other simple geometries such as plug flow through a circular tube or a past a dissolving sphere. It appears that analytical solutions do not exist to the more realistic, although still highly idealized model, in which v is replaced by $U(1-(y/L)^2$, that describes non-ideal flow between two plates (or in a

tube if y is replaced by r and L by the pipe radius). Further complications arise in the diffusion-advection equation if the diffusion coefficients are coupled as in Eqn 4.5). In industrial applications, heterogeneities in the channel wall will lead to turbulence near the wall, leading to still further complications in any hydrodynamic modelling. The utility of the rate expressions obtain in this study to removal of carbonate scale in industrial conditions is limited, both by the need for numerical solutions to the equations describing the scale removal, and because there is very poor control of the hydrodynamics around the dissolving scale. However, from knowledge of scale removal rates in one solution and at a known flow rate, it should be possible to estimate the scale removal rates in different solution compositions.

Although it is unlikely that absolute dissolution rates can be calculated using the models presented here, the utility of some strategies used to increase dissolution rates can be studied. For example, increasing turbulence in the etching solution will increase the dissolution rate. Well stirred, less chemically aggressive solutions may remove scales at greater rate than poorly stirred, stronger acids. As well the models can be used to test if certain additives to the solution will be expected to significantly alter the rate of scale removal.

If a reaction is diffusion controlled, its rate will increase if the solubility of the solid is increased. It seems likely that adding a solute that complexes a significant proportion of the calcium in solution may increase the dissolution rate, by increasing the solubility of calcite. The model presented in Chapter 4 was adapted to test the affect of using a acid, HX, whose conjugate base, X^-, forms a strong complex with calcium. The equations considered in Chapter 4 were recast to include the species CaX^+ and CaX_2° instead of $CaHCO_3^+$ and $CaCO_3$. The CaX^+ complex was strong, complexing over 80% of the calcium when $(X^-) = 1.\times10^{-3}$ moles $kg^{-1} \gg (Ca^{2+})$. The self-diffusion coefficient of the complex CaX^+ was set to be slightly less than the value for Ca. The results of a few simulations ($T = 150°C$, $\delta = 6\mu m$, [HX(b)] = 1.0 mmole kg^{-1}) suggest that the increase in dissolution rate, due to the increased solubility, was trivial. Furthermore, by decreasing the mobility of the complex, the rate of

dissolution could be reduced by forming the complex (at least in solutions when both systems were well undersaturated). Thus, a strategy for increasing descaling rates based solely on introducing an acid whose conjugate base forms a strong calcium complex will likely fail. The equations presented in Chapter 4 can also be recast to calculate how conjugate bases with higher valances will change the dissolution rate. This was tested in a run which considered a strong diprotonated acid (*e.g.* H_2SO_4) instead of HCl. If the self diffusion coefficient for the conjugate base of this acid was the same as for Cl^-, the dissolution rate was found to increase less than 10% over the rate calculated for an HCl solution with the same bulk TIC and Ca concentration and bulk pH. In order to model the consequences of adding a complexing agent such as Na_3EDTA to complex the calcium the model presented in Chapter 4 must be further modified to consider a fourth component.

It may also be tempting to search for a solution additive that would render the calcite surface more susceptible to acid attack. Such a strategy was tested using the conditions mentioned in the previous paragraph, but increasing the rate constant, k_1, by a factor of ten. The calculated rate of dissolution increased by a factor of two. Although the sensitivity of the dissolution rate on the various input parameters can be tested more completely, it is likely that the best strategy for increasing scale removal rates will be based on reducing the stagnant film thickness rather than trying to find solution additives.

Dissolution rates can be estimated with reasonable accuracy by treating δ as a fit parameter and assuming a diffusion limited reaction, but the calculated solution composition within the stagnant film will not be accurate. This can be demonstrated by comparing results of the calculations presented in Chap. 4 with those presented by Sjöberg and Rickard (1984a) and Lancia *et al.* (1991). Both Sjöberg and Rickard (1984a) and Lancia *et al.* (1991) could reproduce experimental rate data using a diffusion based model of calcite dissolution. Both models predict shifts in the solution pH of several units between the crystal surface and the bulk solution. The model presented in Chap. 4 suggests that the shift in pH for bulk solution compositions

under conditions similar to those used in these two studies should be only about 0.5 of a pH unit. Sjöberg and Rickard (1984a) fail to consider the possibility that there could be a concentration gradient in Cl^-. Consequently, in order to balance the charge associated with the Ca^{2+} introduced by the calcite dissolution, without the Cl^-, an increase in bicarbonate and carbonate is required. Lancia *et al.* (1991) assumed a pure diffusion limited reaction and found that pH gradients of several units could be supported around a dissolving calcite grain. Although these assumptions do not seriously affect the rate calculation, they do lead to erroneous conclusions about the chemical environment near the calcite.

7.2 Trace Element Partitioning

Accurate models of the solution composition and the processes leading to this composition are important for analysing the behaviour of trace elements around dissolving or precipitating carbonates. The pH gradients of a magnitude of those calculated by Lancia *et al.* (1991) and Sjöberg and Rickard (1984a) leads to incorrect assumptions about what would happen if a solution containing a soluble form of any metal that forms insoluble hydroxides was brought in contact with calcite. These models predict that any dissolving carbonate will be armoured rapidly by insoluble hydroxides. The saturation state of hydroxides will not change appreciably around dissolving calcite as a result of to the relatively small pH shifts reported in Chap. 4. More interesting results can be obtained by considering the behaviour of trace elements during diffusion limited carbonate precipitation.

7.2.1 Zonations within Grain

The incorporation of manganese into calcite has been extensively studied (see Machel and Burton, 1991). Recently, Reeder *et al.* (1990) observed that calcite grown in unstirred, highly supersaturated, Mn bearing solutions developed concentric oscillatory zones with differing Mn concentrations. The formation of these zones is most likely

due to diffusion within the solution. Similar compositional zoning in plagioclase has been attributed by Haase *et al.* (1980) to a growth law that is limited by diffusion but also sensitive to the melt composition adjacent to and the composition of the crystallizing grain. Although the solution from which the grain is growing is different, a similar feedback loop may affect the partitioning of trace elements in calcite.

A possible mechanism by which compositional zonation can form in calcite is described below. Initially, the calcite is introduced into a homogeneous solution, but since Mn is incorporated preferentially into the growing solid, it will be depleted rapidly from the solution near the crystal. Calcite precipitation kinetics are sensitive to impurities, so as Mn is depleted from the solution the precipitation rate will increase, leading to a Mn depleted zone in the calcite. The increased rate of precipitation will lead to an increased flux towards the surface, which will lead to a replenishment of Mn in the stagnant film. Eventually, the Mn concentration at the solid/solution interface will increase to such an extent that a Mn-rich zone will precipitate. This will than lead to a Mn depletion, and another Ca-rich zone. Detailed analysis of the time dependent diffusion equation is required to determine if this process will result in oscillatory zonations or a simple steady state, in which the rate of incorporation of Mn into the crystal becomes constant. Wang and Merino (1992) recently analysed a similar model and found that oscillatory solutions were possible. However, a simple, order of magnitude, mass balance calculation, applied to the results of Reeder *et al.* (1990) suggests that diffusional processes are most likely involved in the development of the zones.

The period (the length of time required to deposit one complete compositional zone) of oscillatory solutions to the time dependent diffusion equation describing the above model should be on the order of 1 – 10 times the average time required for an ion to diffuse from the bulk solution to the surface. In this time only about 1 - 10 times the total mass of dissolved carbonate present in the stagnant layer may precipitate. This suggests that the separation between Mn-rich zones increase with the Ca in solution. This may explain why Reeder *et al.* (1990) could only grow zoned

crystals in highly supersaturated (0.2 mole kg^{-1} Ca), unstirred, solutions. Reeder *et al.* (1990) also failed to grow zoned crystals in highly supersaturated, stirred solutions, even at stirring rates as low as 8 rpm. The zonations formed in the unstirred solutions were about 10 microns thick (Reeder, 1991). A 10 μm thickness of calcite contains about 0.25 μmoles of Ca per cm^2. This much Ca is present in a 1 cm^2 column of 0.2 molar Ca solution that is 1250 μm long. Thus, if the stagnant zone surrounding a crystal in an unstirred solution is on the order of 1 mm there is a potential to precipitate a zone of calcite 10 μm thick before the composition of the stagnant film will respond to a perturbation, such as the rapid depletion of Mn. A stagnant film thickness of about 1 mm may be reasonable for an unstirred solution, although not for a stirred solution.

7.2.2 Trace Element Partitioning and Precipitation Rates

Another aspect of trace element incorporation that can be addressed quantitatively using the models developed in Chaps. 4 and 6 involves the manner in which precipitation rates affect trace element distribution coefficients. The distribution of trace elements in calcite, particularly those elements which affect the cathodoluminescence properties of calcite, most notably Mn and Fe, is of interest to carbonate petrologists. Machel and Burton (1991) review the factors that influence iron and manganese distribution in calcite and dolomite as well as the utility of data obtained from such distributions.

The distribution of a trace element, Me, between a solution and carbonate solid can be described in terms of a distribution coefficient, which is defined by some equilibrium constant type expression. One expression for a distribution coefficient, $\mathcal{D}_{Me}$, is

$$\mathcal{D}_{Me} = \frac{X_{Me}[Ca^{2+}]}{X_{Ca}[Me^{2+}]}, \qquad 7.5$$

in which X_A is the mole fraction of A in the carbonate. Distribution coefficients, obtained by measuring the concentration of Me incorporated in a carbonate grown in a solution of known composition, have been found to vary with the precipitation

rate (*e.g.* Lorens, 1981; Dromgoole and Walter, 1990). If the precipitation rates are sufficiently rapid concentration gradients, similar to those formed around dissolving calcite grains, will form.

Generally, it appears that elements preferentially incorporated into the calcite structure (*e.g.* Mn) tend to have lower distribution coefficients at higher growth rates, but those elements that are excluded from the calcite structure (*e.g.* Sr) tend to have higher distribution coefficients at higher precipitation rates. Although there are conceptual models that explain these observations (Lahann and Siebert, 1982; Kinsman and Holland, 1969; Lorens, 1981; Mucci, 1988), solute diffusional processes may also be important in this respect. The conceptual model essentially argues that increasing the precipitation rate will decrease the time that the reactions that redistribute the cations around the surface after they have been adsorbed will operate. In other words, adsorbed cations will have less time to find their optimal position on the surface (or in the case of excluded cations, to kick themselves off the surface). However; the observed trends in distribution coefficients are also expected from diffusional considerations; an element will be even more depleted than Ca near a precipitating grain if it is preferentially incorporated into the structure, hence the distribution coefficient (based on bulk solution composition) will be lower than would be obtained in the limit of no growth (no concentration gradients). Two preliminary calculations are presented below. The first model is based on a simple diffusional model, fluxes are strictly proportional to concentration gradients (and uncoupled) and speciation is ignored. This model should give some indication of the pertinent parameters and whether any diffusional considerations need to be considered. The second model considers coupled diffusion and is used to test if the first model is sensible.

A simplified model of diffusion can give information about the conditions under which the distribution coefficient is likely to be affected by diffusional gradients. Assuming that the concentration gradient around the precipitating grain is time invariant, the mole fractions in Eqn 7.5 can be replaced with the elemental fluxes so

that Eqn 7.5 will be

$$\mathcal{D} = J_{\mathrm{Me}}[\mathrm{Ca}^{2+}]/J_{\mathrm{Ca}}[\mathrm{Me}^{2+}]. \qquad 7.6$$

If the gradients are significant the activities in Eqns 7.5 and 7.6 should be replaced with surface activities, to give

$$\mathcal{D} = J_{\mathrm{Me}}(\mathrm{Ca}^{2+}{}_s)/J_{\mathrm{Ca}}(\mathrm{Me}^{2+}{}_s). \qquad 7.7$$

If the fluxes are assumed to be simply proportional to the concentration gradients, and differences between D_{Ca} and D_{Me} and activity coefficients are ignored, Eqn 7.7 can be expressed as

$$\mathcal{D} = \frac{((\mathrm{Me}_b) - (\mathrm{Me}_s))(\mathrm{Ca}_s)}{((\mathrm{Ca}_b) - (\mathrm{Ca}_s))(\mathrm{Me}_s)}. \qquad 7.8$$

Since J_{Ca} is equal to the precipitation rate, r_{ppn}, $(= ((\mathrm{Ca}_b^{2+}) - (\mathrm{Ca}_s^{2+}))/D_{Ca}\delta)$ the surface concentrations can be related to the precipitation rate by

$$(\mathrm{Ca}_s) = (\mathrm{Ca}_b) - \delta r_{ppn}/D_{\mathrm{Ca}} \qquad 7.9a$$

and

$$(\mathrm{Me}_s) = (\mathrm{Me}_b)\frac{D_{\mathrm{Ca}}(\mathrm{Ca}_s)}{D_{\mathrm{Ca}}(\mathrm{Ca}_s) + \delta\mathcal{D}r_{ppn}}. \qquad 7.9b$$

The observed distribution coefficient, $\mathcal{D}'$, is

$$\mathcal{D}' = J_{\mathrm{Me}}(\mathrm{Ca}_b)/J_{\mathrm{Ca}}(\mathrm{Me}_b). \qquad 7.10$$

Eqn. 7.10 can be re-written (using Eqns. 7.7 and 7.9a and 7.9b) as

$$\mathcal{D}' = \frac{\mathcal{D}D_{Ca}Ca_b}{\delta r_{ppn}(\mathcal{D}-1) + D_{\mathrm{Ca}}\mathrm{Ca}_b}. \qquad 7.11$$

In the limits of $r_{ppn} = 0$, $D_{\mathrm{Ca}} \to \infty$ or $\mathcal{D} = 1$, Eqn. 7.11 reduces to

$$\mathcal{D}' = \mathcal{D},$$

as expected.

This analysis suggests that the dimensionless quantity $\Gamma = \delta r_{ppn}/D(\mathrm{Ca}_b)$ is critical in determining the extent to which the observed $\mathcal{D}'$ differs from $\mathcal{D}$. Typically, at 25°C, D will be about 10^{-5} cm^2 s^{-1} and δ is on the order of 10μm (10^{-3} cm). Precipitation

rates reported in by Dromgoole and Walter (1990) range from 450-50,000 μmol m^{-2} hr^{-1} (1.25 $\times 10^{-8}$ mmol cm^{-2} s^{-1} -1.39 $\times 10^{-6}$ mmol cm^{-2} s^{-1}). Dromgoole and Walter (1990) used a 0.1 molar Ca (0.1 mmole cm^{-3}) solution for their experiments which lead to values of Γ of between 1.25 $\times 10^{-5}$ and 1.4 $\times 10^{-3}$. Throughout this range of values Eqn. 7.11 suggests that there will be no appreciable departure between $\mathcal{D}$ and $\mathcal{D}'$.

To test the above, relatively simple, model the program developed to model dolomite dissolution presented in Chap. 6 was adapted by replacing the Mg flux (equal to the rate of dolomite dissolution) with a flux of Mn proportional to the calcium flux. The distribution coefficient, $\mathcal{D}$, defines the Me flux relative to the precipitation rate (Eqn. 7.7); Eqn. 7.7 and 7.10 can be rearranged to give

$$\mathcal{D}' = \mathcal{D}(\mathrm{Ca_b})(\mathrm{Me_s})/(\mathrm{Ca_s})(\mathrm{Me_b}).$$

Calculated values of $\mathcal{D}'$ are plotted as a function of precipitation rate in Fig. 7.1. The values of $\mathcal{D}'$ calculated from Eqn. 7.11 are also shown as a solid line in this figure. There is general agreement between the shape and location at which there becomes a significant departure of $\mathcal{D}$ from $\mathcal{D}'$, but it is clear that Eqn. 7.11 will overestimate the distribution coefficient.

The single most important factor neglected in the above calculations is the formation of aqueous complexes. Within the stagnant film the solution will become increasingly acidic as the surface is approached. If a significant pH gradient is developed in the film the percentage of Mn that is uncomplexed will tend to increase near the surface. Changes in speciation would not have affected the experiments of Dromgoole and Walter (1990), which were conducted in relatively acidic solutions (pH 5.5 - 6.7), but they may be important in more basic solutions. On the basis of these calculations it is apparent that the variation in distribution coefficients with precipitation rate seen experimentally at 25°C (*e.g.* Dromgoole and Walter, 1990) is not due to diffusional processes, but must be related to processes occurring at the crystal surface (*e.g.* similar to those proposed by Kinsman and Holland (1969)). The calculations also demonstrate that Eqn. 7.11 will predict reasonably whether or not

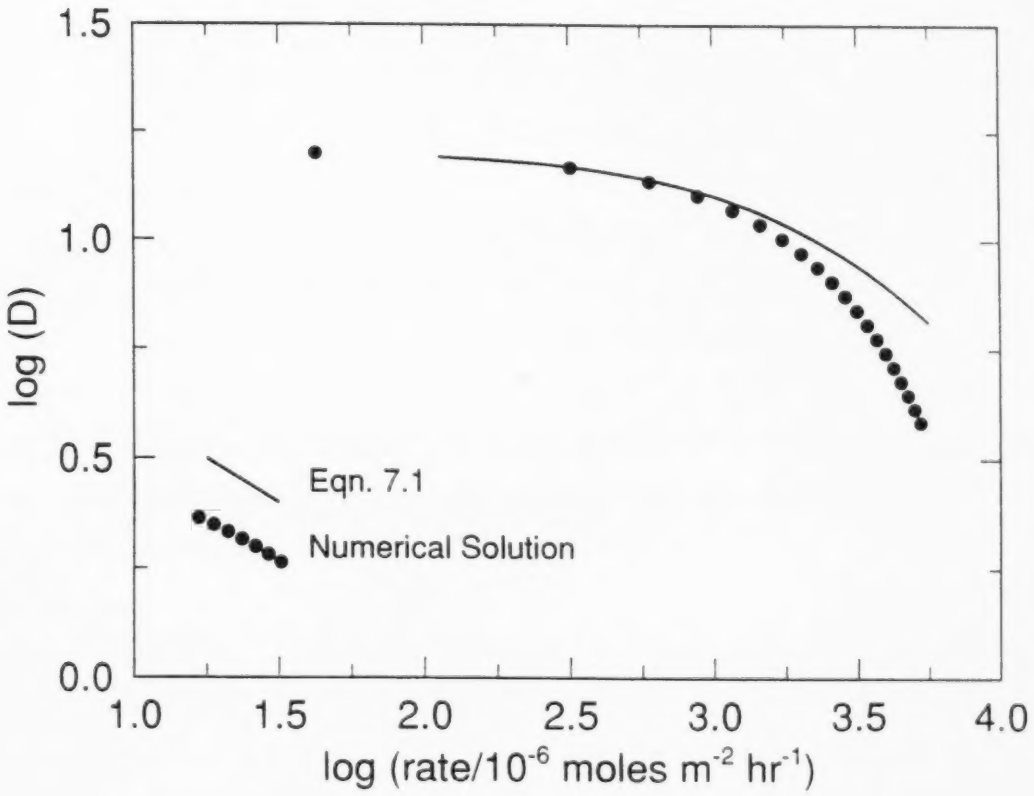

Figure 7.1: Calculated distribution coefficients as a function of precipitation rate assuming the bulk solution contained 10^{-4} moles kg^{-1} Ca, and 5×10^{-6} moles kg^{-1} Me. The precipitation rate was increased by increasing the Na_2CO_3 in the bulk solution. The value of δ used in these calculations was 5 μm. The solid line was calculated from Eqn. 7.11.

diffusional profiles within stagnant film will affect trace element partition coefficients.

Chapter 8

Summary and Conclusions

The rates of dissolution of carbonate minerals are increasingly controlled by diffusion through the solution surrounding the solid as temperature increases. Consequently, the dissolution rate becomes progressively more dependent on the parameters describing the solution flow around the grain with increasing temperature, and the bulk solution composition becomes a less reliable indicator of the chemical environment at the solid/solution interface.

Despite this observation, the rate of calcite dissolution at temperatures between 25 and 200°C is well described by the rate expression proposed by PWP (Eqn. 3.1 - $\frac{dC_a}{dt} = k_1^C[H^+] + k_2^C[H_2CO_3] + k_3^C[H_2O] - k_4^C[Ca^{2+}][HCO_3^-]$). The activities in Eqn. 3.1 are those in the bulk solution. The value of k_1^C is poorly constrained by the data presented here except at 100°C at a stirring rate of 500 rpm. The rate constant, k_2^C, was found to have a maximum near 150°C; the decrease almost certainly being a result of the retrograde nature of calcite solubility. The rate constant, k_3^C, fits well with the extrapolation of PWP data above 25°C with an activation energy of about 25 kJ mole^{-1}.

While it was demonstrated that a rate law of the form proposed by PWP for lower temperatures will fit the higher temperature experimental data, any concentration gradients present at 25°C will be greater at higher temperatures. In order to better understand why the rate data can be fit with the low temperature rate

expression, numerical solutions to the equation describing electrostatically coupled diffusion through a stagnant film were obtained. The boundary conditions attached to the diffusion equation are that the bulk solution composition is fixed and the flux from the dissolving surface is given by the rate expression proposed by PWP, with an important change. The rate is calculated using the solution composition at the solid/solution interface, rather than the bulk solution composition. The calculated concentration profiles developed around a dissolving calcite grain demonstrate that the assumptions made by PWP concerning the forward reaction are valid at 25°C. However, their model to explain the back reaction is not supported by the calculations.

The rate constants for the surface reaction were extrapolated, from the temperature dependence given by PWP, to 150°C, and the calculations of the concentration profiles were repeated. The results demonstrate that, although the solution composition at the solid/solution interface is very different than that of the bulk solution, Eqn. 3.1 can relate the calculated rates to the bulk solution composition. If the stagnant film assumed to be surrounding the calcite grain was about 25 μm, a regression of the calculated rates to Eqn. 3.1 gave rate constants similar to those observed experimentally.

The experimental results demonstrate that the difference between calcite and dolomite dissolution rates decreases with temperature. For example, the run conditions for the calcite run W150288 and the dolomite run 270391 were quite similar ($\sim$ 200° and 36 mmol kg^{-1} TIC) and the dissolution rates measured in the most dilute solutions differed by only a factor of about 4. In a similar solution at 25°C the difference is about a factor of 15. The rate expression proposed by Busenberg and Plummer (1982) for dolomite dissolution was less successful at describing these experimental rates than Eqn. 3.1 was at describing the calcite data. With the exception of the 200°C data, an expression that did not consider any back reaction could, for the most part, be fit to the experimental results. The experimental results demonstrate a stirring rate dependence in k_1^D at 100°C and above. As with calcite, the solution

composition immediately adjacent to the dissolving dolomite grains becomes more basic than the bulk solution, and the measured solution composition becomes less representative of the conditions near the grain. Further increases in temperature increase the sensitivity of the dissolution rate to the stirring rate. As well, the rate constant k_2 is less sensitive to the dolomite specimen at 100°C than at 150°C. This suggests that it is solubility rather than the defect structure which is determining the dissolution rate. By 200°C it is likely that the concentration gradients surrounding the dolomite crystal are so great as to make any analysis without consideration of a back reaction meaningless. In order to fit rate data with a mechanistic rate expression better control of the hydrodynamics in the solution surrounding the grain is required. Without this control, neither the solution composition at the surface nor the form of the forward rate expression can be predicted.

An approach similar to that used to model the concentration gradients around calcite grains was used to calculate the profiles developed around dolomite dissolving in HCl bearing solutions. Values of the rate constants k_1^D - k_3^D were extrapolated to 150°C from the temperature dependence reported in Busenberg and Plummer (1982). The calculations clearly demonstrated that, although the rate of proton consumption was half order at the surface, the apparent reaction order increased with temperature. The calculated increase of reaction order with temperature was not as great was reported by Busenberg and Plummer (1982). The assumptions made to simplify the model limited the temperature range over which the calculation was valid. No back reaction was included in the calculation; however, the calculated surface solution composition at 150°C was oversaturated with respect to dolomite even in quite aggressive solutions. This requires that a back reaction term must be included in the model. Until experiments can be performed under better defined hydrodynamic conditions it will be very difficult to separate all the factors determining the rate of dolomite dissolution.

Diffusional processes can cause the concentration of the solutes that affect the rate of dissolution to differ between the bulk solution and the solution at the surface.

The extent to which they can they alter the partitioning of trace elements between bulk solution and a precipitating solid was also investigated. A kinetic effect which related the distribution coefficient and the precipitation rate was distinguished. At 25°C the calculated effect was much less pronounced than observed variations between distribution coefficients and precipitation rates (*e.g.* Dromgoole and Walter, 1990). The calculations of the concentration gradients formed around dissolving grains at higher temperature indicate that much greater concentration gradients develop at higher temperatures. This suggests that further, more detailed models (*i.e.* provisions for the consideration of more solutes), may prove useful in understanding aspects of trace element partitioning in carbonates.

The composition of the aqueous phase at the solid/solution interface must be discerned before any interpretation of any rate sensitive processes can be begun. Models of processes as diverse as rates of removal rates of carbonate scales found in boiler systems, or diagenetic redistribution of elements between carbonates and solutions must include some consideration of transport processes, and preferably including a fully coupled treatment of diffusion coefficients, in order to be considered as anything but empirical, and very limited, models.

References

Aagaard P. and H.C. Helgeson, 1982, Thermodynamic and kinetic constraints on reaction rates among minerals and aqueous solutions. I. Theoretical considerations. *Amer. J. Sci.*, **282**, 237-285.

Anderson D.E. and D.L. Graf, 1976, Multicomponent electrolyte diffusion. *Ann. Rev. Earth Plant. Sci.*, **4**, 95-121.

Atkins P.W., 1982, *Physical Chemistry. 2nd ed.* Oxford University Press, Oxford, 1081p.

Berner R.A., 1978, Rate control of mineral dissolution under near surface conditions, *Am. J. Sci.*, **278**, 1235-1252.

Berner R.A., 1981, Kinetics of weathering and diagenesis. In: *Kinetics of Geochemical Processes.* A.C. Lasaga and R.J. Kirkpatrick (eds.), *Rev. Mineral.* **8**, 111-134.

Bignold G.J., A.D. Brewer, and B. Hearn, 1971, Specific conductivity and ionic product of water between 50 and 271°C. *Trans. Far. Soc.*, **67**, 2419-2430.

Bird G., J. Boon and T. Stone, 1986, Silica transport during steam injection into oil sands. I. Dissolution and precipitation kinetics of quartz: new results and

review of existing data. *Chem. Geol.*, **54**, 69-80.

Bourcier W.L., G.C. Ulmer, and H.L. Barnes, 1987, Hydrothermal pH sensors of ZrO_2, Pd hydrides, and Ir oxides. In: *Hydrothermal experimental techniques*. G.C. Ulmer and H.L. Barnes (eds.) John Wiley.

Bowers T.S. and H.P. Jr. Taylor, 1985, An integrated chemical and stable–isotope model of the origin of midocean ridge hot spring systems. *J. Geophys. Res.*, **90**, 12,583-12,606.

Busenberg E. and L.N. Plummer, 1982, The kinetics of dissolution of dolomite in CO_2-H_2O systems at 1.5° to 65°C and 0 to 1 atm P_{CO_2}. *Am. J. Sci.*, **282**, 45-78.

Busenberg E. and L.N. Plummer, 1986, A comparative study of the dissolution and crystal growth kinetics of calcite and aragonite. In: *Studies in diagenesis*. F.A. Mumpton (ed.),*USGS Bull.* **1578**, 139-168.

Callahan F.J., 1974, *Swagelok tube fitting and installation manual.* Markad Service Co., Cleveland, Oh., 276p.

Chou L. and R. Wollast, 1984, Study of the weathering of albite at room temperature and pressure with a fluidized bed reactor. *Geochim. Cosmochim. Acta* **48**, 2205-2217.

Chou L. and R. Wollast, 1985, Steady-state kinetics and dissolution mechanisms of albite. *Amer. J. Sci.*, **285**, 963-993.

Chou L., R.M. Garrels and R. Wollast, 1989, A comparative study of the kinetics and mechanisms of dissolution of carbonate minerals. *Chem. Geol.*, **78**, 269-282.

Compton R.G. and P.J. Daly, 1984, The dissolution kinetics of Iceland spar single crystals. *Jour. Colloid Interface Sci.*, **101**, 159-166.

Compton R.G. and P.J. Daly, 1987, The dissolution/precipitation kinetics of calcium carbonate: An assessment of various kinetic equations using a rotating disk method. *J. Colloid and Interface Sci.*, **115**, 493-498.

Compton R.G., K.L. Pritchard, and P.R. Unwin, 1989, The direct measurement of dissolution kinetics at the calcite/water interface. *J. Chem. Soc. Chem. Commun.*, **4**, 249-251.

Compton R.G., C.T. Walker, P.R. Walker, and P.R. Unwin, 1990, Dissolution kinetics of Carrera marble, Portland stone and several limestones in acidic waters. *J. Chem. Soc. Faraday Trans.*, **86**, 849-854.

Correns C.W. and W. von Engelhardt, 1938, Neue Untersuchungen uber die Verwitterung des Kalifeldspates. *Chemie det Erde*, **12**, 1-22.

Davis J.A., C.C. Fuller, and A.D. Cook, 1987, Mechanisms of trace metal sorption by calcite: adsorption of Cd^{2+} and subsequent solid solution formation. *Geochim. Cosmochim. Acta*, **51**, 1477-1490.

Dibble W.E. Jr. and W.A. Tiller, 1981, Non-equilibrium water/rock interactions –I. Model for interface controlled reactions. *Geochim. Cosmochim. Acta*, **45**, 79-92.

Domenico P.A. and F.W. Schwartz, 1990, *Physical and Chemical Hydrogeology*. John Wiley, New York, 824p.

Dreybrodt W. and D. Buhmann, 1991, A mass transfer model for dissolution and precipitation of calcite from solutions in turbulent motion. *Chem. Geol.*, **90**, 107-122.

Dromgoole E.L. and L.M. Walter, 1990, Iron and manganese incorporation into calcite: effects of growth kinetics, temperature, and solution chemistry. *Chem. Geol.*, **81**, 311-336.

Faure G., 1991, *Principles and applications of inorganic geochemistry*. Macmillian, New York, 626p.

Faux R.F., E. Busenberg, and L.N. Plummer, 1986, The dissolution kinetics of magnesite from 25° - 85°C and pH's of 0 - 10 at atmospheric P_{CO_2}. Geol. Soc. Am., Abstr. Prog., 18(6), 599

Fein J.B. and J.V. Walther, 1987, Calcite solubility in supercritical CO_2-H_2O fluids. *Geochim. Cosmochim. Acta,* **51**, 1665-1673.

Ferret J., R. Gout, Y. Kihn, and J. Sevely, 1987, The influence of grinding on the dissolution kinetics of calcite. *Phys. Chem. Min.*, **15**, 163-170.

Frear G.L. and J. Johnston, 1929, Solubility of calcium carbonate (calcite) in certain aqueous solution at 25°C. *Amer. Chem. Soc. Jour.*, **51**, 2082-2093.

Garrels R.M. and C.L. Christ, 1965, *Solutions, Minerals and Equilibria.* Freeman Cooper, San Fransisco, Cal., 450p.

Gerald C.F., 1978, *Applied numerical analysis, 2nd ed.* Addison-Wesley, Menlo Park, Cal., 560p.

Glasstone S., K.J. Laidler, and H. Eyring, 1941, *The theory of rate processes.* McGraw-Hill, New York, 611p.

Gunter W.D., and E.H. Perkins, 1991, Use of calcite as a CO_2 geobarometer for estimation of reservoir pressures in thermally assisted oil recovery. *Can. Miner.*, **29**, 755-765.

Haase C.S., J. Chadam, D. Feinn, and P. Ortoleva, 1980, Oscillatory zoning in plagioclase feldspar. *Science,* **209**, 272-274.

Helgeson H.C., 1969, Thermodynamics of hydrothermal systems at elevated temperatures and pressures. *Am. J. Sci.*, **267**, 729-804.

Helgeson H.C., and D.H. Kirkham, 1974, Theoretical prediction of the thermodynamic behavior of aqueous electrolytes at high temperatures and pressures. I. Summary of the thermodynamic/electrostatic properties of the solvent. *Am. J. Sci.*, **274**, 1089-1198.

Helgeson H.C., W.M. Murphy and P. Aagaard, 1984, Thermodynamic and kinetic constraints on reaction rates among minerals and aqueous solutions. II. Rate

constants, effective area, and the hydrolysis of feldspar. *Geochim. Cosmochim. Acta*, **48**, 2405-2432.

Herman J.S., 1982, *The dissolution kinetics of calcite, dolomite and dolomitic rocks in the carbon dioxide-water system.* Unpublished PhD. thesis, Penn. State, 219p.

Herman J.S. and W.B. White, 1985, Dissolution kinetics of dolomite: Effects of lithology and fluid flow velocity. *Geochim. Cosmochim. Acta*, **49**, 2017-2026.

Holland H.D. and S.D. Malinin, 1979, The solubility and occurrence of non–ore minerals. In: *Geochemistry of hydrothermal ore deposits* H.L. Barnes (ed.), 461-508. John Wiley and Sons.

House W.A., 1981, Kinetics of crystallisation of calcite from calcium bicarbonate solutions. *J. Chem. Soc. Faraday Trans. 1*, **77**, 341-359.

Inskeep W.P. and P.R. Bloom, 1985, An evaluation of rate equations for calcite precipitation kinetics at pCO_2 less than 0.01 atm and pH greater than 8. *Geochim. Cosmochim. Acta*, **49**, 2165-2180.

Keith R.E. and J.J. Gilman, 1960, Dislocation etch pits and plastic deformation in calcite. *Acta Metal*, **8**, 1-10.

Kharaka Y.K., W.D. Gunter, P.K. Aggarwal, E.H. Perkins, and J.D. DeBraal, 1988, SOLMINEQ.88: A computer program code for geochemical modeling of water-rock interactions. *USGS. Water-Resources Investigations Report 88-4227.*

King C.V. and C.L. Liu, 1933, The rate of solution of marble in dilute acids. *Am. Chem. Soc. J.*, **55**, 1928-1940.

Kinsman D.J.J., and H.D. Holland, 1969, The coprecipitation of cations with $CaCa_3$ - IV. The coprecipitation of Sr^{2+} with aragonite between 16° and 96°C. *Geochim. Cosmochim. Acta*, **33**, 1-17.

Lagache M., 1976, New data on the kinetics of the dissolution of alkali feldspar at 200°C in carbon dioxide charged water. *Geochim. Cosmochim Acta*, **40**, 157-161.

Lahann R.W., and R.M. Siebert, 1982, A kinetic model for distribution coefficients and application to Mg-calcites. *Geochim. Cosmochim. Acta*, **46**, 2229-2237.

Lancia A., D. Musmarra, F. Pepe, and G. Volpicelli, 1991, Concentration profiles in the diffusional film in the calcium carbonate dissolution process. *Chem. Engng. Sci.* **46**, 2507-2512.

Lasaga A.C., 1979, The treatment of multi-component diffusion and ion pairs in diagenetic fluxes. *Am. J. Sci.*, **278**, 324-346.

Lasaga A.C., 1981, Rate laws of chemical reactions. In: *Kinetics of Geochemical Processes*. A.C. Lasaga and R.J. Kirkpatrick (eds.), *Reviews in mineralogy*, **8**, 1-68.

Lasaga A.C., 1990, Atomic treatment of mineral-water surface reactions. In: *Mineral-water Interface Chemistry*. M.F. Hochella and A.F. White (eds.), *Rev. in Mineral.*, **23**, 17-85.

Leaist D.G., 1985, Ternary diffusion of carbon dioxide in alkaline solutions of aqueous sodium hydroxide and aqueous sodium carbonate. *Ber. Bunsenges. Phys. Chem.*, **89**, 786-793.

Leaist D.G., 1987, Subsurface dissolution and precipitation during leaching of porous ionic solids. *J. Colloid Inter. Sci.*, **118**, 262-269.

Lerman A., 1979, *Geochemical processes*. John Wiley and Sons, New York, 481p.

Levenspiel O., 1972, *Chemical Reaction Engineering. 2nd ed.* John Wiley, New York, 578p.

Lorens R.B., 1981, Sr, Cd, Mn and Co distribution coefficients in calcite as a function of calcite precipitation rate. *Geochim. Cosmochim. Acta*, **45**, 553-551.

Lund K., H.S. Fogler, and C.C. McCune, 1973, Acidization – I. The dissolution of dolomite in hydrochloric acid. *Chem. Eng. Sci.* **28**, 691-700.

Lund K., H.S. Fogler, and C.C. McCune, 1975, Acidization – II. The dissolution of calcite in hydrochloric acid. *Chem. Eng. Sci.* **30**, 825-835.

Mackenzie F.T., W.D. Bischoff, F.C. Bishop, M. Loijens, J. Schoonmaker, and R. Wollast, 1983, Magnesian calcites: low-temperature occurrence, solubility and solid solution behavior. In: Carbonates: Mineralogy and Chemistry R.J. Reeder (ed.), *Rev. Mineral.* **11**, 97-144.

Machel H.G., and E.A. Burton, 1991, Factors governing catholuminescence in calcite and dolomite, and their implications for studies of carbonate diagenesis. In: *Luminescence microscopy and spectroscopy: Qualitative and Quantitative Applications.* C.E. Barker and O.C. Kopp (eds.) *SEPM Short Course* **25**, 37-58.

Morse J.W., 1974, Dissolution kinetics of calcium carbonate in sea water. III A new method for the study of carbonate reaction kinetics. *Am. J. Sci.* **274**, 97-107.

Morse J.W., 1983, The kinetics of calcium carbonate dissolution and precipitation. In: *Carbonates: Mineralogy and Chemistry* R.J. Reeder (ed.), *Rev. Mineral.* **11**, 227-264.

Mucci A., 1988, Manganese uptake during calcite precipitation from seawater: conditions leading to the formation of a pseudokutnahorite. *Geochim. Cosmochim. Acta,* bf 52, 1859-1868.

Murphy W.M. and H.C. Helgeson, 1989, Thermodynamic and kinetic constraints on reaction rates among minerals and aqueous solutions. IV. Retrieval of rate constants and activation parameters for the hydrolysis of pyroxene, wollastonite, olivine, andalusite, quartz, and nepheline. *Am. J. Sci.* **289**, 17-101.

Murphy W.M., E.H. Oelkers and P.C. Lichtner, 1989, Surface reaction versus diffusion control of mineral dissolution and growth rates in geochemical processes. *Chem. Geol.*, **78**, 357-380.

Nielsen A.E., 1964, *Kinetics of Precipitation*. The MacMillan Company, New York, 151p.

Oelkers E.H. and H.C. Helgeson, 1988, Calculation of the thermodynamic and transport properties of aqueous species at high temperatures: Aqueous tracer diffusion coefficients to 1000°C and 5 kb. *Geochim. Cosmochim. Acta*, bf 52, 63-85.

Paces T., 1973, Steady state kinetics and equilibrium between ground water and granitic rock. *Geochim. Cosmochim. Acta*, **37**, 2641-2663.

Pitzer K.S., and L. Brewer, 1961, *Thermodynamics. 2nd ed.* (revision of 1st ed. by G.N. Lewis and M. Randall, 1923) McGraw-Hill, New York, 723p.

Plummer L.N., and T.M.L. Wigley, 1976, The dissolution of calcite in CO_2–saturated solutions at 25 °C and 1 atmosphere total pressure. *Geochim. Cosmochim. Acta*, **40**, 191-202.

Plummer L.N. and E. Busenberg, 1982, The solubilities of calcite, aragonite and vaterite in the CO_2-H_2O solutions between 0 and 90°C, and an evaluation of the aqueous model for the system $CaCO_3$-CO_2-H_2O. *Geochim. Cosmochim. Acta*, **46**, 1011-1040.

Plummer L.N., T.M.L. Wigley, and D.L. Parkhurst, 1978, The kinetics of calcite dissolution in CO_2-water systems at 5° to 60°C and 0.0 to 1.0 atm CO_2. *Am. J. Sci.* **278**, 179-216.

Plummer L.N., T.M.L. Wigley, and D.L. Parkhurst, 1979, Critical review of the kinetics of calcite dissolution and precipitation. In: *Chemical modeling in aqueous*

systems. Speciation, sorption, solubility, and kinetics E.A. Jenne (ed.) *Amer. Chem. Soc. Symposium Series* **93**, 537-573.

Posey-Dowty J., D. Crerar, R. Hellman, and C. Chang, 1986, Kinetics of mineral water reactions: theory, design and application of circulating hydrothermal equipment. *Am. Miner.* **71**, 85-94.

Reeder R.J, R.O. Fagioli, and W.J. Meyers, 1990, Oscillatory zoning of Mn in solution-grown calcite crystals. *Earth Sci. Rev.* **29** 39-46.

Reeder R.J, 1991, An overview of zoning in carbonate minerals. In: *Luminescence microscopy and spectroscopy: Qualitative and Quantitative Applications.* C.E. Barker and O.C. Kopp (eds.) *SEPM Short Course 25,* 77-82.

Rickard D. and E.L. Sjöberg, 1983, Mixed control of calcite dissolution rates. *Am. J. Sci.* **283**, 815-830.

Rimstidt J.D. and H.L. Barnes, 1980, The kinetics of silca-water reactions. *Geochim. Cosmochim. Acta,* **44**, 1683-1699.

Rimstidt J.D. and P.M. Dove, 1986, Mineral/solution reaction rates in a mixed flow reactor; wollastonite hydrolysis. *Geochim. Cosmochim. Acta,* **50**, 2509-2516.

Robinson, R.A. and R.H. Stokes, 1962, *Electrolyte Solutions, 2nd ed.* Academic Press, New York.

Schott J., S. Brantley, D. Crerar, C. Guy, M. Borcsik, and W. Christian, 1989, Dissolution of strained calcite. *Geochim. Cosmochim. Acta,* **53**, 373-382.

Sharp W.E. and G.C. Kennedy, 1965, The system CaO–CO_2–H_2O in the two phase region calcite and aqueous solution. *J. Geol.* **73**, 391-403.

Shiraki R. and S.L. Brantley, 1992, Precipitation kinetics of calcite at elevated temperatures. In. *Water Rock Interaction WRI-7* Y.K. Kharaka and A.S. Maest (eds.) 111-114

Sjöberg E.L. and D.T. Rickard, 1983, The influence of experimental design on the rate of calcite dissolution. *Geochim. Cosmochim. Acta*, **47**, 2281-2285.

Sjöberg E.L. and D.T. Rickard, 1984a, Calcite dissolution kinetics: Surface speciation and the origin of the variable pH dependence. *Chem. Geol.*, **42**, 119-136.

Sjöberg E.L. and D.T. Rickard, 1984b, Temperature dependence of calcite dissolution kinetics between 1 and 62 °C at pH 2.7 to 8.4 in aqueous solutions. *Geochim. Cosmochim. Acta*, **48**, 485-493.

Sposito G., 1990, Molecular models of ion adsorption on mineral surfaces. In: *Mineral-water Interface Chemistry*. M.F. Hochella and A.F. White (eds.) *Rev. Mineral.*, **23**, 261-279. Mineralogical Society of America.

Talman S.J., B. Wiwchar, W.D. Gunter, and C.M. Scarfe, 1990, The dissolution kinetics of calcite in the H_2O-CO_2 system along the steam saturation curve to 210°C. In: *Fluid Mineral Interactions: A tribute to H.P. Eugster*. R.J. Spencer and I-Ming Chou (eds.) *The Geochemical Society Special Publication No. 2* 41-55.

Talman S.J. and W.D. Gunter, 1992, Rates of dolomite dissolution in CO_2 and HCl bearing solutions from 100 - 200°C. In: *Water Rock Interaction WRI-7* Y.K. Kharaka and A.S. Maest (ed.) 119-122

Thompson D.W. and P.G. Pownall, 1989, Surface electrical properties of calcite. *J. Colloid Interface Sci.*, **131**, 74-82.

Wallin M. and I. Bjerle, 1989, Rate models for limestone dissolution: A comparison. *Geochim. Cosmochim. Acta*, **53**, 1171-1176.

Wang Y. and E. Merino, 1992, Dynamic model of oscillatory zoning of trace elements in calcite: Double layer, inhibition, and self-organization. *Geochim. Cosmochim. Acta*, **56**, 587-596.

Wieland E., B. Wehrli, and W. Stumm, 1988, The coordination chemistry of weathering: III. A generalization on the dissolution rates of minerals. *Geochim. Cosmochim. Acta*, **52**, 1969-1981.

Wollast R., 1967, Kinetics of the alteration of K-feldspar in buffered solutions at low temperature. *Geochim. Cosmochim. Acta*, **31**, 635-648.

Wood B.J. and J.V. Walther, 1983, Rates of hydrothermal reactions. *Science* **222**, 413-415.

Wood J.R., 1986, Thermal mass transfer in systems containing quartz and calcite. In: *Roles of organic matter in sediment diagenesis*. D.L. Gautier (ed.), *SEPM Special Publication* **38** 169-180.

Zhang J.-W., and G.H. Nancollas, 1990, Mechanisms of growth and dissolution of sparingly soluble salts. In: *Mineral-water Interface Chemistry* M.F. Hochella and A.F. White (eds.) *Rev. Mineral.* **23**, 365-399.

Appendix A

A.1 Raw data from the calcite experiments

The raw data from the runs described in the text are given in the following tables. The values for the cations are all from ICP analysis, pH and C_q are the pH and the TIC of the quenched sample and C is the TIC of the sample which was made basic by adding NaOH. The tic concentration is corrected for dilution by NaOH. The units of concentration are ppm. The last sample of each run is, unless otherwise noted, a standard of 26 ppm Ca. Those entries marked - were not analyzed and those listed as *nd* were below detection.

Table A.1

Run	*Sample*	*Time (hrs.)*	Ca	C	Fe	Mg	K	pH	C_q
*W*130587	1	0.0	1.4	380.	3.4	*nd*	0.4	4.39	230.
	3	0.5	3.0	387.	1.7	*nd*	0.5	4.48	238.
	5	1.5	6.6	395.	0.9	*nd*	0.3	4.56	243.
	7	3.5	11.2	384.	0.5	0.1	0.5	4.83	213.
	9	7.5	16.7	385.	0.4	0.1	0.4	4.83	230.
	11	15.5	20.0	381.	0.4	0.2	0.3	4.76	217.
	13	31.5	21.2	391.	0.4	0.1	0.5	4.80	234.
	15	55.5	21.4	381.	0.4	0.3	0.3	4.79	224.
	17	79.5	21.0	375.	0.4	0.2	0.4	4.85	216.
	19	101.0	21.0	388.	0.6	*nd*	0.4	4.81	246.
	21	–	28.4	–	*nd*	3.1	8.6	–	–
*W*150987	1	0.0	1.4	475.	3.0	0.5	11.3	4.53	170.
	3	0.5	3.3	450.	0.6	0.2	13.0	4.67	118.
	5	1.5	7.5	448.	0.6	0.2	14.9	4.97	110.
	7	3.5	13.1	443.	0.5	0.3	17.9	5.28	92.
	9	6.5	17.6	448.	0.3	0.2	15.2	5.27	95.
	11	14.0	21.8	441.	0.3	0.3	12.9	5.47	99.
	13	31.0	21.6	454.	0.2	0.2	8.3	5.14	181.
	15	57.0	22.2	426.	0.3	0.2	10.8	5.22	170.
	17	81.3	21.8	450.	0.3	0.3	13.2	5.39	115.
	21	–	27.8	–	*nd*	3.1	13.7	–	–
*W*271087	1	0.0	0.7	464.	0.1	0.3	1.7	4.54	12.*
	3	0.5	3.6	458.	0.6	0.1	4.5	4.49	204.
	5	1.5	8.0	466.	0.5	0.2	3.3	4.72	191.
	7	3.5	12.4	474.	0.5	0.2	3.3	4.89	178.
	9	7.0	17.4	488.	0.5	0.2	3.8	5.19	139.
	11	15.0	20.2	471.	0.4	0.2	2.7	5.08	181.
	13	31.0	21.4	472.	0.2	0.2	2.4	5.04	205.
	15	130.4	21.4	284.	0.2	0.3	6.4	5.24	187.
	18	–	26.8	–	*nd*	3.0	7.7	–	
*W*011287	1	0.0	0.9	390.	1.8	0.2	7.02	15.3	
	3	0.5	2.1	385.	0.7	*nd*	*nd*	7.23	2.7
	5	1.5	4.6	380.	0.4	*nd*	*nd*	7.63	15.8
	7	3.5	8.6	386.	0.2	*nd*	*nd*	7.71	14.6
	9	7.5	13.7	390.	0.3	*nd*	*nd*	7.98	17.3
	11	15.0	18.5	392.	*nd*	*nd*	*nd*	8.17	19.4
	13	32.0	21.8	396.	0.1	*nd*	*nd*	8.26	23.1
	15	55.0	21.6	384.	*nd*	0.2	0.2	8.33	25.8
	17	79.0	21.2	385.	0.2	*nd*	*nd*	8.23	27.0
	19	103.0	21.4	–	0.2	0.1	*nd*	8.16	13.8
	21	–	28.2	–	*nd*	3.1	7.7–	–	–

Table A.1: Continued

Run	*Sample*	*Time (hrs.)*	Ca	C	Fe	Mg	pH	C_q
*W*150288	1	0.0	2.2	429.	1.8	0.1	7.39	1.7
	3	0.5	4.4	434.	0.4	*nd*	7.52	2.9
	5	1.5	8.8	354.[a]	0.3	*nd*	7.92	5.8
	7	3.5	14.1	350.[a]	0.2	*nd*	8.26	12.2
	9	7.5	19.3	427.	0.4	*nd*	8.39	16.2
	11	14.0	21.9	338.[a]	0.3	0.2	8.33	14.3
	13	32.0	22.2	414.	0.3	0.1	8.37	16.1
	15	57.0	22.1	396.	0.2	0.1	8.30	13.2
	17	128.0	22.1	385.	0.3	0.2	8.28	13.2
	21	–	28.5	–	*nd*	3.2	–	–
*W*250288	1	0.0	11.2	1140	0.8	*nd*	8.03	7.4
	3	0.5	14.0	1210	1.3	*nd*	8.12	8.9
	5	1.5	18.3	1300	0.3	*nd*	8.22	12.1
	7	3.5	24.8	1300	0.3	0.1	8.01	4.1
	9	7.5	30.4	1160	0.2	0.1	8.00	5.3
	11	15.0	33.2	1220	0.4	*nd*	8.07	5.9
	13	32.0	33.8	1230	0.4	0.2	8.01	5.4
	15	56.0	34.4	1230	0.5	*nd*	8.07	6.5
	17	79.5	33.6	1210	0.5	*nd*	8.01	5.5
	21	–	27.6	–	*nd*	3.1	–	–
*W*140388	1	0.0	5.7	469.	0.7	0.2	7.30	1.2
	3	0.5	5.9	419.	0.3	0.1	7.36	1.0
	5	1.5	8.0	403.	0.2	*nd*	7.35	1.3
	7	3.5	11.6	397.	0.1	0.1	7.52	2.1
	9	7.5	16.7	393.	0.2	0.1	7.69	3.0
	11	15.0	20.2	399.	0.1	0.3	7.78	3.9
	13	33.5	19.7	408.	0.3	0.1	7.62	2.2
	15	–	28.0	–	*nd*	3.1	–	–
	17[b]	–	*nd*	–	*nd*	*nd*	–	–
	19[c]	–	*nd*	–	*nd*	0.1	–	–
*W*160588	2	0.0	1.2	60.	0.2	0.1	6.82	0.4
	4	0.5	1.8	62.	0.2	0.3	6.92	0.7
	6	1.5	3.6	62.	0.1	*nd*	7.24	1.1
	10	3.5	6.6	67.	0.3	0.1	7.41	1.7
	12	7.5	9.6	69.	0.3	0.6	7.71	3.5
	14	13.8	11.2	33.[a]	0.1	0.1	7.66	3.0
	16	24.0	11.6	65.	0.2	0.4	7.68	3.1
	18	48.0	11.3	64.	*nd*	0.2	7.74	3.0
	20	72.0	11.7	62.	0.2	0.2	7.71	3.0
	22	–	27.8	–	0.1	3.1	–	–

Table A.1: Continued

Run	*Sample*	*Time (hrs.)*	Ca	C	Fe	Mg	pH	C_q
*W*310588	2	0.0	0.7	453.	0.5	0.7	6.88	0.6
	4	0.5	3.7	470.	0.2	0.5	7.25	1.2
	6	1.5	8.8	466.	0.3	0.4	7.58	2.2
	8	3.5	14.8	460.	0.2	0.5	7.75	3.5
	10	7.5	19.4	465.	0.1	0.5	7.89	4.6
	12	13.5	21.8	467.	0.2	0.5	7.93	5.0
	14	19.8	22.4	474.	0.1	0.6	7.92	5.4
	16	30.0	22.4	474.	0.2	0.6	7.95	5.6
	18	50.0	22.8	455.	*nd*	0.5	7.99	6.1
	–	–	–	–	–	–	–	–
*W*251088	1	0.0	2.2	85.	*nd*	0.2	–	–
	3	0.5	6.5	88.	*nd*	0.1	–	–
	5	1.0	11.9	91.	*nd*	*nd*	–	–
	7	2.0	19.8	96.	*nd*	0.1	–	–
	9	3.5	26.4	110.	*nd*	*nd*	–	–
	11	8.0	33.4	95.	*nd*	0.2	–	–
	13	15.0	35.6	104.	*nd*	0.2	–	–
	15	35.0	37.2	96.	*nd*	0.3	–	–
	17	52.0	36.8	–	*nd*	0.3	–	–
	19	–	23.6	–	*nd*	0.2	–	–
*W*141288	2	0.0	1.2	87.	0.1	0.5	–	–
	4	0.5	6.6	77.	*nd*	0.3	–	–
	6	1.0	9.6	79.	*nd*	0.1	–	–
	8	2.0	17.9	83.	*nd*	0.3	–	–
	10	3.5	24.4	84.	*nd*	0.3	–	–
	12	7.5	30.4	87.	*nd*	*nd*	–	–
	14	14.7	34.8	91.	*nd*	0.3	–	–
	16	37.2	34.6	87.	0.2	0.3	–	–
	18	61.8	36.4	90.	*nd*	0.3	–	–
	–	–	–	–	–	–	–	–
*W*020389	2[d]	0.0	3.4	0.5	0.1	0.1	8.4	–
	4	0.5	1.1	0.7	0.1	*nd*	8.7	–
	6	1.0	2.0	1.2	0.1	*nd*	6.3	–
	8	2.0	2.9	1.3	0.1	0.2	7.3	–
	10	4.0	4.4	1.8	0.1	*nd*	7.6	–
	12	7.0	5.1	2.1	0.1	0.1	8.6	–
	14	12.0	5.9	2.4	*nd*	*nd*	8.8	–
	16	20.0	6.1	2.5	0.1	*nd*	1.8	–
	18	45.0	6.5	2.6	0.1	0.1	9.2	–
	20	91.0	6.7	3.5	*nd*	*nd*	9.0	–
	22	–	27.0	–	*nd*	3.0	–	–

Table A.1: Continued

Run	*Sample*	*Time (hrs.)*	Ca	C	Fe	Mg	Cl[e]
*W*200389	2	0.0	1.8	195.	0.2	0.2	–
	4	0.5	8.1	200.	*nd*	*nd*	–
	6	1.0	14.6	194.	*nd*	*nd*	–
	8	2.0	24.4	200.	0.3	*nd*	–
	10	4.0	43.6	208.	*nd*	0.1	–
	12	7.0	63.0	238.	0.1	0.2	–
	14	12.7	86.5	203.	*nd*	0.1	–
	16	37.2	106.5	213.	*nd*	0.1	–
	18	46.0	108.0	214.	*nd*	*nd*	–
	20	69.0	109.0	207.	*nd*	0.2	–
	22	–	29.6	–	*nd*	3.4	–
*W*040489	2	0.0	4.7	0.	0.4	0.4	70.9
	4	0.5	19.0	1.	0.7	0.2	69.1
	6	1.0	27.2	1.	0.9	0.1	67.4
	8	1.5	32.0	2.	0.8	0.1	65.7
	10	2.5	35.8	7.	0.5	*nd*	64.1
	12	4.0	39.8	10.	0.2	*nd*	62.5
	14	6.5	42.0	11.	0.3	*nd*	60.9
	16	15.5	44.2	12.	0.4	0.3	59.4
	18	38.8	49.4	12.	0.3	0.1	57.9
	20	69.0	48.0	–	0.2	0.2	56.5
	22	–	28.6	–	*nd*	3.7	–

Table A.1: Raw data from the calcite experiments. Notes – all concentrations are ppm; *a* - Sample froze, CO_2 loss likely; b - Water from infill lines; c - milliQ water; d - Sample contaminated; e - From HCl, assumed to decrease by 2.5% with each sample.

A.2 Dolomite Experimental Details

A.2.1 Detailed notes on Experiments

In a flow through reactor the rate of dissolution of a solid can be varied by changing the physical conditions (crystal surface area, stirring rate) and/or the chemical conditions (input solution composition or flow rate) in the reactor. Most of the runs presented here were performed using a single input solution composition and varying the flow rate through the autoclave to change the solution composition within the reactor. It was found that significant changes in the reaction rate could be achieved by varying the flow rate if the input solution contained HCl (runs 051090, 031290, 181290, 200991), but that the $[H_2CO_3]$ changes in the solution in the autoclave associated with changing the flow rate were too small to appreciably affect the dissolution rate (runs 190790, 131290, 290191, 120291, 200291, 270391). Consequently, in order to establish the manner in which the dissolution rate varies with $[H_2CO_3]$ a technique (see Chapter 2) was developed for the last runs (110591, 240691, 090791) by which CO_2 in the input solution could be changed during the run.

Several of techniques were used to introduce CO_2 into the input solution. Initially, a known pressure of CO_2 was added into an evacuated accumulator, and degassed water was pumped into the accumulator (runs 190790, 131290, 290191, 120291). Two possible problems with this method arose. In one run (131290) the CO_2 pressure in the accumulator was near the lower detection limit of the pressure transducer, and hence the reading may be inaccurate. Also, the H_2CO_3 distribution within the accumulator may not be uniform. In addition, this method was time consuming, since each volume of water added to the accumulator was degassed individually. Two later runs (120291, 200291) involved filling the accumulator with deionized water, degassing the entire volume, removing the accumulator cap, dropping a piece of dry ice into the accumulator and quickly replacing the cap. This was considerably less time consuming; although, it was impossible to control the resulting solution composition accurately. Finally, the technique, described in Chapter 2, involving

introducing fluid CO_2 from a sample tube was developed.

The contents of the CO_2 samples, with one exception, were recovered by discharging the contents of the pressurized sample tubes directly into an airtight syringe containing a known volume of NaOH. Unfortunately, problems arose in the sample treatment. The syringe developed a leak that was fixed for the last 6 runs; as well, some of the samples with higher CO_2 contents were not basified sufficiently to completely fix all the CO_2 in the solution. These two factors both caused a partial loss of CO_2 and hence the CO_2 measurements from several runs were suspect. The CO_2 can be calculated from the measured cation concentrations and solution pH, although this may not be accurate. In one of the HCl runs (181290) the, very low, TIC was recovered by directly discharging the contents of the sample tubes into a phosphoric acid filled vial, which was attached to an evacuated carbon isotope line. The evolved pressure of CO_2 was measured, and the TIC calculated. The technique, while time consuming, worked well; although the first two samples were lost because there was a leak in the vacuum system.

The pH of the outflow solution was continuously monitored to give an indication of the approach to steady state, as well as an independent check of the solution composition. Upon leaving the reactor, the outflow solution was cooled to near room temperature; however, the temperature of the solution at the pH electrode did vary with the flow rate. As well, the room temperature was not constant over the course of the experiment. The electrode was regularly calibrated over the course of the run, but the temperature of the buffer was not necessarily the same as the outflow solution. The pH meter did not have any temperature compensation feature. As a consequence, the pH measurement must be considered to be relatively inaccurate, agreement to $\pm$ 0.1 pH unit should be considered good. However, the pH measurement did provide some useful information. In runs where the pCO_2 was greater than 1 atmosphere CO_2 exsolved immediately from the solution at the back pressure regulator. The measured pH corresponded much more closely with a solution in equilibrium with 1 atmosphere pCO_2 than a solution containing the run TIC. Consequently, in these

Sample	TIC(outlet sample) (ppm)	TIC(inlet sample) (ppm)	TIC(calc) (ppm)
090791$T4$	109	112	90
$T7$	247	219	210
$T10$	412	363	280
$T13$	535	404	280
$T17$	781	574	320
240691$T5$	150	98	110
$T8$	272	213	200
$T11$	445	317	350
$T14$	549	411	340
$T17$	696	528	320

Table A.2: Comparison of carbonate in solution from samples taken from the accumulator (no dead volume) with samples taken after the autoclave. Calculated TIC values were obtained from the measured pH and cations in the sample. The maximum at about 350 ppm corresponds to the solubility of CO_2 at ambient pressures.

cases, the pH presented in Tables 5.1 – 5.3 was calculated for a TIC of about 28 mmole kg^{-1} (about 0.95 bar pCO_2) rather than the run pCO_2.

In those experiments where CO_2 was added to the input solution, the TIC of the solution in the accumulator was evaluated by analysing the solution within the pistonless sample tube that initially contained the CO_2 added to the input solution. Although it should be the same as the TIC of the solution at the outflow, it was found to be considerably lower than the TIC in the output solution (Table A.2).

There are two possible reasons for this discrepancy. The first is that CO_2 may exsolve into the dead volume between the inlet valve on the sample tube and the valve opening the flow system to the sampling system. A second possible reason for the discrepancy is that some CO_2 may not be absorbed into the basified solution during sampling.

Upon opening the flow system to the sample tube, some CO_2 will exsolve into the dead volume. This dead volume is about 3 cc. while the volume of the sample tube is about 17 cc. The CO_2 in the dead volume will eventually end up in the sample tube as a contaminant, however, the extent of contamination depends on the sampling protocol. This contamination may result in an over-estimatation of the

Run	Standard 1 Ca, Mg (ppm)	Standard 2 Ca, Mg (ppm)	Standard 3 Ca, Mg (ppm)
Standards	9.0, 6.4	5.1, 3.7	2.9, 2.1
131290	9.2, 6.9	5.5, 4.1	3.1, 2.2
290191	9.2, 7.0	5.3, 4.0	3.0, 2.3
120291	9.5, 6.4	5.4, 4.0	3.0, 2.3
270391	9.2, 6.8	5.3, 3.9	3.1, 2.2
110591	9.6, 7.0	6.1, 4.0	3.0, 2.2
200991	9.2, 6.8	5.1, 3.7	2.9, 2.2
Averages	9.32, 6.82	5.45, 3.88	3.01, 2.21
σ	0.18, 0.22	0.35, 0.15	0.08, 0.08

Table A.3: Analysis of standard samples submitted along with the run samples.

TIC (assuming the CO_2 fugacity coefficient is 1.) by up to 22 %. A similar sampling method was used in the calcite experiments, but the dead volume was lower, and hence the discrepancy should not be as severe. It seems likely that this problem can be eliminated in the flow reactor by removing the piston from the sample tube and discharging continuously through the sample tube. However, since the recovery of CO_2 from a pistonless sample tube may be incomplete, a sampling procedure that gives reproducible results using both types of sample tubes should be developed.

Calcium and magnesium standards were submitted along with samples from several runs. Table A.3 presents the analysis of these standards. The actual concentration of the standards is given in the first row of Table A.3. The low standard, which is most representative of the concentrations of most of the samples, gives very reproducible results, and the accuracy seems to be about $\pm$ 5% .

The data collected from the experimental runs are presented below. It was noted previously that the data collected was not necessarily self-consistent. These discrepancies are discussed in the following text. A • under the run number in Tables A.4 – A.6 indicates that standard samples were not submitted along with the run samples. Those runs marked with a $\surd$ had three standards submitted along with the run products. In these cases the cation analyses were corrected using the regression line calculated from the standards. The slope of this regression line was less than 8%

Table A.4: Raw data collected from the 100°C runs. Notes - The superscripted digit in the pH column in this and the following tables represents a measured, though inaccurate digit. * and ** some difficulties with gas lines and so analysis probably wrong, *** discarded sample (see text).

Experiment t = 100°C							
Sample	*Stirring rate/* rpm	*flow rate/* mg s^{-1}	Ca/ μmol kg^{-1}	Mg/ μmol kg^{-1}	pH	TIC/ mmol kg^{-1}	Comments
051090	100	0.311	15.	16.	3.1^{5}	–	crystal 1
•		0.178	23.	25.	3.1^{6}	–	HCl =
		0.100	40.	41.	3.2^{2}		1.0 mmolar
		.0333	70	70.	3.4^{1}		
031290	100	0.311	25.	8.	3.3^{5}	12.8	crystal 1
•		0.124	42.	25.	3.4^{5}	13.7	HCl =
		.0533	72.	53.	3.6^{0}	15.7	0.5 mmolar
		.0311	100.	78.	3.8^{0}	17.9	
		0.178	137.	115.	4.1^{5}	15.4	
131290	100	0.311	•	•	4.4^{5}	4.1	crystal 2
√		0.124	8.	5.	4.6^{0}	4.4	
		.0533	18.	17.	4.7^{5}	4.0	
		.0311	35.	32.	4.9^{5}	5.2	
181290	100	0.302	103.	76.	2.6^{2}	0.•	crystal 2
√	600	0.302	96.	92.	2.6^{4}	0.08••HCl =	
	100	0.212	53.	49.	2.6^{3}	0.1372.5 mmolar	
	600	0.212	68.	65.		0.162	HCl
			15.	17.		•••	
270291	630	0.302	10.	12.	4.0^{7}	15.7	crystal 2
√	210	0.290	8.	8.	4.0^{3}	15.2	
	550	0.160	18.	21.	4.1^{3}	16.7	
	550	.0167	120.	120.	4.6^{8}	16.6	
	550	.0533	60.	49.	4.3^{9}	16.1	
est. tic						26.4	
090791	500	0.155	13.	15.	$6.^{3}$	*see*	crystal 3
√	500	0.166	26.	25.	4.6^{0}	*table*	
	500	0.156	42.	36.	4.4^{2}	2.5	
	500	0.182	44.	31.	4.3^{0}		
	500	0.182	46.	32.	4.3^{2}		
	500	0.182	56.	42.	4.3^{4}		
200991	–	–	0.0	0.0	4.1^{5}		crystal 3
	100	0.160	12.	12.	4.5		
	–	–	0.0	0.0	3.0^{3}		
	100	0.160	38.	39.	3.3^{9}		
	500	0.160	75.	76.	3.5^{6}		
	–	–	0.0	0.0	2.7^{6}		
	100	0.178	69.	70.	3.0^{8}		
	500	0.222	126.	125.	3.1^{8}		

from unity, and the intercept generally less than 0.5 ppm.

Experiment $t = 150°C$							
Sample	*Stirring rate/* rpm	*flow rate/* mg s^{-1}	Ca/ μmolkg^{-1}	Mg/ μmolkg^{-1}	pH	TIC mmolkg^{-1}	Comments
190790	100	0.311	40.	37.			crystal 1
•	100	0.186	65.	66.			
290191	100	.0700	16.	17.	$4.7^{9}(20)$	4.9	crystal 2
√	300	0.134	18.	17.	$4.7^{2}(22)$	4.8	
	300	0.284	11.	6.0	4.5^{3}	4.8	
	300	0.391	6.	*bd*	$4.4^{6}(30)$	4.7	
	300	.0222	44.	45.	5.2^{6}	4.6	
200291	500	0.302	20.	13.	4.1^{5}		crystal 2
√	500	0.136	44.	25.	4.3^{6}		
	500	0.167	32.	21.	4.1^{5}		
	500	.0306	145.	137.	4.7^{6}		
	500	.0611	74.	56.	4.5^{6}		
110591	500	0.116	32.5	24.6	–	0.0	crystal 3
√	500	0.109	60.0	57.6	4.93	6.7	
	500	0.076	110.	100.	4.92	11.0	
	260	0.109	100	98.7	4.67	20.0	
	250	0.109	120	111.	4.61	32.0	
	260	0.204	75.0	65.8	4.41	40.0	

Table A.5: Raw data collected from the 150°C runs. The bracketed number following some pH values represents the temperature of the solution in the pH meter.

- 190790 - The pH of the outflow solution was not monitored during run 190790. The ratio Mg/Ca was 1. to within analytical uncertainties, so these values are assumed accurate. Similarly the TIC's agree between the two samples, however, the TIC is lower than the TIC estimated from the amount of CO_2 put into the accumulator. (4.108 V on a 1-5V 0-50 psia transducer, which should result in a solution containing 110 mmoles kg^{-1} TIC). The solution (about 17 mls. of what is expected to be about 0.1 N CO_2) was basified with only about 3 mls of 0.2 N NaOH. This was insufficient to fix all the CO_2, consequently the TIC for this run was estimated at 110 mmole kg^{-1}.

Experiment $t = 200°C$							
Sample	*Stirring rate/* rpm	*flow rate* mgs^{-1}	Ca $\mu molkg^{-1}$	Mg $\mu molkg^{-1}$	pH	TIC $mmolkg^{-1}$	Comments
120291	160	.0522	54.	73.	4.5^{4}	14.7	crystal 2
√	500	0.258	32.	26.	4.3^{1}	15.5	
	500	0.133	49.	42.	4.4^{8}	13.5	
	500	.0203	118.	108.	4.8^{4}	14.2	
270391	550	0.133	58.	60.	4.3^{6}		crystal 2
√	550	0.222	40.	44.	4.2^{5}	30.4	
	550	.0233	108.	106.	4.6^{0}		
	550	.0555	72.	75.	4.4^{5}		
240691	180	0.182	23.	23.			crystal 3
√	500	0.158	38.	36.	4.6^{9}	8.3	
	500	0.160	48.	44.	4.5^{0}	17.5	
	500	0.160	83.	71.	4.4^{5}	26.4	
	500	0.160	82.	69.	4.4^{8}	34.3	
	500	0.196	80.	68.	4.4^{7}	44.0	

Table A.6: Raw data collected from the 200°C runs

- 051090 - The samples from run 051090 all had very high iron contents (mean 3.2 ppm). The iron came from the accumulator, the blank taken from it contained 20. ppm Fe. The accumulator was charged with approximately 1 mmol kg^{-1} HCl, but the reaction with the accumulator can, depending on the Eh of the solution, lower $[H^+]$ below 10^{-3}. It should increase back to 10^{-3} as the iron comes out of solution. The steady state pH could not, however, be predicted from the measured solution composition unless the $[Cl^-]$ was reduced to 0.8×10^{-3} mmol kg^{-1} and the measured [Fe] was included in the charge balance calculation. This results in good agreement between the calculated and measured pH. The calculated pH is given, along with the rest of the assumed solution composition in Table 5.1. Finally, the flow rate for the last sample may not be accurate. It was noted that one of the pumps tripped before the sample was taken. The pH trace suggests that the pump tripped only shortly before the sample was taken so the solution composition should be representative of the steady state solution composition. However, the reason that the pump tripped is either that it was not completely filled, or that is was discharging more rapidly than expected from the recorded flow rate.

- 031290 - The results of 031290 are not consistent. The input solution was made to be 0.5 mmolar HCl and approximately 38 mmolar CO_2. The TIC analyses were all consistently lower than this value, this is likely due to the leak in the syringe used to collect the CO_2. The ratio Ca/Mg is consistently greater than 1; however, the difference between Ca and Mg is roughly constant for each sample ($\sim$ 20 μm kg^{-1}). In Table 5.1 the Mg values are increased by 20 μm kg^{-1}. It can be seen that with these concentrations the calculated pH (column 6 of Table 5.1) agrees quite well with the measured pH (column 6, Table A.4). It is likely that both Ca and Mg are overestimated since there is no provision for other cations in the calculation (*e.g.* Ni); however, the solution composition in Table 5.1 is likely much closer to the actual composition than that listed in Table A.4. The effect on the solution pH resulting from the exsolution of CO_2 before the pH meter is small; cation concentrations change by less than 10% if 28.4 mmolar TIC is used in the calculation.

- 131290 - The results of 131290 are rather difficult to reconcile. The low TIC makes the pH very much more sensitive to the cation concentration than in other runs with higher TIC's and anion concentrations. Reasonable agreement between the measured and calculated solution composition can be achieved by assuming TIC = 4.2 mmol kg^{-1}, and that about 10 μequivalents of cations other than Ca and Mg (*i.e.* Ni) were in the solution. The Mg concentration of the second sample was also increased to 8 μmol kg^{-1}. Table 5.1 gives the calculated pH of this solution at 25°C. The value of 4.2 mmol kg^{-1} for TIC is lower than the estimated run condition of 5.0 mmol kg^{-1}; however, it is in good agreement with the mean of the measured TIC's of 4.4 mmol kg^{-1}. The run conditions were estimated by filling the accumulator with

a measured pCO_2 before it was filled with water. The pCO_2 in the accumulator was measured with a relatively high pressure transducer, so the accuracy of the reading is suspect. The low TIC's from this run mean that the problems associated with the TIC measurement in some other samples (CO_2 loss due to improper basification) were avoided.

- 181290 - The solution data from run 181290 are generally self consistent. The Ca concentration of the first sample is reduced in Table 5.1 to make it the same as the Mg concentration. It also appears that the analyses were mixed up; the cation analyses included more data than there were samples submitted. One solution contained 120 ppm K (as opposed to less than 0.5 ppm in all the other samples) and so was discarded. Since there was no CO_2 added to the input solution, the concentrations of TIC in these samples were calculated from the pressure of CO_2 evolved when the sample tube was discharged directly into an acidic solution. The vacuum system leaked for both the first two samples, so these samples were both lost. The TIC from the third and fourth samples were both about 4×10^{-5} mole kg^{-1} greater than the sum of the cations. This likely arises from a failure to evolve all the CO_2 during the degassing of the input solution.

- 290191 - There was very poor control of the temperature of the output solution (the temperature is given in brackets following the pH in Table A.5) and the temperature of the buffer relative to the sample was not known. This makes the pH measurement sort of meaningless. The TIC was consistent between the samples. The pH's given in Table 5.2 are all at 25, and so cannot be compared with the measured pH. The cations for the third and fourth samples were not consistent, as well as being near the lower limit of the analysis, so they were averaged.

- 120291 - The analysis for this run was generally consistent. The Mg in the first sample was considerably higher than the Ca, and lowered down to the Ca value. The TIC chosen was the highest measured TIC since only this sample was properly basified. After these alterations were made, the agreement between the measured and calculated pH was good.

- 200291 - No TIC's are available for this run. The initial TIC estimate was about 300 ppm; however, the accuracy of this figure is low since CO_2 was added as dry ice. TIC's calculated from the on line pH varied between 220 and 340 ppm. However, with the exception of the last sample, the calculated pH was within 0.1 pH units from the measured pH value if the TIC was 250 ppm. The ratio of Ca/Mg is appreciably larger

than 1 for all the samples, even after correction for the standards. The information available from this run is insufficient to justify any other data manipulation.

- 270291 - The input solution for run 270291 was obtained by discharging 11.6 g of CO_2 into the 10 L accumulator. This should have resulted in solution containing 26.4 mmol kg^{-1} TIC. The measured TIC's were considerably lower than this value (Table A.4); however, the data cannot be reconciled if the measured TIC's are used. Table 5.1 presents the data assuming that the TIC is 26.4 mmol kg^{-1} (317 ppm). The calculated pH's agree very well with the measured values.

- 270391 - Insufficient base was used in 270391 to fix all the TIC in solution, with the exception of one sample which had a TIC of 0.0375 moles kg^{-1}. All the other TIC's were considerably lower than this. A portion of the initial charge of CO_2 in the accumulator was lost. The measured pH fixed the TIC at about very nearly the CO_2 solubility limit (about 28 mmole kg^{-1}). The solution composition used in the rate calculations is based on the one TIC measurement of 0.0375 moles kg^{-1}.

- 110591 - There is good agreement between the measured pH's and those calculated using the measured solution composition. The pH of the last two samples agree with the pH in a solution with 28 mmolar H_2CO_3. In three samples the Ca is greater than the Mg, however, in all cases the discrepancy is within 10% , which is likely within analytical error. The standards of 5.1 ppm Ca and 3.6 ppm Mg were analysed at 6.1 ppm and 4.0 ppm respectively, although the analysis of the lower standards (2.9 ppm Ca and 2.1 ppm Mg) were 3.0 ppm and 2.2 ppm respectively.

- 240691 - The cation ratio in the first two samples is near one, however, there appears to be a systematic deviation from stoichiometric dissolution in the last three samples. The fact that the ratio was essentially one for the first and second sample in both this run and the next makes it possible that the dissolution is non-stoichiometric. The TIC value was taken from the sample drawn from the accumulator (see chapter 2). The pH of the fourth and fifth samples agreed to within 0.05 of a pH unit if the TIC was assumed to be 28 mmole kg^{-1}, which is the solubility of atmospheric CO_2 in an acidic solution.

- 090791 - Also noted in Chap. 2 was that CO_2 exsolved from solution between the back pressure regulator and the pH meter in the high pCO_2 runs. The TIC of the samples from the input solution were not in agreement with the TIC of the outlet

samples (see Chapter 2). The different samples in this run correspond to different TIC's rather than different flow rates. The amount of CO_2 added to the accumulator was weighed out to try to lead to a rather constant increase in TIC between each sample. This is not the case (see Table 2.5, particularly for samples 4 and 5) for either the input or outlet TIC measurement, however, the input solution corresponds more closely to the expected value. The TIC value presented in Table 5.1 are those from the input solution, with the exception of samples 4 and 5 which were obtained by simply incrementing the previous TIC by 10.4 mmol kg^{-1}. Significant errors are possible in these TIC estimates. The calculated pH's for the final three samples were in closer agreement with the measured pH if the Mg concentration was constrained to the Ca concentration.

- 200991 -

Cl analysis of the output from the first sample yielded values of 3.8 and 7.7 ppm. Analysis of a sample drawn from the accumulator gave 2.8 ppm, and the pH of a similar sample suggested 2.5 ppm Cl. The measured pH and cation analysis of the first sample also implied that the Cl concentration was near 2.8 ppm. The flow rate from this sample was not recorded, so it was assumed to be the same as next two. The later two solutions had Cl contents of 6.5×10^{-4} and 1.21×10^{-3} moles kg^{-1} as evaluated by Cl titration. The calculated outflow pH agrees to 0.1 pH unit if these values for (Cl) are used.